To the Graduate Council:

I am submitting herewith a thesis written by Brett S. Okhuysen entitled "Manufacture of Composite Shells Utilizing the Statical-Geometric Properties of Braided Sleeves." I have examined the final copy of this thesis for form and content and recommend that it be accepted in partial fulfillment of the requirements for the degree of Master of Science, with a major in Engineering Science.

Dr. Y. J. Weitsman, Major Professor

We have read this thesis
and recommend its acceptance:

Madhu S. Madhukar

Accepted for the Council:

Associate Vice Chancellor
and Dean of The Graduate School

A NEW FABRICATION TECHNIQUE FOR COMPOSITE SHELLS UTILIZING THE STATICAL-GEOMETRIC PROPERTIES OF BRAIDED SLEEVES

A Thesis

Presented for the

Master of Science

Degree

The University of Tennessee, Knoxville

Brett S. Okhuysen

August 1995

Copyright © Brett Samuel Okhuysen, 1995

All rights reserved.

DEDICATION

This thesis is dedicated to my grandmother, Mrs. Edna Callahan Mobley. I have benefitted greatly over the years from her wisdom, intelligence, and personality. The opportunities that she has generously provided me are uncountable. Over the years the love and encouragement she has given me have propelled me toward numerous goals. I am extraordinarily lucky to have such a fine grandmother. She is an inspiration to me.

ACKNOWLEDGMENTS

I wish to thank my study advisor, Professor Y. J. Weitsman for his generous financial support and guidance throughout this endeavor. I would like to especially thank Professor E. N. Kuznetsov of the University of Illinois, Urbana-Champaign for the inspiration he has given me. Without the many discussions that he provided me, this work would not have been possible. Additionally, I wish to express my gratitude to the other members of my committee, Dr. M. S. Madhukar and Dr. Allen Yu for their support. Additional thanks go out to Dr. T. M. Donnellan of Northrop-Grumman Aircraft for giving me a start in this field as a cooperative engineering student.

I would like to express my gratitude to the Atkins and Pierce company of Covington, Kentucky for the donation of some of the sleeve material used in this work.

I thank the staff of the composite materials branch of the Naval Air Warfare Center in Warminster, Pennsylvania for all they taught me as a co-op student.

I would like to thank my friends Stephanie Vierkötter, J. W. Penland, Brian Erickson, Donald Erdman, Joanna Jankowski, Ranga Kosuri, Sean Anderson, Steve Kolesar, Benny Adams and Timothy Page. Finally I wish to thank my family for their support, guidance, encouragement, and love, especially my sister Catherine J. Okhuysen, and my parents Harry and Charlotte Bruen.

ABSTRACT

Shells constructed from composite materials have several advantages over similar structures made from traditional materials. However, the high cost of manufacturing composite shells inhibits their use in commercial applications, where cost is a dominant concern. A significant factor of this cost is that current fabrication methods for continuous fiber composite shells require fibers to be placed on mandrels to obtain desired shapes. Commonly fibers are placed on a mandrel by three techniques: they are wound as filaments, put in laminate form and wrapped, or braided into tubes, called sleeves, and dressed to the mandrel. Often a new mandrel must be manufactured for each new part produced.

A new method of fabricating composite shells from braided sleeves has been developed in which different sleeves are nested to form a single assembly. This assembly is then subjected to loads so that different sleeves in the assembly manifest different levels of tension. Various shapes are realized by manipulating the patterns of forces on the sleeves, without necessarily incorporating a mandrel. Manipulating the sleeves in this manner is called statically controlling the geometry of the sleeves. By eliminating the mandrel from the fabrication process, statically controlling geometry offers to lower the cost of manufacturing high strength composite shells and render these structures cost effective for commercial applications.

This work demonstrates the feasibility of producing composite shells by the new fabrication method. Statically controlling geometry requires a statical-kinematic model for braided sleeves. The rotationally symmetric Chebyshev net was found to be an effective model for braided sleeves based on the results of an experimental study. After determining

the model, a methodology was established to fabricate shells with the new technique. To carry out statically controlled geometry, simple equipment was constructed and shells of different shapes were fabricated from single sleeves and nested assemblies. Inflatable bladders were placed inside some assemblies to produce additional shapes. Statically controlled geometry was found a suitable method for fabricating many different shapes of composite shells.

TABLE OF CONTENTS

CHAPTER		PAGE
1.	Introduction	1
2.	Theoretical Considerations	
	2.1 Overview	8
	2.2 Mathematical Preliminaries	10
	2.3 Mechanics of Nets	31
3.	Some Rotationally Symmetric Solutions for Nets	
	3.1 Introduction	40
	3.2 Analytical Solutions for Single Sleeves under Uniform Axisymmetric Tension	41
4.	Experimental Determination of a Sleeve Model	
	4.1 Basic Considerations	60
	4.2 Procedure for Single-Sleeve Membrane Fabrication	62
	4.3 Evaluation of Membrane Geometry	65
	4.4 Results	67
5.	Feasibility of Fabricating Composite Shells by Statically Controlled Geometry	
	5.1 Basic Considerations	71
	5.2 Tensioning Device	74
	5.3 Procedure for Shell Fabrication	79
	5.4 Feasibility of Statically Controlled Geometry	83
6.	Conclusion	
	6.1 Summary and Conclusions	89
	6.2 Suggestions for Future Work	91
REFERENCES		93
APPENDICES		96
	APPENDIX A	97
	APPENDIX B	103
VITA		118

LIST OF FIGURES

FIGURE PAGE

2.1 A space curve $C(s)$ with osculating, rectifying, and normal planes defined at a point 13

2.2 A space curve $C(s)$ shown with a position vector $\boldsymbol{R}$ to a point, and the orthonormal triad formed by the unit tangent $\boldsymbol{T}$, principal normal $\boldsymbol{N}$, and binormal $\boldsymbol{B}$ at that point 14

2.3 An arbitrary space curve $C(s)$ described by a field of position vectors $\boldsymbol{R}_n$ and, alternatively, by a field of associated tangent vectors $\boldsymbol{T}_n$ 16

2.4 Some examples of surfaces of revolution: (a) sphere, (b) paraboloid, and (c) catenoid 19

2.5 Manifestation of Gaussian curvature in surfaces of revolution for the clastic ($K>0$), developable ($K=0$), and anticlastic ($K<0$) cases 26

2.6 Elements of the arrays $\boldsymbol{u}$ and $\boldsymbol{v}$ intersecting at an angle ω on a surface at P shown with corresponding 90° offset complementary arrays 30

2.7 Geodesic and Chebyshev curvatures of lines in a plane: (a) non-zero geodesic curvature, (b) zero geodesic curvature, (c) non-zero Chebyshev curvature, and (d) zero Chebyshev curvature 32

2.8 Equilibrium of a filament in a general configuration (top) and a singular rectilinear configuration (bottom) 34

3.1 Unit vector fields $\boldsymbol{u}$ and $\boldsymbol{v}$ shown with respect to the lines of principal curvature represented by s and ϕ at a point on a surface with rotational symmetry 45

3.2 An axisymmetric net with arrays $\boldsymbol{u}$ and $\boldsymbol{v}$ shown (a) in the general case and (b) with reflection symmetry 47

3.3 Relationship of principal curvatures to coordinate variables on a surface of revolution 51

3.4 Analytical solutions for each net type: (a) one-sheet hyperboloid of revolution formed by a geodesic net, and (b) hyperbolic pseudosphere of revolution formed by a Chebyshev net 59

4.1 Unit cells for three cases: (a) actual pattern of the braided sleeves, (b) Chebyshev model of the sleeve allowing only rotation at tow intersections, and (c) geodesic model of the sleeve with no interaction between tows 61

4.2 Schematic diagram of the device used to place the braided sleeves in uniform, axisymmetric tension 63

4.3 Schematic diagram of the measuring device used to obtain the membrane geometric data 66

4.4 Experimental results and theoretical predictions for membrane with 10 inch axial length 69

4.5 Experimental results and theoretical predictions for membrane with 17 inch axial length 70

5.1 Theoretical profile predictions for Chebyshev nets with nominal diameters of 9 inches and 11 inches 72

5.2 (a) Asymptotic configurations for sleeves 1 and 2 when $d_{n1}<d_{n2}$, (b) sleeves are nested with some combination of T_1 and T_2 to form an assembly, (c) extreme cases for which the assembly approaches its asymptotic limits. (d_n-nominal diameter, T-tension) 75

5.3 Conceptual diagram for producing a clastic shell: (a) a sleeve or nested assembly under nominal tension, (b) an inflatable is inserted into the structure, (c) fluid is pumped into the inflatable to produce internal pressure, (d) a prescribed shape is obtained corresponding to a required level of pressure 76

5.4 Schematic diagram of the tensioning device 77

5.5 Photographs of the tensioning device 80

5.6 Example of a shell fabricated from a nested assembly of two sleeves 84

5.7 A clastic shell with positive Gaussian curvature produced by internal pressure 85

5.8 Example of a clastic shell fabricated with internal pressure and external loads (indicated by white bands around the shell) 86

5.9 Shell without rotational symmetry fabricated with elliptical end disks 87

5.10 Two identical rotationally symmetric membranes with 10 inch end diameters and 17 inch axial length 88

CHAPTER 1

Introduction

Composite materials are used extensively in high-performance, high-cost applications like aerospace and defense. However, to be of wider application composites must integrate into the mainstream of structural component manufacturing. This integration entails a shift in demand from higher cost to lower cost materials. In order to compete with traditional "lower cost" materials such as metals, efficient manufacturing techniques for composite structures must be found. An important class of such structures is shells. In this thesis the feasibility of fabricating composite shells by a new method with many potential advantages over current techniques is studied.

Composites are materials made up of different components with distinct interfaces. The simplest composites consist of two materials: a basic phase called a matrix and a reinforcing component such as fibers. Matrices may be metals, ceramics, or polymers. The most common composites are polymer matrix composites (PMC's). Polymer matrix composites are divided into two broad classes: thermosets, where the polymer chains are chemically cross linked, and thermoplastics, where the long polymeric chain molecules interact through entanglements. Epoxy, which is a thermoset, was used for the work herein because it can be cured at room temperature.

In general, a matrix may be reinforced by particulates or fibers. The most common reinforcement consists of continuous fibers, resulting in high strength composites. Fibers may also be chopped, in which case they act primarily as crack inhibitors and to a lesser extent as load carrying objects. Continuous fibers are

advantageous because of their high modulus and high strength to weight ratio, called specific strength. In structural applications, fibers are typically made of glass, graphite, boron, Kevlar or silicon carbide. Continuous fibers may be bundled into strings called tows, which are available in various sizes.

The fibers and matrix are combined to form a composite material system. The mechanical properties of the material depend on the orientation of the fibers relative to some datum. For instance, a composite's strength and modulus in the direction parallel to the reinforcing fibers are much greater than in the directions orthogonal to it, due to the high specific strength and high specific modulus of the fibers. This characteristic generally leads to highly anisotropic material properties with high strength to weight ratios in preferred orientations. A glass-epoxy material system is used to demonstrate the new fabrication technique, but the method is not limited to this case.

The manufacturing of any structure from polymer matrix composites involves three major steps. First, the component materials must be combined. Second, the composite material must be shaped into a prescribed geometry with a material configuration that maximizes the advantages of anisotropicity in the structure. Third, the matrix must be processed so that it sustains loads and binds the reinforcements together. This processing is called curing, which usually involves placing the part in an autoclave or oven and heating it according to an appropriate temperature profile. Unfortunately, the same qualities that give composites such versatility, namely the custom design and construction of the material to suit a given application, cause manufacturing costs to be large.

In practice, many engineering applications involve parts that may be modeled as shells. Shells are ubiquitous structural elements that may be found in a variety of

applications such as pressure vessels, nozzles and rocket motor cases. The most common shell structures are rotationally symmetric, or axisymmetric, and therefore this case will be brought into focus. This work deals with the fabrication of shells from composite materials. With current manufacturing technology, fabrication of composite shells is a slow process. Consequently, composite shells are very expensive. The cost of producing a shell from a composite material may inhibit implementation of an advanced material despite the variety of advantages over other materials.

There are three primary techniques for fabricating composite shells: filament winding, lamination and braiding. In filament winding, continuous tows are impregnated with resin and wound around a mandrel. Filament winding is used mostly for structures with large curvatures, such as spherical and cylindrical pressure vessels [1]. The second method is layup with unidirectional tape prepreg. The principle behind this approach is that if the curvature of the surface being produced is sufficiently small, then the minimal skewness of the fibers that result from dressing the tape to the surface will be negligible. This technique is frequently used to manufacture aircraft control surfaces. The third procedure involves braiding tows onto a mandrel. Tows are interlaced at various angles so that they completely cover the mandrel. Resin is then applied to the braid while it is on the mandrel. Alternatively, a braid may be produced without a mandrel, forming a sleeve. The sleeve may then be dressed to a mandrel. This alternative uncouples the braiding process from the layup process. One advantage of braided sleeves is that they may be pre-impregnated with resin before they are dressed to the mandrel. The most common use for braided sleeves is to produce cylindrical composite shells.

An expense that is common to all the foregoing techniques is that a mandrel must be manufactured specifically for the geometry of the part being produced. Another key issue involved in all three methods discussed above is that the mandrel must be removed

after the composite shell is processed. In the case of anticlastic and developable shells, mandrel removal can be difficult for practical reasons. If the shell is clastic, then removing the mandrel intact is topologically impossible. For this reason, mandrels are often made of a water-soluble material so that they may be dissolved after the part is processed [2]. Since such a mandrel may be used only once, the cost of producing the composite part increases from the additional burden of constructing a new mandrel for each unit.

As discussed above, braided sleeves are manufactured and dressed to a mandrel of the desired shape to produce a composite shell. However, this method is a special case of a more general potential usage of the braided sleeve in shell production. When the sleeve is dressed on a mandrel, a displacement condition is placed on the sleeve; it is fixed to the surface of the mandrel. The sleeve varies its shape to fit the surface by changes in the angle between the constituent tow arrays and by movement of the tows relative to one another. The question arises: can the sleeve be shaped by other combinations of load and displacement conditions? By following this idea, it is sought to eliminate the mandrel from the fabrication process altogether and thereby reduce manufacturing costs. A patent based upon this concept was recently issued by the United States Patent and Trademark Office [3].

A braided sleeve is a type of net, made up of interlaced tows. Nets have a characteristic uncommon in structural systems; their geometry is related to the magnitude and direction of static loads applied to the system. A change in the loading conditions of a sleeve may thus change the configuration of the sleeve without strain. This phenomenon is called statically induced geometry. The elements that describe the relationship between the load patterns and the geometric configurations of the system are called the statical-geometric properties of the sleeve. These statical-geometric properties may be utilized to

generate a shape without a mandrel.

Kuznetsov and Weitsman [4] suggest that laminated composite shells may be fabricated by nesting braided sleeves. They also offer a generic predictive solution for the shapes of rotationally symmetric nested assemblies. However, to utilize this solution a model for the braided sleeve must be selected. In [4], two analytical net models are suggested as candidates to represent the behavior of a braided sleeve, but no specific decision is made regarding the appropriate choice. The determination of a realistic model can be made by applying a simple load configuration, such as uniform axisymmetric tension, on a single sleeve and observing its shape. Upon comparing predictive solutions derived from each candidate model with experimental results, the best model can be chosen.

Chapter 2 lays the theoretical groundwork necessary for understanding the behavior of nets. Differential geometry is an indispensable tool for the description of nets, therefore basic differential geometry relevant to the discussion of nets and braided sleeves is reviewed. Braided sleeves have the capability for statically induced geometry because they are underconstrained systems. These little known systems are discussed briefly. The principles of statics are then combined with the differential geometry of nets to yield a mathematical model that predicts the shape of a type of net under a given load. Solutions of the modeling equations may then be utilized for design purposes.

Chapter 3 presents an implementation of the fundamental concepts discussed in Chapter 2 so that explicit solutions may be generated for specific cases. Two cases are developed as candidates for modeling a sleeve: the geodesic net and the Chebyshev net. Different characteristics of sleeves are present in each model. The key issue for predicting the kinematic behavior of the sleeve is to find the type of net that models the sleeve most

realistically. Once the appropriate net type is established, the potential for applying the predictive analysis more complicated systems such as nested sleeves exists.

Chapter 4 describes the process of selecting a model for braided sleeves. An experimental study was performed to determine the most appropriate model of a single sleeve. The practical aspects of braided sleeves are discussed and the procedure for fabricating axisymmetric membranes from single sleeves is delineated. In addition, equipment and procedures are developed to evaluate the geometry of the membranes produced in the study. The theoretical results derived in Chapter 3 and the experimental data obtained in the study are compared, and a model for braided sleeves is selected.

The feasibility of producing structures beyond single sleeve axisymmetric geometries is addressed in Chapter 5. Specifically, producing shells from nested assemblies is considered. A device that was constructed to apply unusual patterns of tension to a nested assembly is discussed. Utilizing this tensioning device, the fabrication of nested assemblies and non-axisymmetric geometries is demonstrated. In addition to tension applied to the end of the sleeve, the sleeve may be subjected to internal pressure by an inflatable bladder. External loads may also be applied to the outer surface of the sleeve assembly. Shapes are produced involving combinations of these mechanisms.

Chapter 6 concludes this investigation of a new fabrication method for composite shells. Conclusions drawn from the study are rendered and the potential advantages of the new technique are elucidated. Finally, suggestions for future research to develop the method beyond the experimental stage are presented.

This study is the first step toward developing the technology of statically controlled geometry for the manufacture of composite shells. Manufacture of composite shells by manipulation of the statics of braided sleeves has the potential to reduce the cost

of producing some types of shells from composite materials. There are also many possibilities to reduce costs involving the integration of statically controlled geometry with current composite shell fabrication technology. Additionally, this technique may be useful when other shell production methods cannot be applied, such as in the production of ceramic matrix composites.

With the advantages discussed previously, statically controlled geometry of braided sleeves may offer an alternative other composite shell production techniques, or be used in conjunction with them, to reduce manufacturing costs of some composite shells. By lowering production costs the technique has the potential to be an economically viable alternative to the manufacture of structural components from such traditional materials as metals and monolithic ceramics. With competitive manufacturing costs, implementing statically controlled geometry would advance the state of the art of manufacturing structures from composite materials.

CHAPTER 2

Theoretical Considerations

2.1 Overview

The transformation from a pliable braided sleeve to a rigid shell is accomplished by subjecting the sleeve to a tensile force field. By specifying the characteristics of the sleeves and the pattern of loading, the shape of the resulting structure may be predicted. The principle of static equilibrium is used to obtain the shape of a sleeve under a specified load. The braided sleeves used in this study are modeled as rotationally symmetric nets, but the concept of shell fabrication by statically controlled geometry may be carried beyond the simple case of a single braided sleeve under tension to nested assemblies of sleeves with and without rotational symmetry and external loading.

Some terminology is useful in order to focus the present ideas. A filament is the basic constituent of a net. A filament may be a cable, wire, string, thread, or some material fiber. This fundamental component is intentionally ambiguous so that the definition of the net does not preclude any detailed internal filament structure. For example, a fishing net is made up of intersecting cords that are filaments of the net. These cords have their own structure, but this structure is of little relevance to the overall shape of the fishing net. The geometric representation of a filament is a curve. A group of filaments that are distinct in space and do not intersect is called an array of filaments, or simply an array. The mathematical model of an array is a set of non-intersecting curves.

A net is an object composed of two or more distinct, intersecting arrays of

filaments. Furthermore, under any deformation, the foregoing arrays of filaments are assumed to remain intersecting. Since most braids and weaves are made up of two arrays, the current discussion will be limited to that case. In most nets filaments have low bending stiffness, which gives the net large variability of configuration; a shrimping net will catch five shrimp or five thousand, adapting to each situation. The low bending stiffness of the filament coupled with its geometry cause the filament to buckle under very small compressive loads. Therefore, it is assumed that filaments cannot sustain compressive loads. Consequently, a net consisting of such structures will not be able to support compressive loads.

An analytical description of braids and membranes is accomplished through geometry. For statical-geometric fabrication of composite parts, we are interested in the mathematical description of braids and membranes. The mathematical analogies of braids and membranes are nets and surfaces and the principal tool for describing these objects is differential geometry. A brief review of the relevant concepts of differential geometry useful for describing nets is given in Section 2.2. In Section 2.3, nets are discussed terms of statics, allowing expressions that predict the geometries of sleeves to be presented in Chapter 3.

For a comprehensive introduction to classical differential geometry see Struik [5]. In addition, McConnell [6] is a useful reference for tensorial differential geometry and its application to traditional problems in physics, while Nakahara [7] contains a modern discussion of the subject based on topology. Shulikovsky [8] is an authoritative reference for the differential geometry of nets. The mechanical behavior of nets has been explored by Kuznetsov [9] [10] [11], Pipkin [12], Pipkin and Rivlin [13], and Rivlin [14]. By describing the geometry and mechanics of nets, the model of the fabrication process has been formulated in [4]. However, the type of net that best models a braided sleeve was

not specified conclusively in that work. This issue will be addressed in detail in Chapters 3 and 4.

2.2 Mathematical Preliminaries

In the material that follows, the components of vectors and tensors will often be written in indicial notation, utilizing the Einstein summation convention. Therefore, a repeated lowercase index indicates summation. A superscript index indicates the contravariant components of the object, while a subscript denotes the covariant components. To distinguish surface tensors from space tensors, we employ Greek indices to indicate summation from one to three, while Roman indices should be summed from one to two. Further, if a subscript or superscript is denoted by a capital letter, then that letter is merely an instrument of identification and should not be summed. Occasionally, some lower case subscripts are used also for identification purposes and for adherence to common notation. It is clear from context that these subscripts do not indicate summation.

Consider a three dimensional Euclidean space, E^3, defined by

$$E^3 = \{(x,y,z) \mid x,y,z \in \mathbb{R}\}, \tag{1}$$

where $\mathbb{R}$ is the set of real numbers and (x,y,z) defines a vector. Define vector addition by

$$(a_1,a_2,a_3)+(b_1,b_2,b_3)=(a_1+b_1,a_2+b_2,a_3+b_3) \tag{2}$$

and scalar multiplication by:

$$\alpha(a_1,a_2,a_3)=(\alpha a_1,\alpha a_2,\alpha a_3), \tag{3}$$

where α is a constant. Then E^3 is called a linear vector space.

If we define a set of linearly independent vectors $\boldsymbol{e}_1, \boldsymbol{e}_2, \boldsymbol{e}_3 \in E^3$ then any vector $\boldsymbol{R} = (r_1, r_2, r_3)$ in E^3 can be represented by

$$\boldsymbol{R} = \alpha \boldsymbol{e}_1 + \beta \boldsymbol{e}_2 + \gamma \boldsymbol{e}_3, \tag{4}$$

where $\boldsymbol{e}_1, \boldsymbol{e}_2$ and $\boldsymbol{e}_3$ are called basis vectors and α, β and γ are called components of $\boldsymbol{R}$. This set is designated as a basis of the Euclidean space. The familiar Cartesian basis is defined by the basis vectors:

$$\begin{aligned} \boldsymbol{e}_1 &= (1,0,0) \equiv \boldsymbol{i} \\ \boldsymbol{e}_2 &= (0,1,0) \equiv \boldsymbol{j} \\ \boldsymbol{e}_3 &= (0,0,1) \equiv \boldsymbol{k} \end{aligned} . \tag{5}$$

Assume that physical space is completely described by E^3. Then a point P in physical space is located with Cartesian coordinates by a position vector

$$\boldsymbol{R} = x\boldsymbol{i} + y\boldsymbol{j} + z\boldsymbol{k} . \tag{6}$$

A curve is a one dimensional manifold, which means that open intervals on $\mathbb{R}$ may be mapped onto E^3 by a curve function. Curve functions considered in this thesis are assumed to be differentiable to any order. The map $C: (u_0, u_1) \to E^3$, where (u_0, u_1) is an open interval in $\mathbb{R}$, defines a curve function which traces a curve in three dimensional Euclidean space. With the aid of a parameter t and (6), this curve may be represented in Cartesian coordinates as

$$\boldsymbol{R}(t) = R^{\alpha}(t)\boldsymbol{e}_{\alpha}, \tag{7}$$

where t is on some interval in $\mathbb{R}$, $\boldsymbol{e}_{\alpha}$ are Cartesian basis vectors, and

$$R^{\alpha}(t)=\begin{bmatrix} x(t) \\ y(t) \\ z(t) \end{bmatrix}.$$

To facilitate discussion of the geometry of curves, it is useful to introduce three orthogonal planes. Consider two points on a curve, P and Q. Connect these points by a secant line. In the limit as $P \to Q$, the secant line becomes a tangent line at the point Q and the plane which contains that line as well as the point P is called the osculating plane. At Q, a line orthogonal to the tangent line is a normal to the curve, and the set of all normal lines makes up the normal plane. The third plane is called the rectifying plane and is orthogonal to the first two planes. These three planes are shown in Figure 2.1.

It is now possible to define a set of orthogonal coordinate axes that move along the curve. The intersection of the normal plane and the osculating plane is a line called the principal normal. The intersection of the osculating plane and the rectifying plane is the tangent line. And the line formed by the intersection of the rectifying plane with the normal plane is called the binormal. Unit vectors in the direction of the principal normal, binormal, and tangent directions are denoted, respectively, by $\mathbf{N}$, $\mathbf{B}$, and $\mathbf{T}$. This orthonormal triad is depicted at a point on a space curve in Figure 2.2.

The arc length of a curve, C, in E^3 is found with the aid of a parameter $t \in (u_0, u_1)$, where (u_0, u_1) is an open interval on $\mathbb{R}$:

$$s = \int_{u_0}^{u_1} \| \boldsymbol{R}'(t) \| \, dt. \tag{8}$$

where $\boldsymbol{R}(t) = x(t)\boldsymbol{i} + y(t)\boldsymbol{j} + z(t)\boldsymbol{k}$. Equation (8) may be cast in differential form

$$ds^2 = dx^{\alpha} dx_{\alpha} \tag{9}$$

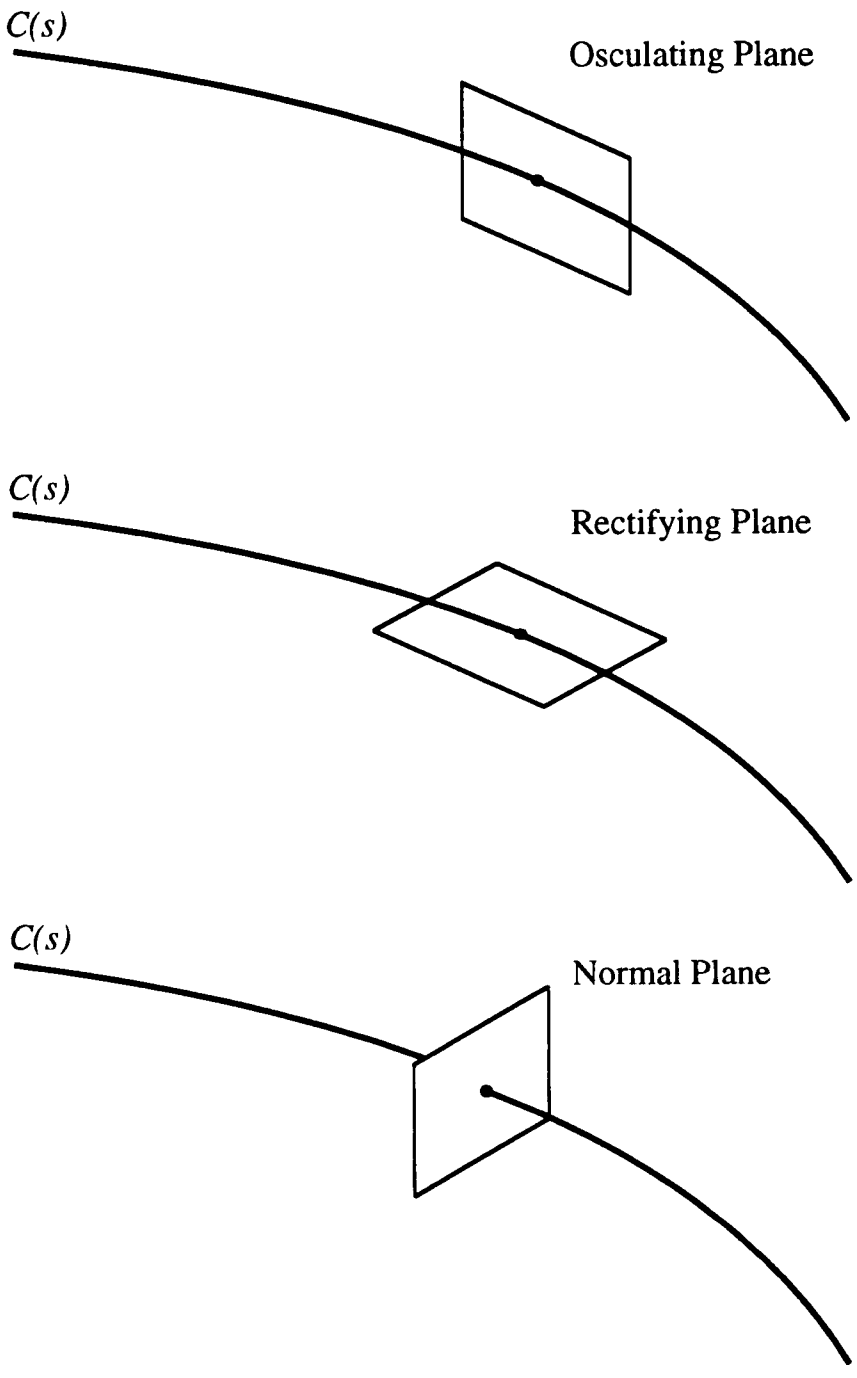

Figure 2.1: A space curve *C(s)* with osculating, rectifying, and normal planes defined at a point.

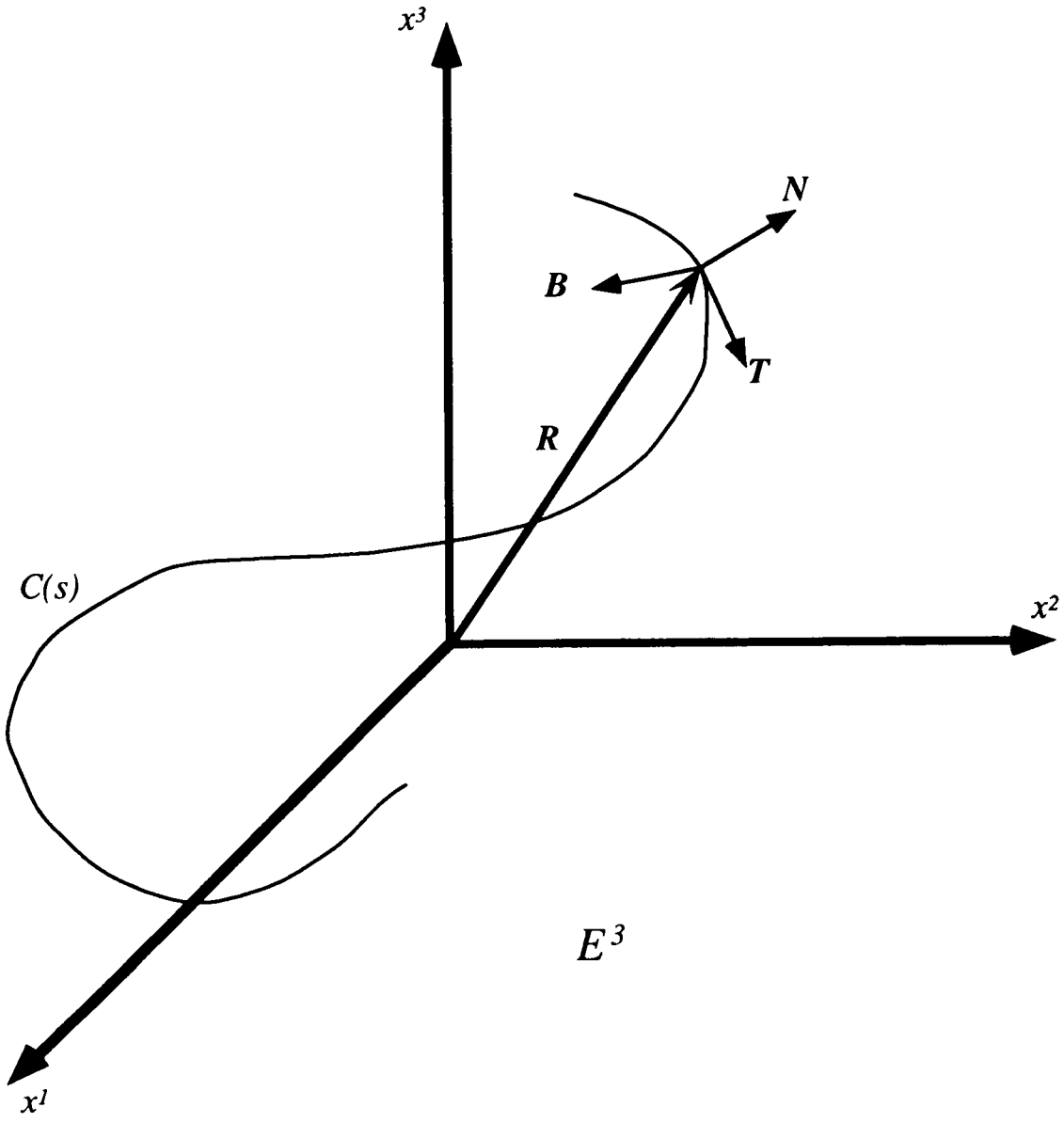

Figure 2.2: A space curve *C(s)* shown with a position vector ***R*** to a point, and the orthornormal triad formed by the unit tangent ***T***, principal normal ***N***, and binormal ***B*** at that point.

It is useful to give $\boldsymbol{R}$ a unit speed parameterization. This re-parameterization is formally accomplished by noting the relationship between s and t in (8) and rewriting (9) as

$$\frac{dx^{\alpha}}{ds}\frac{dx_{\alpha}}{ds}=1. \tag{10}$$

It is now possible to give formal definitions to the unit vectors **N**, **B**, and **T**. From elementary calculus, the unit tangent vector is

$$\boldsymbol{T}=\frac{d\boldsymbol{R}}{ds}. \tag{11}$$

The other definitions along with some auxiliary relationships are contained in the well known Frenet equations:

$$\frac{d}{ds}\begin{bmatrix}\boldsymbol{T}\\ \boldsymbol{N}\\ \boldsymbol{B}\end{bmatrix}=\begin{bmatrix}0 & \kappa & 0\\ -\kappa & 0 & \tau\\ 0 & -\tau & 0\end{bmatrix}\begin{bmatrix}\boldsymbol{T}\\ \boldsymbol{N}\\ \boldsymbol{B}\end{bmatrix}, \tag{12}$$

where $\kappa(s)$ is the curvature of curve C at s and $\tau(s)$ is called the torsion of C. Equations (11) and (12) describe the spatial variation of the orthogonal triad formed by the three unit vectors with the parameter s. For a formal derivation of the Frenet equations (12), see [5], p. 10-20.

An expression for a curve was defined in (7) as a set of position vectors that continuously and smoothly traces a path. Alternatively, a curve may be represented by a one dimensional field of tangent vectors, defined in (11), associated with each position vector (Figure 2.3). Generally, a one dimensional tensor field is a set of tensors that may be mapped bijectively and smoothly to a curve. The field may be expressed as a function that maps a tensor $\boldsymbol{V(t)}$ to every point $\boldsymbol{R(t)}$ on a curve. The concept of a tangent vector field is especially useful in describing the arrays of a net.

The next geometric object associated with nets is the surface. The Cartesian

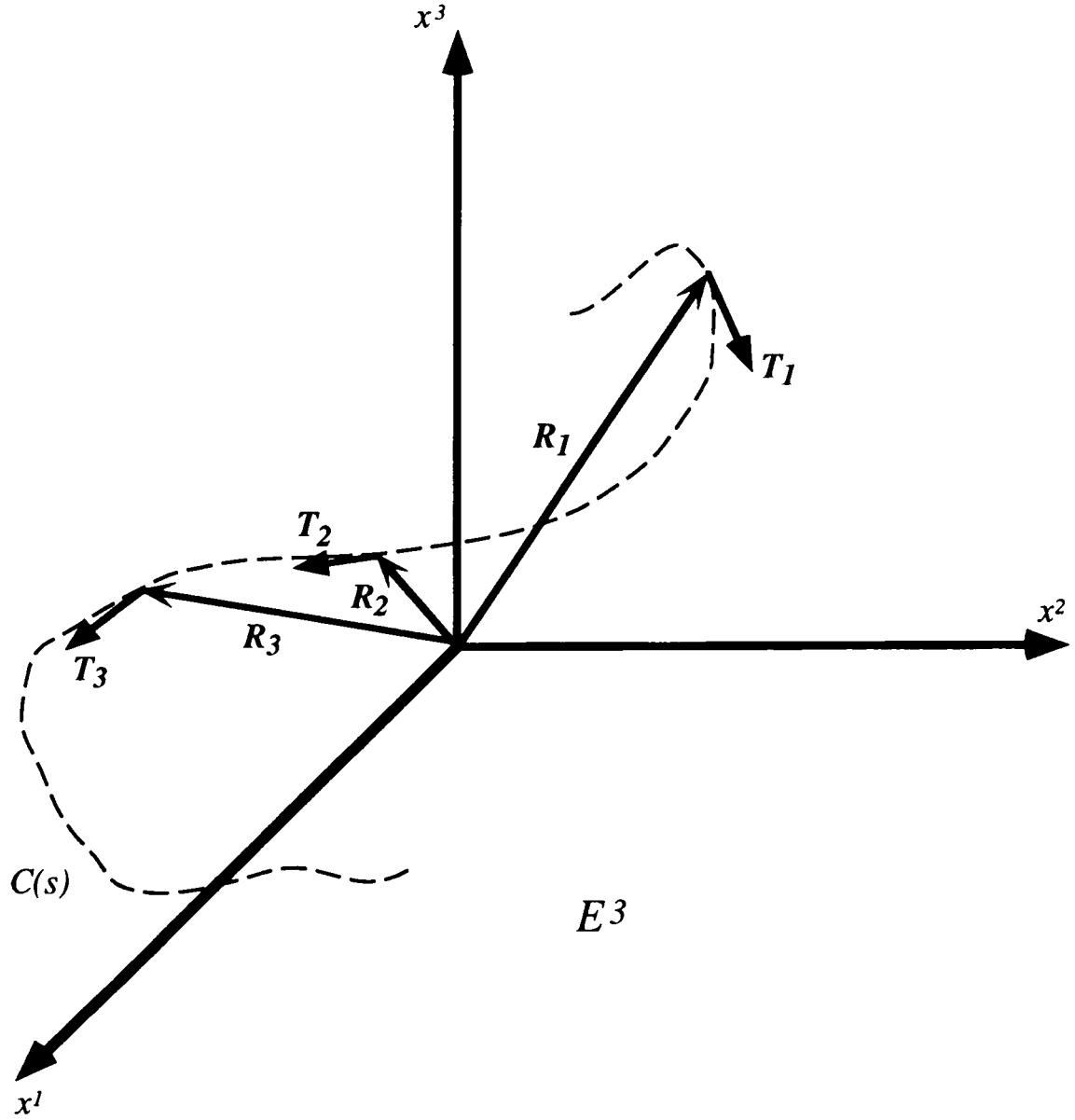

Figure 2.3: An arbitrary space curve $C(s)$ described by a field of position vectors $\boldsymbol{R}_n$ and, alternatively, by a field of associated tangent vectors $\boldsymbol{T}_n$.

product is utilized to define $\mathbb{R}^2$ as

$$\mathbb{R}^2 \equiv \mathbb{R} \times \mathbb{R} = \{(u,v) \mid u \in \mathbb{R} \ \textit{and} \ v \in \mathbb{R}\} \tag{13}$$

A surface is generated in E^3 by a surface function defined with the aid of (13) by $\Sigma: \mathbb{R}^2 \to E^3$ where $u \in (u_0, u_1)$ and $v \in (v_0, v_1)$. An arbitrary surface is denoted by Σ and may be represented in Cartesian coordinates by using (5) and (6):

$$\boldsymbol{R}(u,v) = R^{\alpha}(u,v)\,\boldsymbol{e}_{\alpha}, \tag{14}$$

where

$$R^{\alpha}(u,v) = \begin{bmatrix} x(u,v) \\ y(u,v) \\ z(u,v) \end{bmatrix}.$$

The partial derivatives $\boldsymbol{R}$ are expressed by the notation:

$$\boldsymbol{R}_{,u} = \frac{\partial \boldsymbol{R}}{\partial u} \ \text{and} \ \boldsymbol{R}_{,v} = \frac{\partial \boldsymbol{R}}{\partial v}. \tag{15}$$

A surface is a two dimensional manifold that is locally homeomorphic to $\mathbb{R}^2$, which implies that $\boldsymbol{R}_{,u}$ and $\boldsymbol{R}_{,v}$ are linearly independent and the surface function is invertible. The parametric lines on a surface for a given surface function define a net. A point on the surface Σ can be expressed two ways. A point P on Σ is still a point in E^3, therefore P can be expressed in terms of coordinates $\{x,y,z\}$. Alternatively P can be expressed as a surface vector with the coordinates $\{u,v\}$ defined by

$$\boldsymbol{x} = x^i (\boldsymbol{e}_P)_i \tag{16}$$

where $(\boldsymbol{e}_P)_i$ is a basis at P and $x^1 = u$ and $x^2 = v$. The basis is found from the expression

$$(\boldsymbol{e}_P)_i = \frac{\partial \boldsymbol{R}_P}{\partial x^i} \equiv \boldsymbol{R}_{,i}, \tag{17}$$

where $\boldsymbol{R}_P$ is the position vector for P. This basis may be used to express any vector in the tangent plane to a surface at a point. Note that the base vectors in (17) are local to a point in the manifold defined in (14), in contrast to the global Cartesian basis (5). Differentials in the three dimensional space system and the two dimensional surface system are then related by

$$dR^{\alpha} = \frac{\partial R^{\alpha}}{\partial x^i} dx^i \tag{18}$$

Surfaces of revolution are of primary interest in this study. A surface of revolution may be produced by a generator curve rotated about a line called an axis of rotational symmetry. For simplicity, denote the axis of symmetry by the z axis. When the generator is coplanar with the axis of rotational symmetry, then it is called a profile curve. A profile curve is also called a meridian of the surface. If the meridional curve is defined by $z=f(r)$, then the surface of revolution can be represented by

$$\begin{aligned} x &= r\cos\phi \\ y &= r\sin\phi \\ z &= f(r) \end{aligned} \tag{19}$$

Equations (19) represent one of the parameterizations of a surface of revolution. An arbitrary surface of revolution with the coordinate isomorphism (19) is denoted $\Sigma(r,\phi)$. Several such surfaces are shown in Figure 2.4. The surface is covered by the intersections of parallel circles that are perpendicular to the axis of symmetry and meridians that are traced by the function $z=f(r)$. Since the surface is embedded in E^3, every point on the surface is also a point in the space. Note that a point on the surface may be specified by the space coordinates $\{x,y,z\}$ or a set of surface coordinates $\{r,\phi\}$. If

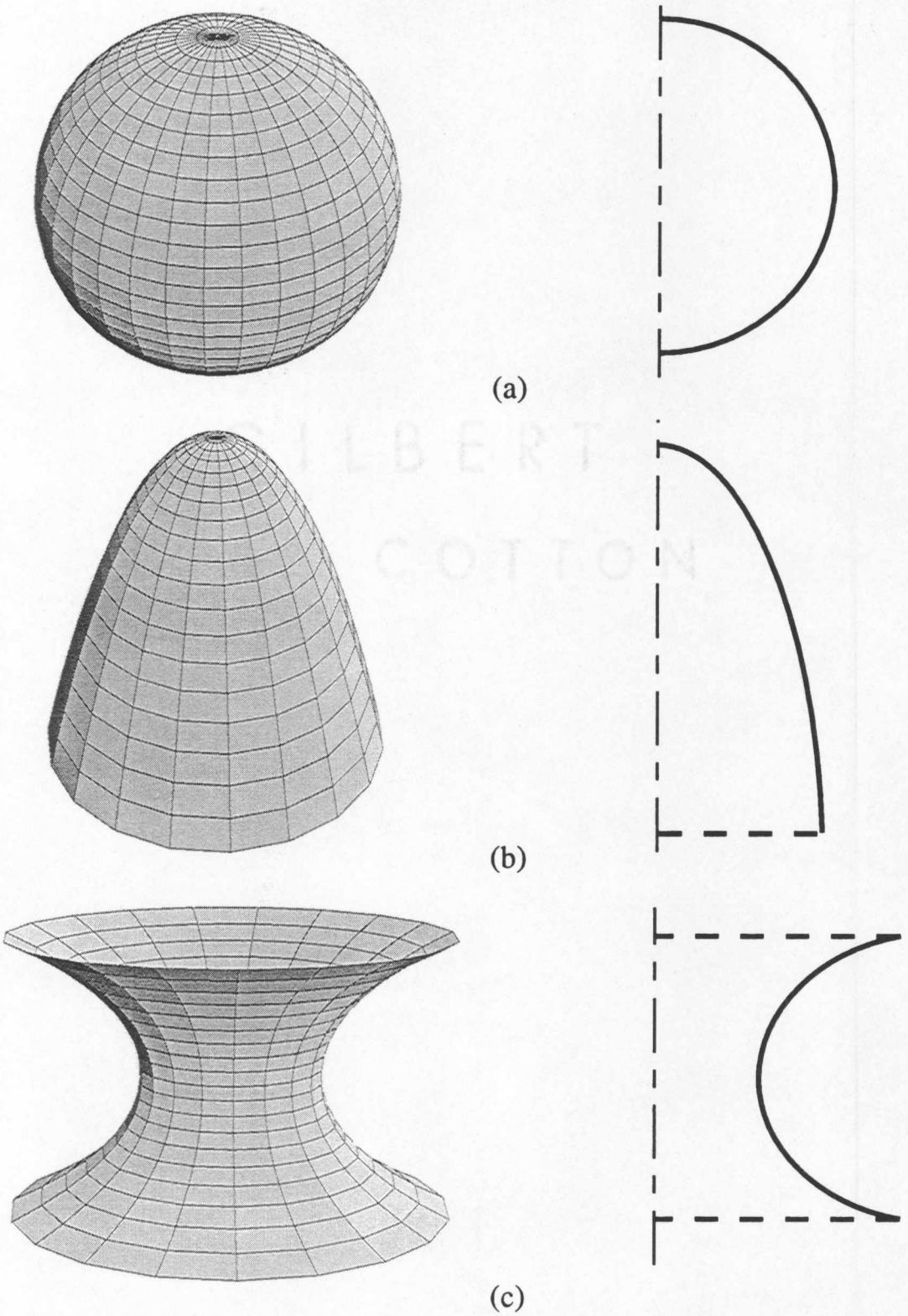

Figure 2.4: Some examples of surfaces of revolution: (a) sphere, (b) paraboloid, and (c) catenoid.

a space curve, $C(t)$, is constrained to lie on $\Sigma(r,\phi)$, then by (19)

$$\begin{aligned} x(t) &= r(t)\ cos\ \phi(t) \\ y(t) &= r(t)\ sin\ \phi(t)\ . \\ z(t) &= f[r(t)] \end{aligned} \tag{20}$$

In view of (20), the arc length defined by (8) may be written

$$s = \int_{u_0}^{u_1} \sqrt{\left(1+f'(r)^2\right)\left(\frac{dr}{dt}\right)^2 + r^2\left(\frac{d\phi}{dt}\right)^2}\ dt. \tag{21}$$

The integrand in (21) contains a symmetric quadratic form that may be written succinctly as

$$\frac{ds}{dt} = \sqrt{g_{ij}\frac{dx^i}{dt}\frac{dx^j}{dt}} \tag{22}$$

where $x^1 = u$ and $x^2 = v$ for a general parametrization and $x^1 = r$, $x^2 = \phi$ for $\Sigma(r,\phi)$. The expression g_{ij} is a second order tensor called the metric tensor of the surface. In general, components of the surface metric may be calculated by

$$g_{ij} = \frac{\partial R^\alpha}{\partial x^i}\frac{\partial R^\alpha}{\partial x^j}\ . \tag{23}$$

Equation (22) is often written

$$ds^2 = g_{ij}dx^i dx^j\ . \tag{24}$$

This expression is a generalization of the Pythagorean theorem. The right hand side (RHS) of (24) is called the first fundamental (quadratic) form of the surface. Further, if $\boldsymbol{u}$ and $\boldsymbol{v}$ are surface unit vector fields defined by

$$u^i(s) = \frac{dx^i}{ds}\ ,\ v^i(s) = \frac{dy^i}{ds}\ , \tag{25}$$

then the curves are said to have a unit speed parameterization. When $\boldsymbol{u}$ and $\boldsymbol{v}$ intersect, i.

e. $x^i = y^i$ at P, then the angle θ between them at P is given by the inner product

$$\cos\theta = g_{ij}u^i v^j. \tag{26}$$

The metric of a surface defines distance and angle on that surface. It is notable that the metric tensor is independent of the surrounding space. Returning to the surface of revolution, $\Sigma(r,\phi)$, the metric is

$$g_{ij} = \begin{bmatrix} 1+f'(r)^2 & 0 \\ 0 & r^2 \end{bmatrix}. \tag{27}$$

The contravariant metric tensor is defined by

$$g_{ij}g^{jk} = \delta_i^k, \tag{28}$$

where δ_i^k is the Kronecker delta. Therefore the associated contravariant metric tensor for $\Sigma(r,\phi)$ is

$$g^{ij} = \begin{bmatrix} \frac{1}{1+f'(r)^2} & 0 \\ 0 & \frac{1}{r^2} \end{bmatrix}. \tag{29}$$

The first fundamental form contains information intrinsic to the surface. However, to completely describe the surface, the orientation of each point on the surface with respect to the surrounding space must be established[1]. The change in orientation of points on a surface relates the local bending of that surface. This feature resembles elementary considerations of classical beam theory, in which bending can be quantified by the orientation of normal vectors to the beam's axis.

The unit normal vector is defined at a point P on a surface by the cross product of two independent tangent vectors at P normalized to unity:

---

[1]All surfaces considered in this thesis are orientable, thus the issue of orientability will not be addressed.

$$\boldsymbol{n} = \frac{\boldsymbol{R}_{,u} \times \boldsymbol{R}_{,v}}{\left\| \boldsymbol{R}_{,u} \times \boldsymbol{R}_{,v} \right\|}. \tag{30}$$

For $\Sigma(r,\phi)$, considering (7) and (20),

$$\begin{aligned} \boldsymbol{R}_{,r} &= \cos\phi\, \boldsymbol{i} + \sin\phi\, \boldsymbol{j} + f'(r)\boldsymbol{k} \\ \boldsymbol{R}_{,\phi} &= -r\sin\phi\, \boldsymbol{i} + r\cos\phi\, \boldsymbol{j} \end{aligned} \tag{31}$$

hence (30) takes the form

$$\boldsymbol{n} = -\frac{1}{\sqrt{1+f'(r)^2}} \left[f'(r)\cos\phi\, \boldsymbol{i} + f'(r)\sin\phi\, \boldsymbol{j} - \boldsymbol{k} \right]. \tag{32}$$

Recall that from the Frenet equations (12) the curvature vector of a space curve, C, is

$$\boldsymbol{\kappa} \equiv \frac{d\boldsymbol{T}}{ds} = \kappa \boldsymbol{N}, \tag{33}$$

where $\boldsymbol{T}$ is the unit tangent vector of C and $\boldsymbol{N}$ is the unit principal normal vector to C. If $C \subset \Sigma$, then the projection of the curvature vector along the surface normal is called the normal curvature vector of the point on the surface and is denoted

$$\boldsymbol{\kappa}_n = \kappa_n \boldsymbol{n}, \tag{34}$$

with no sum on n, where

$$\kappa_n = \boldsymbol{\kappa} \cdot \boldsymbol{n}. \tag{35}$$

The normal curvature is a measure of how the surface bends in the neighborhood of P.

Visually, the normal curvature of a surface Σ at P, defined relative to the curve C with tangent vector $\boldsymbol{T}$ embedded in Σ, is the curvature of the arc formed by the intersection of the surface with a plane containing $\boldsymbol{T}$ and the surface normal $\boldsymbol{n}$. Since $\boldsymbol{n}$ is orthogonal to $\boldsymbol{T}$,

$$\frac{d\boldsymbol{T}}{ds} \cdot \boldsymbol{n} = -\boldsymbol{T} \cdot \frac{d\boldsymbol{n}}{ds} \tag{36}$$

and (35) reads

$$\kappa_n = -\frac{d\boldsymbol{R}}{ds}\cdot\frac{d\boldsymbol{n}}{ds}. \tag{37}$$

For Σ, $\boldsymbol{R}=\boldsymbol{R}(u,v)$ and $\boldsymbol{n}=\boldsymbol{n}(u,v)$ therefore

$$\begin{aligned} d\boldsymbol{R} &= \boldsymbol{R}_{,u}du+\boldsymbol{R}_{,v}dv \\ d\boldsymbol{n} &= \boldsymbol{n}_{,u}du+\boldsymbol{n}_{,v}dv \end{aligned}. \tag{38}$$

Considering (38), the numerator for the RHS in (37) is

$$-d\boldsymbol{R}\cdot d\boldsymbol{n} = -\frac{\partial R^{\alpha}}{\partial x^{i}}\frac{\partial n^{\alpha}}{\partial x^{j}}dx^{i}dx^{j} \tag{39}$$

where $x^1 = u$ and $x^2 = v$. Equation (39) is a symmetric (since $\boldsymbol{R}_{,i}$ is orthogonal to $\boldsymbol{n}$) quadratic form, called the second fundamental form of the surface. The coefficients of (39) constitute a second fundamental tensor,

$$h_{ij} = \begin{bmatrix} (\boldsymbol{R}_{,u}\cdot\boldsymbol{n}_{,u}) & (\boldsymbol{R}_{,u}\cdot\boldsymbol{n}_{,v}) \\ (\boldsymbol{R}_{,v}\cdot\boldsymbol{n}_{,u}) & (\boldsymbol{R}_{,v}\cdot\boldsymbol{n}_{,v}) \end{bmatrix}. \tag{40}$$

By differentiating (32) with respect to r and ϕ and substituting with (31) into equation (40) with $u=r$ and $v=\phi$, the second fundamental tensor for a surface of revolution, $\Sigma(r,\phi)$, is found to be

$$h_{ij} = \frac{1}{\sqrt{1+f'(r)^2}}\begin{bmatrix} f''(r) & 0 \\ 0 & r f'(r) \end{bmatrix}. \tag{41}$$

It is possible to obtain further insight into the properties of the surface by deriving the so called shape tensor, S^i_j, from the foregoing two fundamental forms. For that purpose consider the derivatives of the unit normal vector, $\boldsymbol{n}$ with respect to the surface parameters u and v at P. These derivatives are vectors orthogonal to $\boldsymbol{n}$, and so they lie in the tangent plane to the surface at P. The tangent plane is a linear vector space defined at P by the parametric tangent vectors $\boldsymbol{u}$ and $\boldsymbol{v}$. Therefore, the vectors $\boldsymbol{n}_{,u}$ and $\boldsymbol{n}_{,v}$ may be

expressed as a linear combination of $\boldsymbol{u}$ and $\boldsymbol{v}$:

$$\begin{aligned} \boldsymbol{n}_{,u} &= S_1^1 \boldsymbol{u} + S_2^1 \boldsymbol{v} \\ \boldsymbol{n}_{,v} &= S_1^2 \boldsymbol{u} + S_2^2 \boldsymbol{v} \end{aligned} . \tag{42}$$

By taking the inner products of both of equations (42) with $\boldsymbol{u}$ and $\boldsymbol{v}$, and noting that $\boldsymbol{u} = \boldsymbol{R}_{,u}$ and $\boldsymbol{v} = \boldsymbol{R}_{,v}$ we find

$$\begin{aligned} \boldsymbol{R}_{,u} \cdot \boldsymbol{n}_{,u} &= S_1^1 g_{11} + S_2^1 g_{12} \\ \boldsymbol{R}_{,v} \cdot \boldsymbol{n}_{,u} &= S_1^1 g_{21} + S_2^1 g_{22} \\ \boldsymbol{R}_{,u} \cdot \boldsymbol{n}_{,v} &= S_1^2 g_{11} + S_2^2 g_{12} \\ \boldsymbol{R}_{,v} \cdot \boldsymbol{n}_{,v} &= S_1^2 g_{21} + S_2^2 g_{22} \end{aligned}$$

But from the definition of the second fundamental tensor in (40), it is evident that

$$h_{ij} = -S_j^k g_{ik} . \tag{43}$$

Equations (42) may now be written

$$n^{\alpha}{}_{,j} = -S_j^i R^{\alpha}{}_{,i} , \tag{44}$$

where

$$S_j^i = -g^{ik} h_{kj} . \tag{45}$$

is the shape tensor of the surface. The shape tensor is just the negative of the second fundamental tensor with mixed covariant and contravariant components. Equations (44) are known as the Weingarten equations of the surface. Using (45), with (29) and (41), the shape tensor for

$\boldsymbol{\Sigma}(r,\phi)$ is

$$S_j^i = -\frac{1}{\sqrt{1+f'(r)^2}} \begin{bmatrix} \frac{f''}{1+f'(r)^2} & 0 \\ 0 & \frac{f'}{r} \end{bmatrix} . \tag{46}$$

The determinant of the shape tensor is an invariant called the Gaussian curvature, K:

$$K = Det\left(S^i_j\right). \tag{47}$$

The sign of the Gaussian curvature (which is also called total curvature) may be used to classify three types of surfaces. The three possibilities correspond to hyperbolic, parabolic, and elliptic points on the surface when K is negative, zero, and positive, respectively. The manifestation of the Gaussian curvature of a surface is very easy to visualize; the three cases are demonstrated by surfaces of revolution in Figure 2.5. A surface with positive Gaussian curvature is called clastic, a surface with negative Gaussian curvature is anticlastic, and a surface with zero Gaussian curvature is known as developable. If $K=0$, and $\boldsymbol{S=0}$, then the surface is a plane. In this work, rotationally symmetric surfaces with negative Gaussian curvature will be of primary concern.

Substituting (44) into the normal curvature definition in equation (37) while noting (39) yields the normal curvature in terms of the shape tensor:

$$\kappa_n = g^{jk} S^i_j R^{\alpha}{}_{,i} R^{\alpha}{}_{,k}. \tag{48}$$

The extremal values of the normal curvature at P, which are the eigenvalues of the shape tensor, are called principal curvatures. The corresponding eigenvectors, with components normalized to unity, represent the unit principal vectors that are tangent to the surface. On a surface, there will be two principal curvatures, denoted by κ_1 and κ_2 in the sequel. Curves on a surface that consist of principal direction vectors are called lines of principal curvature. If the eigenvalues are not unique, then the principal curvatures are equal, and the point is called an umbilic. Umbilic points are excluded from consideration in this work. Therefore surfaces under consideration will have two lines of principal curvature, from which a principal basis may be formed in the tangent plane at P.

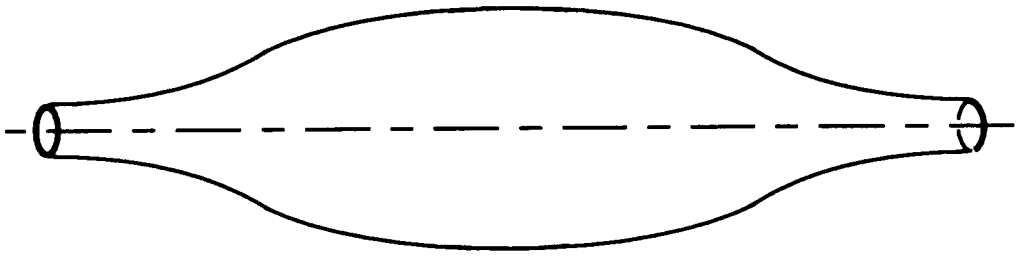

Clastic

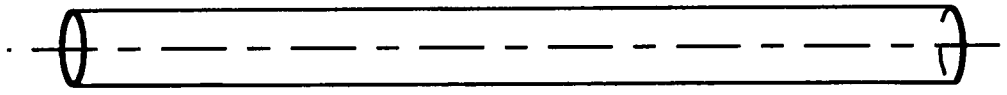

Developable

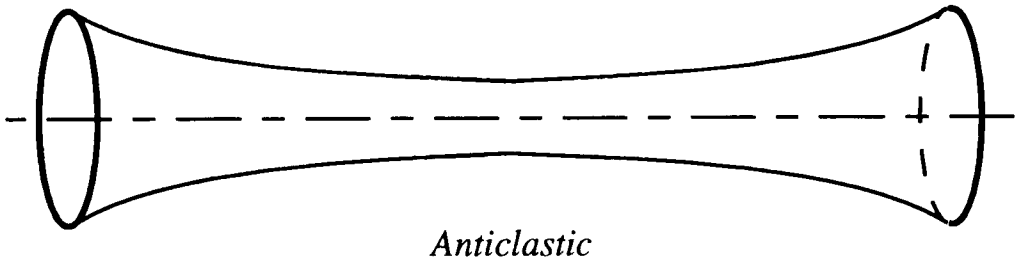

Anticlastic

Figure 2.5: Manifestation of Gaussian curvature in surfaces of revolution for the clastic ($K>0$), developable ($K=0$), and anticlastic ($K<0$) cases.

Furthermore, since the lines of principal curvature are formed from the eigenvectors of the shape operator, they are orthogonal on the surface. Finally, if the principal curvatures are of different sign at a point P, there is a tangent vector at P for which the normal curvature vanishes. That vector is termed asymptotic. A curve defined by asymptotic vectors exclusively is called an asymptotic curve. If a net consists of two families asymptotic curves, then it is an asymptotic net.

Consider an arbitrary unit vector $\boldsymbol{t}$, tangent to Σ at P, expressed in terms of the local unit orthogonal principal basis $\{\boldsymbol{e}_1, \boldsymbol{e}_2\}$ so that

$$\boldsymbol{t} = cos\ \alpha\, \boldsymbol{e}_1 + sin\ \alpha\, \boldsymbol{e}_2, \tag{49}$$

where $\boldsymbol{e}_1$ and $\boldsymbol{e}_2$ have unit magnitude. It can be shown that, when referred to the principal basis, the shape tensor reduces to

$$S^i_j = -\begin{bmatrix} \kappa_1 & 0 \\ 0 & \kappa_2 \end{bmatrix}. \tag{50}$$

where κ_1 and κ_2 are the principal curvatures. Substituting (49) and (50) into the expression for the normal curvature (48) and recalling that $\boldsymbol{t} = R^{\beta}{}_{,i}\boldsymbol{e}^{i}$, yields Euler's theorem:

$$\kappa_n = \kappa_1 \cos^2\alpha + \kappa_2 \sin^2\alpha. \tag{51}$$

As noted in (34), the normal curvature was defined as the projection of the curvature of an arc on a surface Σ at the point P in the direction of the surface normal. Consider this arc as a unit vector field on the surface

$$\boldsymbol{u} = u^i(s)\,\boldsymbol{e}_i(s). \tag{52}$$

The complementary projection of the curvature lies in the tangent plane at P and is

orthogonal to the surface normal $\boldsymbol{n}$ and the tangent vector $\boldsymbol{u}$. This component of the curvature is called the geodesic curvature, γ, of the surface. Denoting the direction of the geodesic curvature vector by the unit vector $\tilde{\boldsymbol{u}}$, the geodesic curvature can be expressed using the first Frenet equation (33) applied in the tangent plane at a point on the curve defined by the unit tangent vector field $\boldsymbol{u}$ in the surface:

$$\frac{d\boldsymbol{u}}{ds} = \gamma \tilde{\boldsymbol{u}} . \tag{53}$$

Until this time, we have only differentiated Cartesian vectors, where it sufficed to consider the derivatives of the components only, since they were referred to a constant basis. In general, this is not the case. In (52), the basis at one point on the surface is different from that at another point. The tangent planes at the two different points are two separate linear vector spaces. In order to compare the two spaces, a connection must be defined. Since the basis varies with location, employment of the product rule of differentiation in the evaluation of (53) yields,

$$\frac{d\boldsymbol{u}}{ds} = \frac{du^i}{ds}\boldsymbol{e}_i + u^i \frac{d\boldsymbol{e}_i}{ds}. \tag{54}$$

Denote

$$\frac{d\boldsymbol{e}_i}{ds} = \Gamma^j_{ik}\boldsymbol{e}_j u^k, \tag{55}$$

where

$$\Gamma^j_{ik} = \boldsymbol{e}^j \boldsymbol{e}_{i,k} \tag{56}$$

are the coefficients of the connection. A straightforward calculation yields that the non-vanishing connection coefficients for $\Sigma(r,\phi)$ are

$$\Gamma^1_{11}=\frac{f'(r)f''(r)}{1+f'(r)^2}$$
$$\Gamma^2_{12}=\Gamma^2_{21}=\frac{1}{r} \qquad (57)$$
$$\Gamma^1_{22}=-\frac{r}{1+f'(r)^2}$$

Applying the chain rule to (54) and taking into account (55), we obtain the well known expression for the covariant derivative

$$u^i{}_{,j}=\frac{\partial u^i}{\partial x^j}+\Gamma^i_{jk}u^k \qquad (58)$$

where

$$\frac{du^i}{ds}=u^i{}_{,j}u^j. \qquad (59)$$

It is useful to introduce the complementary unit vector fields (Figure 2.6)

$$\tilde{u}^i=g^{ij}\varepsilon_{jk}u^k$$
$$\tilde{u}_i=g_{ij}\varepsilon^{jk}u_k \quad , \qquad (60)$$

where ε_{ij} is the antisymmetric permutation tensor, and define the transversal vector along $\boldsymbol{u}$,

$$(t_u)_i=u^j{}_{,i}\tilde{u}_j. \qquad \text{(no sum on } u) \qquad (61)$$

The transversal vector can be expressed using (58) and (60) as

$$(t_u)_i=\varepsilon_{jk}\left(\frac{\partial u^j}{\partial x^i}u^k+\Gamma^j_{li}u^lu^k\right). \qquad (62)$$

If two curves $\boldsymbol{u}$ and $\boldsymbol{v}$ are offset by an angle ω at a point on the surface, then the infinitesimal rotation vector is defined as

$$\omega_i=\frac{d\omega}{dx^i}. \qquad (63)$$

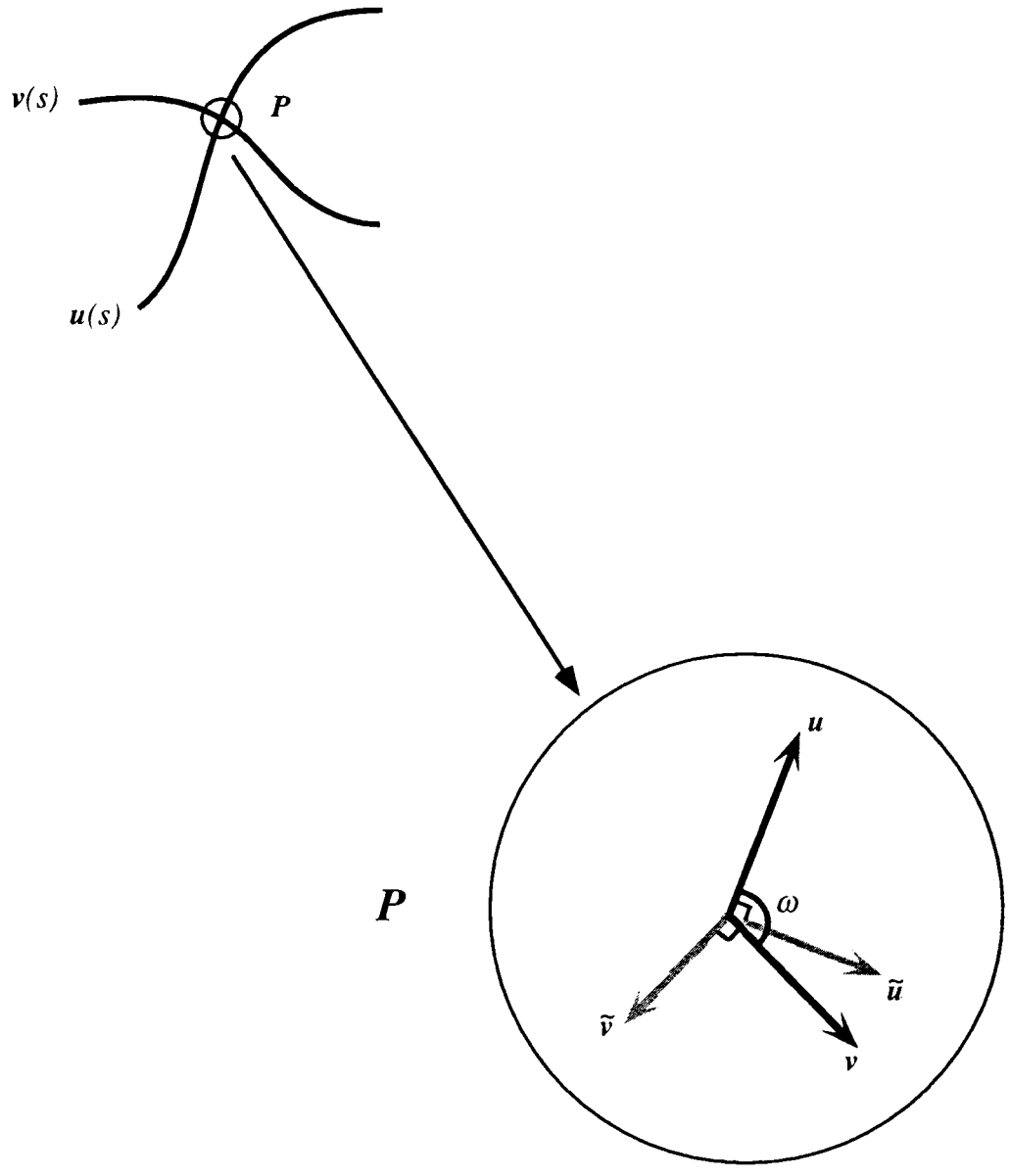

Figure 2.6: Elements of the arrays ***u*** and ***v*** intersecting at an angle ω on a surface at ***P*** shown with corresponding 90° offset complementary arrays.

The infinitesimal rotation vector can be written in terms of the transversal vectors of each curve as

$$\omega_i = (t_u)_i - (t_v)_i. \tag{64}$$

In view of (53), (58), (59) and (62), the geodesic curvature of the curve u^i can be expressed

$$\gamma_u = (t_u)_i u^i. \qquad \text{(no sum on } u\text{)} \tag{65}$$

The geodesic curvature is a measure of the rotation of successive unit tangent vectors of the field u^i along a curve defined by u^i about the surface normal. The length of a curve with zero geodesic curvature is the shortest in-surface distance between two points on the surface. Such a curve is called a geodesic line.

This idea may be generalized to an arbitrary unit vector field along a curve C through P. Consider a field of unit vectors v^i along C not tangent to the curve defined by u^i Another invariant that is formally similar to (65) is found by taking the scalar product of the transversal vector of $\boldsymbol{u}$ with the corresponding element of $\boldsymbol{v}$:

$$\lambda_v = (t_u)_i v^i. \qquad \text{(no sum on } v\text{)} \tag{66}$$

This invariant is called the Chebyshev curvature. The Chebyshev curvature measures the degree of parallelism between successive members of v^i along C. Examples of geodesic and Chebyshev curvatures of curves in a plane are given in Figure 2.7.

2.3 Mechanics of Nets

The logical starting point for developing the mechanical model for braided sleeves

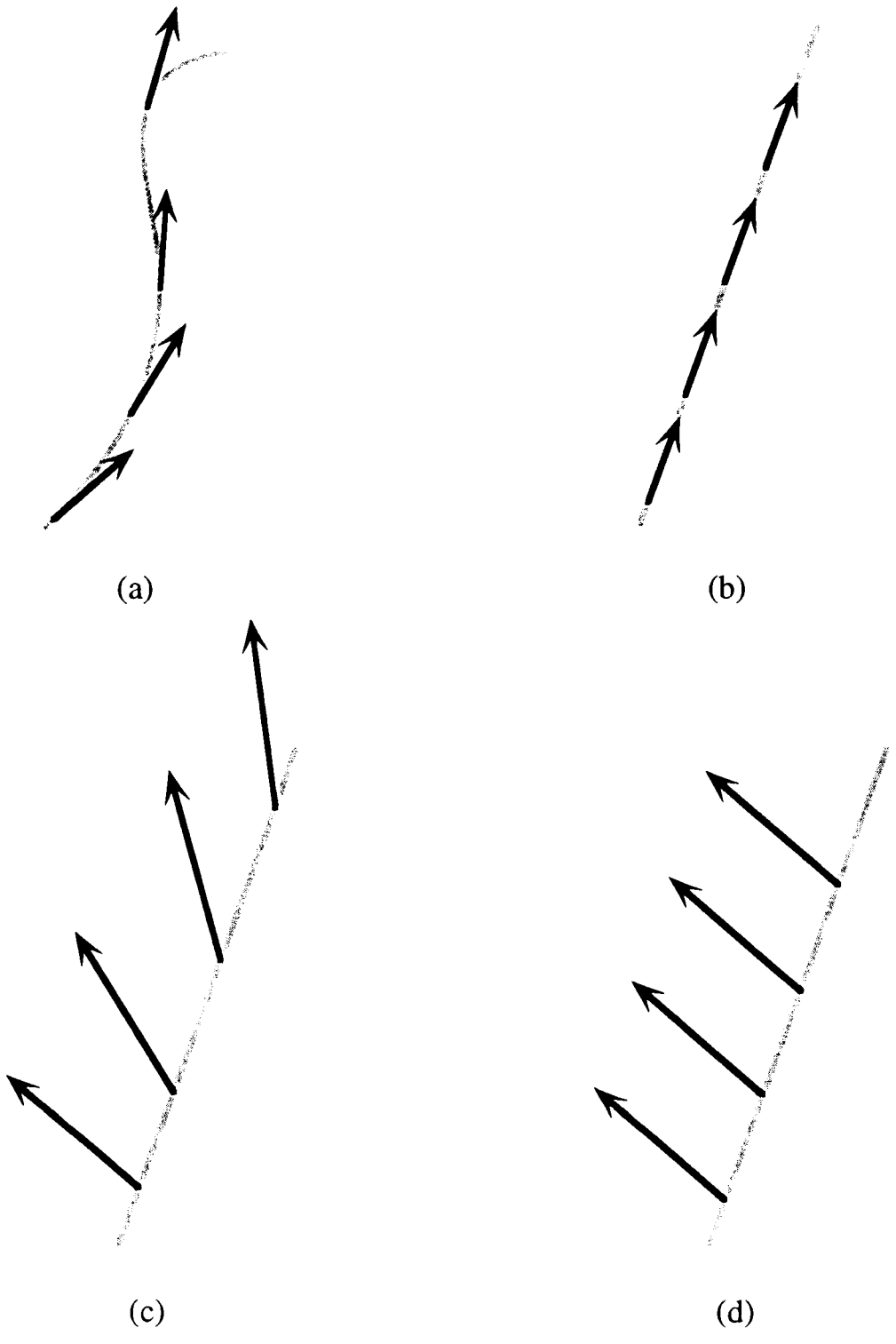

Figure 2.7: Geodesic and Chebyshev curvatures of lines in a plane: (a) non-zero geodesic curvature, (b) zero geodesic curvature, (c) non-zero Chebyshev curvature, and (d) zero Chebyshev curvature.

is to examine the mechanical behavior of an inextensible filament. As noted in Section 2.1, the filament is the fundamental constituent of a net. For a braided sleeve, the filament is a tow of material fibers. Consider the filament whose position is indicated by the curve $C(s)$. Assume that the filament is embedded in a Euclidean space and assume that one end is fixed in space. Because the filament has no bending stiffness, it cannot internally balance arbitrary applied forces. The only mechanism for balancing external forces is tension. The equilibrium equation for a filament is found from the balance of forces on a differential element shown in Figure 2.8 to be

$$\frac{d\boldsymbol{F}}{ds} = \boldsymbol{P}, \tag{67}$$

where $\boldsymbol{F}(s)$ is the tension in the filament and $\boldsymbol{P}$ represents external loads applied to the filament. Expanding the derivative in (67) and multiplying the result by the unit tangent $\boldsymbol{T}$, the principal normal $\boldsymbol{N}$, and the unit binormal $\boldsymbol{B}$ vectors gives three equilibrium equations,

$$\begin{aligned} \frac{dF}{ds} &= P_T \\ F\kappa &= P_N \\ 0 &= P_B \end{aligned} \tag{68}$$

where F is the scalar tension and κ is the curvature of the filament. From (68c), the system cannot attain static equilibrium if there is any binormal component of the external load. Eliminating F, we obtain a relationship between the loads, tangential and principal normal, and the curvature of the filament:

$$\frac{d}{ds}\left(\frac{P_N}{\kappa}\right) = P_T. \tag{69}$$

If the load $\boldsymbol{P}$ is prescribed, then the system will be in static equilibrium in the configuration given by the curvature in (69). However, given a configuration, the load $\boldsymbol{P}$

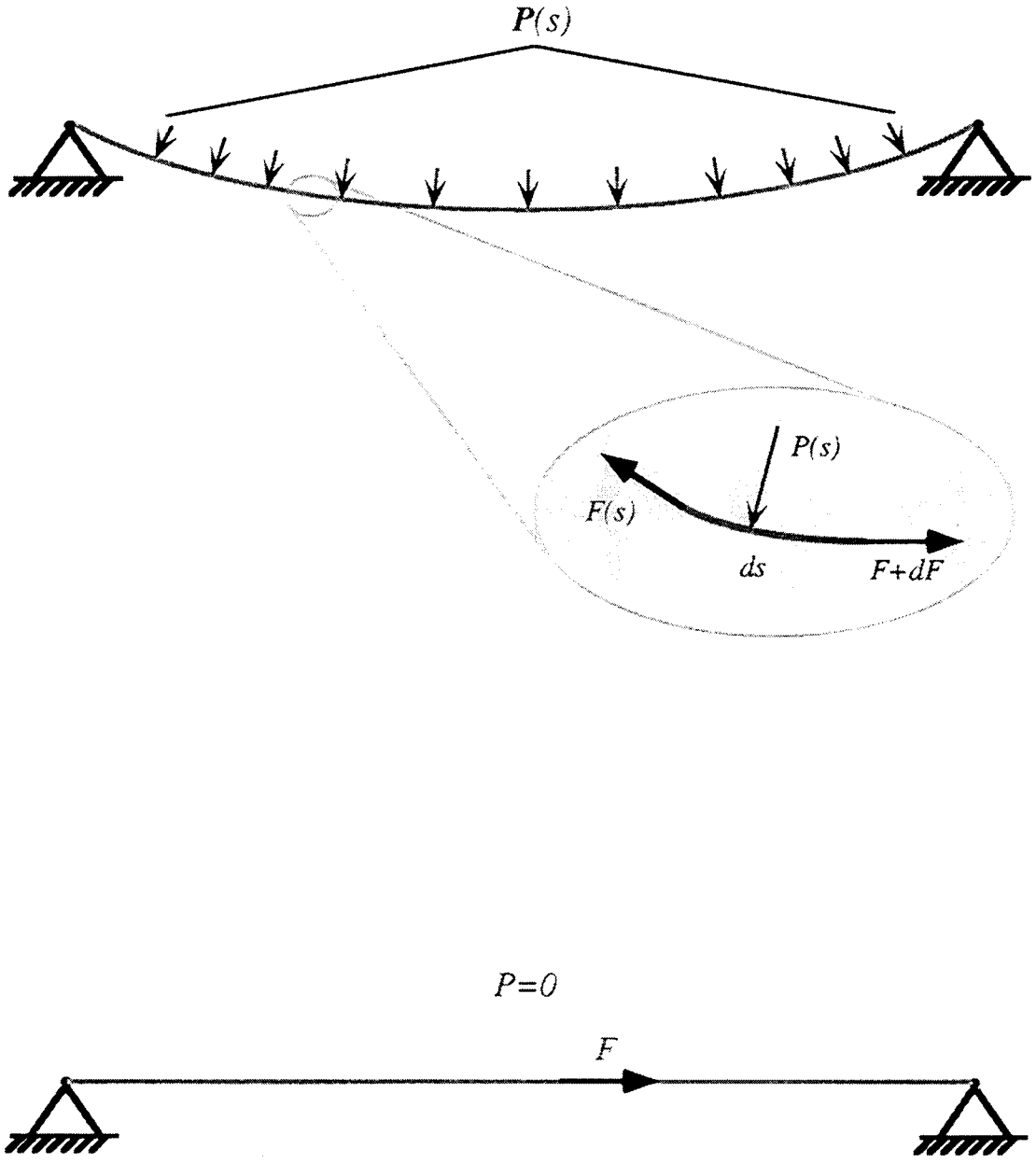

Figure 2.8: Equilibrium of a filament in a general configuration (top) and a singular rectilinear configuration (bottom).

is indeterminate since a proportional change in P_N and P_T will leave (69), and thereby the configuration, unchanged. If the configuration of the system is specified, only the pattern of the load may be obtained from equation (69). This relationship between statics and geometry enables the design of filament geometries by applying external loads.

These results are extend to a class of structural system that Kuznetsov [9] terms underconstrained systems. In the absence of external loads (68) becomes

$$\begin{matrix} \frac{dF}{ds}=0 \\ F\kappa=0 \end{matrix}, \tag{70}$$

Equations (70) are called the homogeneous equilibrium equations of the filament. Solving for F, equations (70) admit a trivial solution, $F=0$. However, if the curvature κ is zero, then the system has an infinite number of solutions for constant F. The curvature is a geometric parameter of the system, and when it vanishes, the filament is a straight line. This status of the filament is called a singular configuration of the system. All other configurations cannot remain in static equilibrium for non-vanishing tension in the cord; in that case the system becomes dynamic.

Such a simple and intuitively obvious outcome demonstrates a very important point. The result shows that the filament, which is a dynamic system in general, possesses a singular configuration that is static. There is a mathematical principle that if there exists a non-trivial solution to a homogeneous system of equations, then the system is not independent. The existence of a singular configuration indicates that the local dimension of the configuration is less than the local dimension of the external load, and therefore the system is underconstrained. It is possible to statically control the geometry of such an underconstrained system. Furthermore, when the system is not independent the non-homogeneous system of equations does not have a unique solution, as was

shown in (69) for the case of the filament.

Traditionally, the external load on the system is called the applied load, while the resultant tension would be termed a reaction to that load. This correlation between external causes and internal effects occurs in all commonly familiar structures. However, this terminology is misleading in the present circumstances where a reaction may be present in the structure even in the absence of external load. Thus, tension is referred to as an internal force, rather than a reaction. The applied load is called an external force. Static equilibrium is brought about by the balance between internal and external forces. If there is a non-trivial solution to the homogeneous equilibrium equations, then internal forces balance themselves.

Next consider two filaments, $U(u)$ and $V(v)$, intersecting at an angle ω. This system is two dimensional, therefore equilibrium for each filament becomes

$$\begin{aligned} \frac{\partial}{\partial u}(\boldsymbol{F}_U\ dv)\,du &= \boldsymbol{P}_U^{\circ}\ du\,dv\,sin\ \omega \\ \frac{\partial}{\partial v}(\boldsymbol{F}_V\ du)\,dv &= \boldsymbol{P}_V^{\circ}\ du\,dv\,sin\ \omega \end{aligned} \tag{71}$$

where $\boldsymbol{F}_U = F_U\boldsymbol{u}$ is the tension per unit length acting on dv, $\boldsymbol{F}_V = F_V\boldsymbol{v}$ is the tension per unit length acting on du, ω is the angle at the intersection, and $\boldsymbol{P}_U^{\circ}$ and $\boldsymbol{P}_V^{\circ}$ are the external loads per unit area on each filament at the intersection. If there are no external forces on the system, then two possibilities exist. Either $\boldsymbol{P}_U^{\circ}$ and $\boldsymbol{P}_V^{\circ}$ are both identically zero so that the filaments decouple, or $\boldsymbol{P}_U^{\circ} + \boldsymbol{P}_V^{\circ} = 0$ in which case $\boldsymbol{P}_U^{\circ}$ and $\boldsymbol{P}_V^{\circ}$ are due to mutual interaction between filaments. In the first case, the results for both filaments are the same as the solution of (70); they are straight lines. In the second instance, equations (71) may be superposed to form

$$\frac{\partial}{\partial u}\boldsymbol{F}_U\,du\,dv+\frac{\partial}{\partial v}\boldsymbol{F}_V\,du\,dv=0\ . \tag{72}$$

This result may be extended to two arrays of filaments. In that case, equation (72) is the homogeneous equilibrium equation for a net on which every point is an intersection. Further , the general equilibrium equation for a net is

$$\frac{\partial}{\partial u}\boldsymbol{F}_U\,du\,dv+\frac{\partial}{\partial v}\boldsymbol{F}_V\,du\,dv=\boldsymbol{P}^{\circ}\sin\omega\,du\,dv\ , \tag{73}$$

where $\boldsymbol{P}^{\circ}$ is external load applied to the net.

Nets have not received wide attention in structural mechanics because the ability to radically change configuration under changing load conditions renders them unsuitable for structural applications. However, this ability embodies a net's usefulness in other applications. Nets are capable of very large deformations, which is generally not desirable if the goal of a structure is to maintain its configuration, and thus its structural integrity, under a variety of loads. However, if the goal is to produce a range of shapes for different load patterns, then nets are well suited. We want to utilize the low bending stiffness of filaments to manufacture different shapes from nets under various loads.

An important distinction needs to be emphasized regarding the term deformation. The deformation of a net considered herein is kinematic deformation, due to lack of constraint in the system. This motion is distinct from deformation due to material strain. In reality, material strain occurs in filaments, but it is assumed to be very small compared with the kinematic motion. For the purpose of finding useful configurations of nets, filaments are considered to be inextensible. This assumption is justified when dealing with the application of nets in composite structure fabrication where material fibers are generally very stiff. Material deformation is important for the stress analysis and design considerations of the composite structure, however it is a completely different

phenomenon from kinematic deformation which describes the shape of the net. It is the latter aspect which is discussed herein.

A methodology is needed to classify nets. One way to classify nets is by the interaction between its constituent arrays. Specifically, net classification may be based upon the manner in which arrays interact with each other. Abstractly, the arrays occupy the same space at every intersection of the filaments. Physically, this idea may be realized by forming the net from some material in a mold, but this is impractical for many applications and uncommon. More often filaments are interlaced to form a net, as occurs in braids or weaves. Specifically, filaments are interlaced to form a circular cylindrical tube for a braided sleeve.

A net has been defined as two arrays of intersecting filaments. Exactly how the arrays interact at an intersection needs to be elaborated. An intersection is a point of interaction between filaments that may be expressed in terms of their relative motions. The primary mechanisms that control interaction for a braid or weave are friction and tightness, the latter being related to the density of the braid. Tightness describes the proximity of neighboring filaments in the braid. The presence or absence of friction and tightness strongly influences the static-geometric behavior of nets and provides a suitable means for their classification.

Two simple types of interaction will be considered for a net with arrays U and V. The first case is that two arrays move over one another with no resistance. It is well known that an unrestricted filament will assume a geodesic trajectory when placed in tension (see [6], p. 249-251). When both arrays of a net assume geodesic trajectories, the net is called a geodesic net. By definition, a geodesic curve has zero geodesic curvature at every point. Therefore the analytical criterion for a geodesic net is

$$\gamma_U = \gamma_V = 0. \tag{74}$$

The second case corresponds to the condition that the $\boldsymbol{U}$ array can only translate along the u curves, i.e. along itself, and there can be no component of motion along the $\boldsymbol{V}$ array. Under this condition, the $\boldsymbol{V}$ is an array of parallel curves along $\boldsymbol{U}$ and $\boldsymbol{U}$ forms another array of parallel curves along $\boldsymbol{V}$. The analytical criterion for parallel elements of one array along another is the vanishing of the Chebyshev curvature, namely

$$\lambda_U = \lambda_V = 0 \tag{75}$$

A net with vanishing Chebyshev curvatures is called a Chebyshev net.

At this stage, all the necessary tools for analytically dealing with braided sleeves have been defined. Additionally, the theoretical basis has been established for controlling certain structures, in particular nets, by statical means, yielding a predictive analytical framework for their kinematic behavior. This theoretical possibility provides the motivation for the new fabrication technique.

CHAPTER 3

Some Rotationally Symmetric Solutions for Nets

3.1 Introduction

It is intuitively clear that the concepts developed for nets in the foregoing chapter may be extended to describe braided sleeves. For a given sleeve, different shapes may be produced by applying by various loads. Before the shape of the sleeve can be predicted, the nature of the interaction between the braided tows must be ascertained. This interaction may be quantified by an analytical relationship that maps the angle between the braided tows to every point on the surface of the sleeve. Establishing this relationship is tantamount to specifying the type of net used to describe braided sleeves.

Two types of nets were introduced in Chapter 2, geodesic and Chebyshev. Motivated by the arguments of [3], these types will be elucidated in order to model braided sleeves. The sleeve is considered to be in a cylindrical configuration initially, with its arrays described by helical trajectories therefore, in this state, the sleeve is simultaneously a geodesic net and a Chebyshev net. When the sleeve is loaded, the tows will undergo motion. This motion can be expressed in terms of two components: translation of the tows relative to one another and rotation of tows about surface normals at tow intersections. If the tows are able to translate without restraint, they will tend toward geodesic trajectories, and the geodesic quality of the sleeve will be preserved at the expense of the Chebyshev character. If the tows are not able to translate, only rotation about intersection normals is possible. In this case the tows are inhibited from geodesic trajectories and the sleeve will maintain its Chebyshev character.

In reality, the intersections of the sleeve are not fixed. This characteristic suggests that a sleeve may behave kinematically as a geodesic net. However, for high density braiding the movement of the tows is restricted. Additional restriction may manifest from the presence of friction between the tows. Due to these restrictions, the normal rotation at tow intersections may be the dominant mode of kinematic behavior and consequently the intersections may be considered fixed with respect to translation. In this case, then the Chebyshev character of the sleeve is maintained at the expense of the geodisicity of the sleeve arrays.

The determination of the type of net formed in reality for a given braided sleeve is achieved by measuring actual surface geometries and comparing the data with analytical solutions for geodesic and Chebyshev nets. The actual geometries are generated by placing sleeves under tension and locking in their shapes by applying matrix materials, such as epoxy, which harden upon cure. These shapes are then compared with the analytic results derived below. In this chapter, we focus attention on solutions for each type of net under specific circumstances which correspond to the experimental verification detailed in Chapter 4.

3.2 Analytical Solutions for Single Sleeves under Uniform Axisymmetric Tension

In order to ascertain the nature of the interaction between the tows of a braided tube, the sleeve was considered in a configuration produced by uniform axisymmetric tension. This load/configuration case was selected because it is conceptually simple and straightforward to implement experimentally. Two types of nets, geodesic and Chebyshev, were contemplated as candidates to model braided sleeves. Specifying the

type of net yields a geometric relationship necessary to obtain an expression for the shape of the net. In the following development, theoretical expressions are derived for each type of net. These expressions are used to compare the predicted shape of each net to the actual shape of a braided sleeve produced experimentally.

All sleeves under analytical consideration in this thesis are assumed to be in an axisymmetric configuration. In Chapter 2, a parameterization of a surface of revolution in terms of its radius r and the angle ϕ was defined in equations (19). It is mathematically convenient to invert the third of equations (19) to get $r=f(z)$ so that the surface is parameterized by the axial distance z and ϕ, rather than r and ϕ. This parameterization produces expressions that are better suited to the purposes of this work. An arbitrary rotationally symmetric surface with this parameterization is denoted by $\Sigma(z,\phi)$, and in view of (19), the coordinate isomorphism for $\Sigma(z,\phi)$ is

$$\begin{aligned} x &= r(z)\ cos\ \phi \\ y &= r(z)\ sin\ \phi\ . \\ z &= z \end{aligned} \tag{76}$$

The theoretical considerations presented previously may now be applied to the specific case of $\Sigma(z,\phi)$ to derive expressions for the various objects associated with the differential geometry of curves and surfaces. These objects may then be used to describe the configuration of an axisymmetric braided sleeve. According to (17) the basis vectors corresponding to the parameterization (76) are

$$\begin{aligned} \boldsymbol{e}_z &= r'(z)\ cos\ \phi\ \boldsymbol{i} + r'(z)\ sin\ \phi\ \boldsymbol{j} + \boldsymbol{k} \\ \boldsymbol{e}_\phi &= -r(z)\ sin\ \phi\ \boldsymbol{i} + r(z)\ cos\ \phi\ \boldsymbol{j} \end{aligned}\ , \tag{77}$$

where the prime denotes differentiation with respect to z. Then from (23) with (17) and (77) the metric tensor is

$$g_{ij}=\begin{bmatrix} 1+r'^2 & 0 \\ 0 & r^2 \end{bmatrix} \tag{78}$$

and by (28) the contravariant metric tensor is

$$g^{ij}=\begin{bmatrix} \frac{1}{1+r'^2} & 0 \\ 0 & \frac{1}{r^2} \end{bmatrix}. \tag{79}$$

The unit normal for $\Sigma(z,\phi)$ is

$$\boldsymbol{n}=-\frac{1}{\sqrt{1+r'^2}}\left[\cos\phi\,\boldsymbol{i}+\sin\phi\,\boldsymbol{j}-r'\,\boldsymbol{k}\right] \tag{80}$$

from substituting (77) into (30) after recalling (17). The second fundamental tensor is found by differentiating (80) and placing the appropriate expressions into (40) to yield

$$h_{ij}=\frac{1}{\sqrt{1+r'^2}}\begin{bmatrix} r'' & 0 \\ 0 & -r \end{bmatrix} \tag{81}$$

Substitution of (79) and (81) into (45) yields the shape tensor,

$$S^i_j=\frac{1}{\sqrt{1+r'^2}}\begin{bmatrix} -\frac{r''}{1+r'^2} & 0 \\ 0 & \frac{1}{r} \end{bmatrix}. \tag{82}$$

Since the fundamental tensors expressed in (78) and (81) are diagonal, the basis defined in (77) is the principal basis and the orthogonal coordinate lines are lines of principal curvature. As was shown in (50), when the principal basis is employed the principal curvatures are the diagonal elements of the shape tensor. Therefore expressions for the principal curvatures are contained in (82). The lines of principal curvature may be written as unit vector fields s and ϕ on the surface of revolution in terms of the basis (77):

$$s^i=\begin{bmatrix} \frac{1}{\sqrt{1+r'^2}} \\ 0 \end{bmatrix} \qquad \phi^i=\begin{bmatrix} 0 \\ \frac{1}{r} \end{bmatrix} \tag{83}$$

The vector field s represents a meridional curve and ϕ defines a parallel circle or latitude on the surface. A parallel circle is defined at every point on the domain of the surface along the axis of revolution. Parallel circles have radius r and lie in planes perpendicular to the z axis.

The connection coefficients for $\Sigma(z,\phi)$ are found from (56) considering (77):

$$\begin{aligned}
\Gamma^1_{11} &= \frac{r'r''}{1+(r')^2} \\
\Gamma^1_{12} &= \Gamma^1_{21} = 0 \\
\Gamma^1_{22} &= -\frac{rr'}{1+(r')^2} \\
\Gamma^2_{11} &= 0 \\
\Gamma^2_{12} &= \Gamma^2_{21} = \frac{r'}{r} \\
\Gamma^2_{22} &= 0
\end{aligned} \quad , \tag{84}$$

from which the transversal vectors for the curves s and ϕ defined in (83) are calculated in a straightforward manner with equation (62) as

$$(t_s)_i = \begin{bmatrix} 0 \\ \frac{r'}{\sqrt{1+r'^2}} \end{bmatrix} \tag{85}$$

and

$$(t_\phi)_i = \begin{bmatrix} 0 \\ \frac{r'}{\sqrt{1+r'^2}} \end{bmatrix}. \tag{86}$$

Consider now an arbitrary curve u shown in Figure 3.1 and represented by a field of unit tangent vectors. With the principal basis (77), this field can be expressed

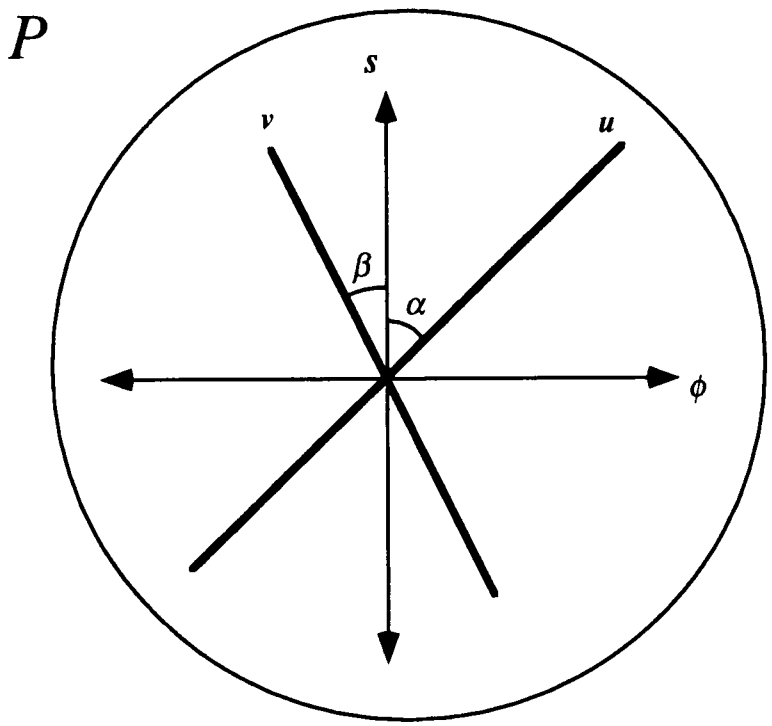

Figure 3.1: Unit vector fields $\boldsymbol{u}$ and $\boldsymbol{v}$ shown with respect to the lines of principal curvature represented by $\boldsymbol{s}$ and ϕ at a point on a surface with rotational symmetry.

$$u^i = \begin{bmatrix} \frac{\cos\alpha}{\sqrt{1+r'^2}} \\ \frac{\sin\alpha}{r} \end{bmatrix}, \tag{87}$$

where α is the angle between u and s at a point on the surface. In addition, consider a second curve v also shown in Figure 3.1. This curve can be described by

$$v^i = \begin{bmatrix} \frac{\cos\beta}{\sqrt{1+r'^2}} \\ -\frac{\sin\beta}{r} \end{bmatrix}. \tag{88}$$

From equation (64) with (85) and (87), the transversal vectors of u and v are

$$(t_u)_i = \begin{bmatrix} \alpha' \\ \frac{r'}{\sqrt{1+r'^2}} \end{bmatrix} \tag{89}$$

and

$$(t_v)_i = \begin{bmatrix} \beta' \\ \frac{r'}{\sqrt{1+r'^2}} \end{bmatrix}, \tag{90}$$

respectively.

In addition to rotational symmetry, a second symmetry may be assumed for braided sleeves. The arrays of a sleeve are counterwound such that, on average, the angles at an intersection between a tow of each array and the meridian of the net surface are of equal magnitude. Using the meridian as a zero-angle reference line, and denoting the angles of the arrays at the intersection as α and β for the arrays u and v, respectively, the tows are described by the condition $\beta = -\alpha$. This type of symmetry is called reflection symmetry with respect to the meridian, or simply reflection symmetry. Reflection symmetry is shown in Figure 3.2.

Consider now equilibrium of a sleeve under uniform axisymmetric tension with no external loads. In the absence of such loads, the equilibrium equation for a net (73) with

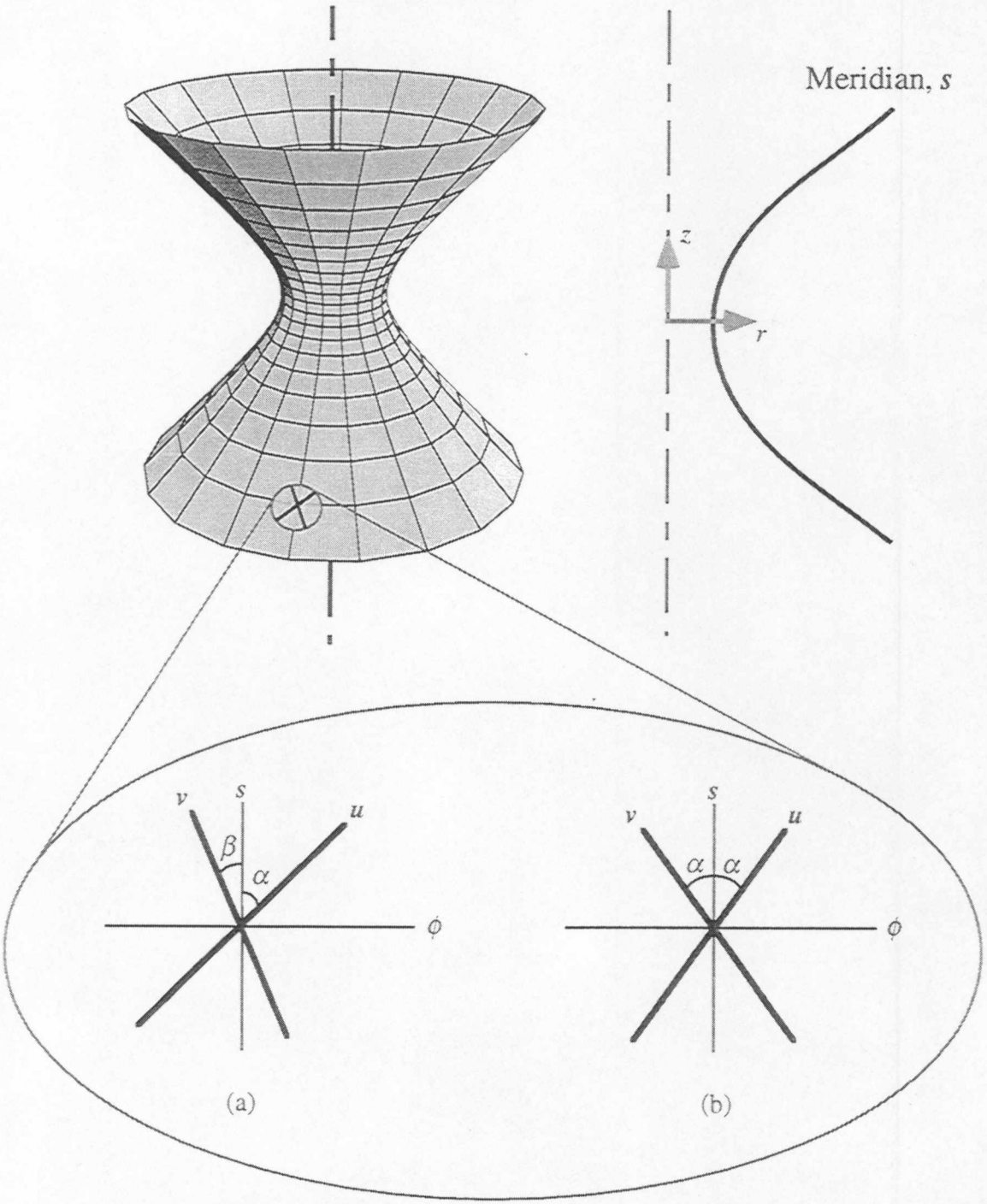

Figure 3.2: An axisymmetric net with arrays ***u*** and ***v*** shown (a) in the general case and (b) with reflection symmetry.

$\boldsymbol{P}^{o}=\boldsymbol{0}$ takes the form

$$\frac{\partial \boldsymbol{T}_U}{\partial u} + \frac{\partial \boldsymbol{T}_V}{\partial v} = \boldsymbol{0} \tag{91}$$

The inner product of (91) and the unit normal vector of the net surface yields the scalar equilibrium equation in the normal direction

$$T_U\left(\frac{\partial \boldsymbol{u}}{\partial u}\cdot\boldsymbol{n}\right)+T_V\left(\frac{\partial \boldsymbol{v}}{\partial v}\cdot\boldsymbol{n}\right)=0. \tag{92}$$

The first Frenet equation (12) applied to $\boldsymbol{u}$ and $\boldsymbol{v}$ yields,

$$\frac{\partial \boldsymbol{u}}{\partial u}=\kappa_u \quad , \quad \frac{\partial \boldsymbol{v}}{\partial v}=\kappa_v \ , \tag{93}$$

where κ_u, κ_v denote the curvatures of the filaments. By noting the definition of the normal curvature (35), (92) may then be written

$$T_U(\kappa_u)_n + T_V(\kappa_v)_n = 0 \qquad \text{(no sum on } u \text{ and } v\text{)} \tag{94}$$

By hypothesis, both arrays are in tension, therefore T_U and T_V are strictly positive. Consequently, equation (94) implies that if there are no external loads on the sleeve, the normal curvatures of the net must have opposite signs. Furthermore, if the normal curvatures of two curves through a point have opposite sign, then the principal curvatures at that point will be of opposite sign also. Noting equations (47) and (50), it is evident that the Gaussian curvature of any surface formed by this net must be negative regardless of any symmetry considerations. Since the sleeve is tensioned uniformly and axisymmetrically, $T_U = T_V$ and the normal curvatures of the resulting net surface must satisfy

$$(\kappa_u)_n+(\kappa_v)_n=0. \tag{95}$$

Using Euler's equation (51), the normal curvatures in (95) may be expressed as

$$\begin{aligned} (\kappa_u)_n &= \kappa_1 \cos^2\alpha + \kappa_2 \sin^2\alpha \\ (\kappa_v)_n &= \kappa_1 \cos^2\beta + \kappa_2 \sin^2\beta \end{aligned} \quad . \tag{96}$$

A reflection symmetric net has the property $\alpha = -\beta$, therefore considering (96),

$$(\kappa_u)_n = (\kappa_v)_n . \tag{97}$$

In light of (97), equation (95) is satisfied if and only if the normal curvatures of both arrays vanish. This result indicates that the sleeve will take the shape of an asymptotic net when it is subjected to uniform, axisymmetric tension.

For an asymptotic net, the net angle may be conveniently related to the principal curvatures by considering Euler's theorem for each array as in the system of equations expressed in (96) with the normal curvatures set to zero. When reflection symmetry is assumed, this system degenerates into a single independent equation:

$$\kappa_1 \cos^2\alpha + \kappa_2 \sin^2\alpha = 0 \tag{98}$$

The basis corresponding to $\Sigma(z,\phi)$ is principal and the principal curvatures are found from (82) upon recalling equation (50):

$$\kappa_1 = -\frac{r''}{\left(1+r'^2\right)^{3/2}} \tag{99}$$

and

$$\kappa_2 = \frac{1}{r\sqrt{1+r'^2}} . \tag{100}$$

On a surface of revolution, the principal curves corresponding to κ_2 are circles with radii $r = R \sin\theta$, where R is the radius of a circle contained in the normal plane of the profile curve and θ is the angle between R and the axis of symmetry. The normal plane is defined at the point where the profile curve and this circle contact one another.

This relationship is demonstrated in Figure 3.3. By definition $\kappa_2 = 1/R$ therefore,

$$\kappa_2 = \frac{\sin\theta}{r}. \tag{101}$$

From Figure 3.3, it is noted that the meridional curve of a surface can be described by

$$\frac{dz}{dr} = \tan\theta. \tag{102}$$

Comparing κ_1 to κ_2 in expressions (99) and (100) it is deduced that on a surface of revolution

$$\kappa_1 = \frac{d}{dr}(r\kappa_2). \tag{103}$$

Substituting (103) into (98) yields the equation:

$$\frac{d\kappa_2}{dr} = -\frac{\kappa_2}{r\cos^2\alpha}. \tag{104}$$

Equations (103) and (104) completely determine the principal curvatures, and thus the surface formed by the axisymmetric, asymptotic net. However, equation (104) contains the term α, which is an unknown function of r. To solve this equation, it is necessary to incorporate a relationship between r and α, which is obtainable upon specifying the type of net.

Consider first the case of rotationally symmetric, reflection symmetric geodesic nets. Substitution of (87) and (89) and then (88) and (90) into equation (65) yields the following expressions for the geodesic curvature of each array of the net:

$$\gamma_u = \frac{1}{r\sqrt{1+r'^2}}\left[r\alpha'\cos\alpha + r'\sin\alpha\right] \tag{105}$$

and

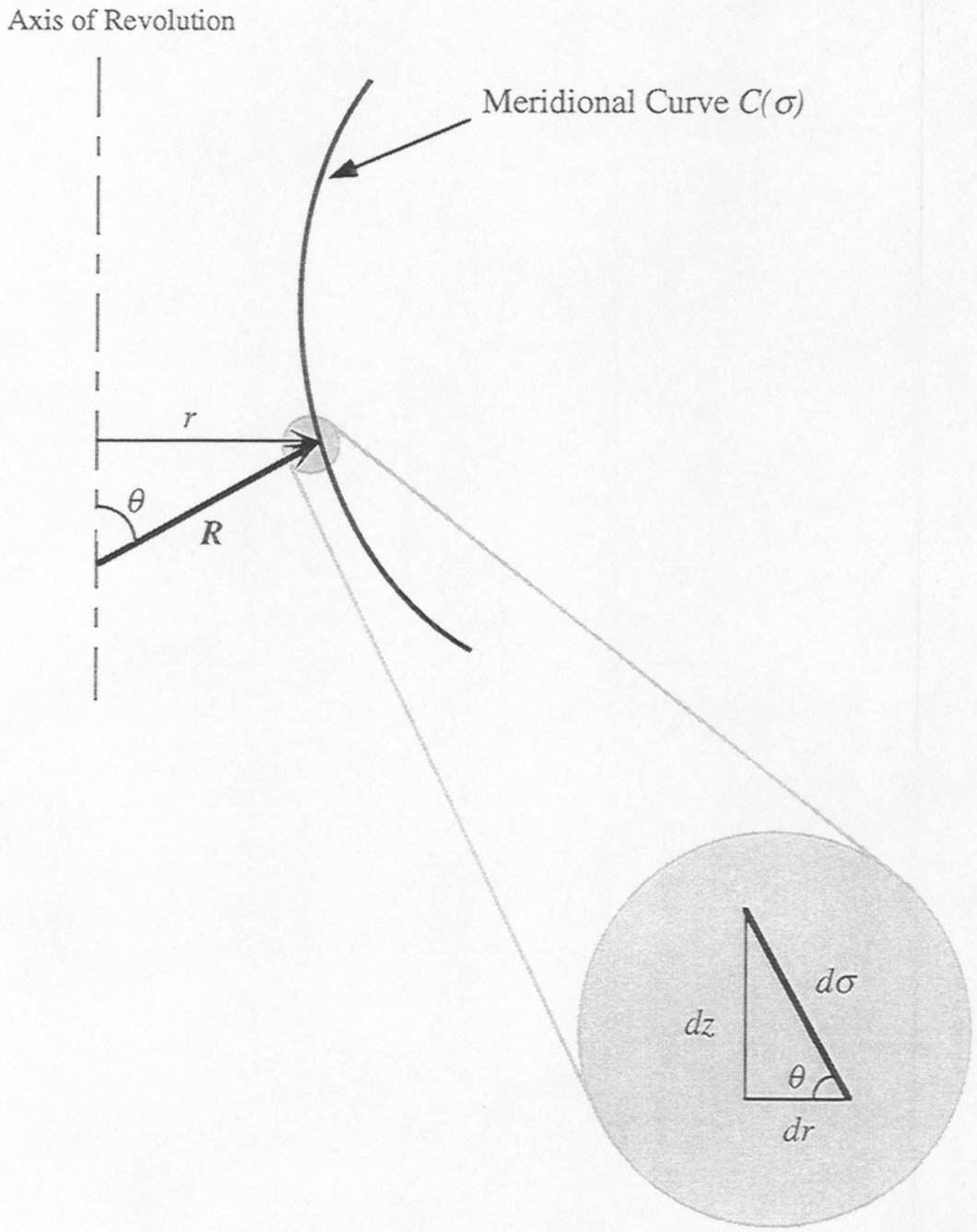

Figure 3.3: Relationship of principal curvatures to coordinate variables on a surface of revolution.

$$\gamma_v = \frac{1}{r\sqrt{1+r'^2}}[r\beta' \cos\beta + r' \sin\beta]. \tag{106}$$

Upon recalling (74), the requirement that the geodesic curvature of each array of a geodesic net vanish reduces the expressions (105) and (106) to read

$$r\alpha' \cos\alpha + r' \sin\alpha = 0 \tag{107}$$

and

$$r\beta' \cos\beta + r' \sin\beta = 0. \tag{108}$$

In view of the assumed reflection symmetry, we have $\alpha = -\beta$, thus (107) and (108) condense into a single equation

$$ctn\ \alpha\, d\alpha = -\frac{dr}{r} \tag{109}$$

Integration of equation (109) results in the well known Clairaut formula,

$$r = \frac{r_{min}}{\sin\alpha} \tag{110}$$

where r_{min} is the minimum radius possible for the net. This constant radius is realized when $\alpha = \pi/2$, but it may be calculated from $r_{min} = r_o \sin\alpha_o$ at any reference parallel where r_o and α_o are known.

With expression (110) at hand, it is now possible to determine the shape of the geodesic net. Substituting (110) into (104) and solving the resulting differential equation gives

$$\kappa_2 = \frac{c}{\sqrt{r^2 - r_{min}^2}}, \tag{111}$$

where c is an arbitrary constant. Comparing (111) and (101) and regarding (110) the constant c can be written

$$c = \sin\theta \cos\alpha, \tag{112}$$

where θ is the angle between the surface normal and the axis of symmetry. Let r_e denote the equatorial radius namely, the radius of the axisymmetric surface at a parallel corresponding to a relative minimum or maximum of the meridional curve. At an equator, the surface normal vector lies in the same plane as the parallel circle which corresponds to $\theta = \pi/2$. If an equator is assumed to exist on the surface, then c may be expressed using (110) and (112) as

$$c = \cos\alpha_e = \sqrt{1 - \left(\frac{r_{min}}{r_e}\right)^2}. \tag{113}$$

The differential equation that describes the profile curve is found from (101), (102) and (111) to be

$$\frac{dz}{dr} = \frac{cr}{r_{min}\sqrt{\left(\frac{r}{r_e}\right)^2 - 1}}. \tag{114}$$

Solving (114) yields the expression for the profile of a rotationally, reflectively symmetric asymptotic geodesic net:

$$r = \pm r_e \sqrt{1 + \frac{z^2 r_{min}^2}{r_e^2\left(r_e^2 - r_{min}^2\right)}}, \tag{115}$$

which is a hyperbola in the plane formed by r and z. The resulting surface of revolution is a one-sheet hyperboloid of revolution.

Consider now the case of rotationally symmetric Chebyshev nets with rotational and reflection symmetries. These nets are characterized by the condition (75) namely, null Chebyshev curvatures of the constituent arrays. Substituting (87) and (90) and then (88) and (89) into (66) yields the following expressions for the Chebyshev curvatures

$$\lambda_u = \frac{1}{r\sqrt{1 + r'^2}}\left[r\beta' \cos\alpha + r' \sin\alpha\right] \tag{116}$$

and

$$\lambda_v = \frac{1}{r\sqrt{1+r'^2}}\left[r\alpha' \cos\beta + r' \sin\beta\right] \tag{117}$$

Upon considering reflection symmetry, namely $\beta = -\alpha$, the above equations duplicate each other. Subsequently, the vanishing of the Chebyshev curvature gives

$$\frac{dr}{r} = ctn\ \alpha\, d\alpha. \tag{118}$$

The general solution to this equation is

$$r = C \sin\alpha \tag{119}$$

By noting that a Chebyshev net attains a maximum radius when $\alpha = \pi/2$, (119) may be written

$$r = r_{max} \sin\alpha. \tag{120}$$

Upon combining (120) with equations (103) and (104), it is possible to express the principal curvatures of a Chebyshev net:

$$\begin{aligned} \kappa_1 &= -\frac{C\tilde{r}}{\sqrt{1-\tilde{r}^2}} \\ \kappa_2 &= \frac{C\sqrt{1-\tilde{r}^2}}{\tilde{r}} \end{aligned}, \tag{121}$$

where $\tilde{r} = r/r_{max}$ and C is a constant of integration with dimension of inverse length. Recalling (47) and (50) then, in view of (121), the Gaussian curvature becomes

$$K = \kappa_1 \kappa_2 = -C^2, \tag{122}$$

demonstrating that an asymptotic Chebyshev net will form a surface of constant negative Gaussian curvature. This result was proved by Voss [15] in 1882. General expressions for the profile curves of axisymmetric surfaces of constant negative curvature that are relevant for calculating the shape of a braided sleeve are derived below.

Comparing expressions (101) and (121) we get

$$\sin\theta = Cr_{\max}\sqrt{1-\tilde{r}^2}\,. \tag{123}$$

Let c denote Cr_{max} so that, with (121), $c = \sin\theta_o / \cos\alpha_o$. Putting (123) into (102) yields:

$$\frac{dz}{dr} = \frac{c\sqrt{1-\tilde{r}^2}}{\sqrt{(1-c^2)+(c\tilde{r})^2}}\,. \tag{124}$$

It is immediately apparent that for the case $\sin\theta_o = \cos\alpha_o$ we obtain $c = 1$. Then (124) may be solved analytically to yield:

$$z = \sqrt{r_{\max}^2 - r^2} - r_{\max}\, ln\left(\frac{r_{\max}+\sqrt{r_{\max}^2-r^2}}{r}\right). \tag{125}$$

This expression describes a tractrix. A rotation surface with a tractrix as its profile curve is a parabolic pseudospere of revolution. We now seek solutions for the hyperbolic and elliptic cases corresponding to $c>1$ and $c<1$, respectively.

The simplest way to obtain a formal solution for the shape of a rotation surface of constant curvature with $c \neq 1$ is to consider the most general parameterization of the principal coordinate system on that surface denoted by $\Sigma(\sigma,\phi)$, where σ is some arbitrary parameter. In analogy with (77), we now have

$$\begin{aligned} \boldsymbol{e}_\sigma &= r'(\cos\phi\, \boldsymbol{i} + \sin\phi\, \boldsymbol{j}) + z'\boldsymbol{k} \\ \boldsymbol{e}_\phi &= -r(\sin\phi\, \boldsymbol{i} - \cos\phi\, \boldsymbol{j}) \end{aligned} \tag{126}$$

where the prime indicates differentiation with respect to σ. While the foregoing base vectors have the same direction as those found in (77) or (7), a substantial advantage accrues by letting σ be the arc length along the meridional curve, while r and z are radial and axial distances. From (126) the differential arc length of a curve on the surface is

$$ds^2 = \left(r'^2 + z'^2\right) d\sigma^2 + r^2 d\phi^2 . \tag{127}$$

Since the parameter σ is arbitrary, it may be chosen such that the meridional curve has unit speed. In that case

$$r'^2 + z'^2 = 1 \tag{128}$$

and the differential meridional arc length shown in Figure 3.3 is

$$d\sigma = \sqrt{1 + \left(\frac{dr}{dz}\right)^2}\ dz . \tag{129}$$

The first fundamental tensor derived from (17), (23), and (126) is found to be

$$g_{ij} = \begin{bmatrix} 1 & 0 \\ 0 & r^2 \end{bmatrix} \tag{130}$$

In light of (17), (30), (40) and (126), the second fundamental tensor for $\Sigma(\sigma,\phi)$ is

$$h_{ij} = \begin{bmatrix} r''z' - r'z'' & 0 \\ 0 & -rz' \end{bmatrix} \tag{131}$$

and , in view of (45), the shape tensor corresponding to (122) and (123) is

$$S^i_j = \begin{bmatrix} r''z' - r'z'' & 0 \\ 0 & -\dfrac{z'}{r} \end{bmatrix} \tag{132}$$

By definition (42), the Gaussian curvature of $\Sigma(\sigma,\phi)$ is the determinant of (132). Taking the derivative of (128) with respect to σ into account, the Gaussian curvature may be expressed as

$$K = -\frac{1}{r}\frac{d^2 r}{d\sigma^2} . \tag{133}$$

It was shown in (122) that the surface resulting from an asymptotic, axisymmetric Chebyshev net has constant negative Gaussian curvature and therefore the general solution of (133) can be obtained as

$$r(\sigma)=A\ cosh\ \frac{\sigma}{\sqrt{K}}+B\ sinh\ \frac{\sigma}{\sqrt{K}} \tag{134}$$

For the case of $c > 1$, equation (124) indicates that there exists a radius, r_e, for which

$$\left.\frac{dz}{dr}\right|_{r\to r_e} \to \infty. \tag{135}$$

The point on the meridional curve corresponding to r_e is a critical point, either a relative minimum or maximum. The circle corresponding to this radius on the surface is distinguished as an equator. Furthermore equation (135) implies that

$$\left.\frac{dr}{dz}\right|_{r\to r_e} \to 0. \tag{136}$$

Let $z=0$ at $r=r_e$ and since σ is arbitrary, let $\sigma=0$ at $r=r_e$ also; then

$$r(\sigma=0)=r_e. \tag{137}$$

As $r \to r_e$ equation (129) implies that $d\sigma=dz$ and (136) becomes

$$r'(\sigma=0)=0. \tag{138}$$

When boundary conditions (137) and (138) are applied to (134), the solution of equation (133) for $c>1$ is revealed. By introducing the variable $\bar{\sigma}=\sigma/\sqrt{r_{max}^2-r_e^2}$ this solution can be written

$$r(\sigma) = r_e\ cosh\ \bar{\sigma}. \tag{139a}$$

Equation (139a) is an expression of the radius in terms of the meridional arc length, σ. To obtain the axial coordinate z, corresponding to any given r equation (128) is used, whereby

$$z(\sigma) = \int_0^{\bar{\sigma}} \sqrt{r_{max}^2 - r_e^2\ cosh^2\ t}\ dt. \tag{139b}$$

Together, equations (140) describe the profile curve of a hyperbolic pseudosphere.

Although the case $c < 1$ is of lesser relevance for nets that can be readily deployed in the experimental program discussed in Chapter 4, the solution for this case is listed for the sake of completeness. This solution reads

$$r(\sigma) = b \sinh \frac{\sigma}{\sqrt{K}} \tag{140a}$$

whereby

$$z(\sigma) = \int_0^{\sigma} \sqrt{1 + K b^2 \cosh^2 \left(\frac{t}{\sqrt{K}}\right)}\, dt \tag{140b}$$

and b is a constant. Equations (140) trace the meridian of an elliptic pseudosphere.

A braided sleeve placed in uniform axisymmetric tension forms a singular, asymptotic, rotationally and reflectionally symmetric net. The shape of such a net is embodied by a surface of revolution. The type of surface of revolution that is formed depends on the nature of the filament intersections in the net. Either no friction manifests at the intersections, allowing unlimited filament movement and resulting in a geodesic net or friction restricts filament movement, so that only filament rotations about the surface normal are permitted, resulting in a Chebyshev net. The surfaces of revolution corresponding to these net types are the one-sheet hyperboloid of revolution for the geodesic net and the pseudospheres of revolution for the Chebyshev net. The relevent pseudosphere for this work is the hyperbolic case. The surfaces obtained from each model are shown in Figure 3.4.

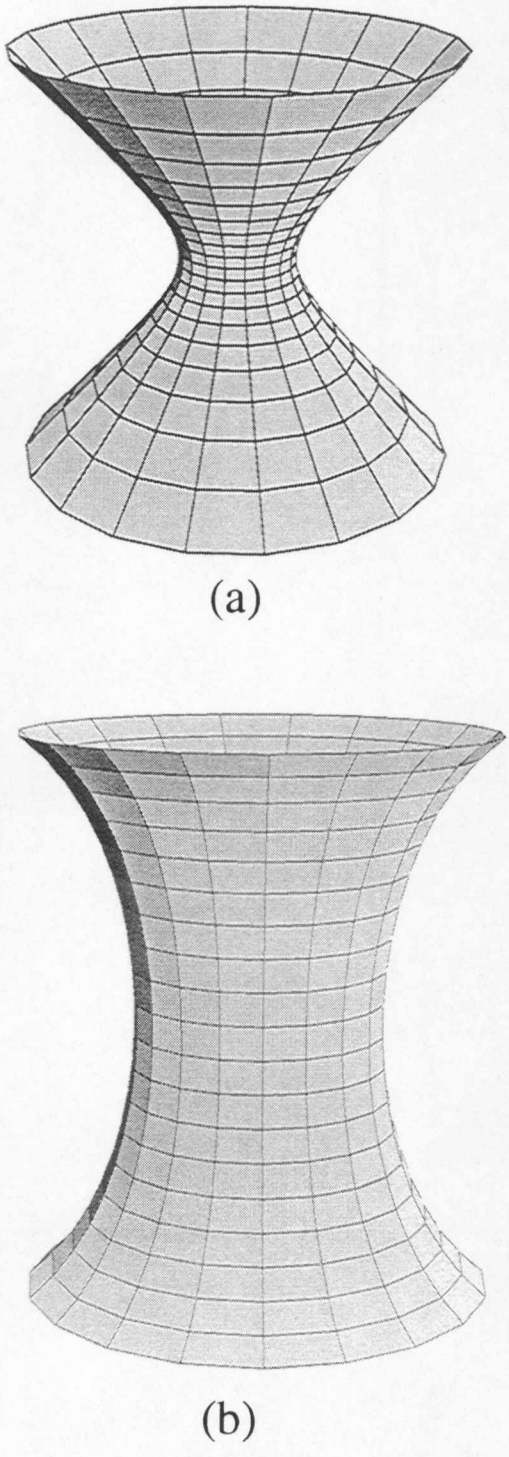

Figure 3.4: Analytical solutions for each net type: (a) one-sheet hyperboloid of revolution formed by a geodesic net, and (b) hyperbolic pseudosphere of revolution formed by a Chebyshev net.

CHAPTER 4

Experimental Determination of a Sleeve Model

4.1 Basic Considerations

Braided sleeves are produced by counterwinding two arrays of fiber tows to form a circular cylindrical tube. In addition to counterwinding, the arrays are interlaced such that tows of each array cross over one another periodically. In the continuum model of the net presented within Chapter 2, filaments were considered to occupy the same space, and subsequently the model does not directly account for the local geometry of interlacing tows. This local geometry affects the type of interaction present at an intersection. When sleeves are braided tightly, with small separations between neighboring filaments, movement of the tows tends to be restricted. If we assume these intersections are fixed with respect to translation, the sleeve may be considered a Chebyshev net. If a sleeve is braided loosely, with greater distance between the filaments, then tows may have some mobility. In the case of unlimited mobility, the sleeve would have characteristics of a geodesic net. The pattern of the unit cell of a braided sleeve is shown with the treatment of the corresponding region by each of the models in Figure 4.1.

In its "reference configuration" the braided sleeve has a circular cylindrical shape, with a reference diameter called the nominal diameter. The tows of an array are wound at a constant angle with respect to the meridian of the circular tube. Furthermore, the angles of the two arrays are equal in magnitude, but of opposite sense. This magnitude of the angles is called the braid angle of the sleeve. If asymmetric loads are applied, then the symmetry of the reference configuration may be lost, but under rotationally symmetric

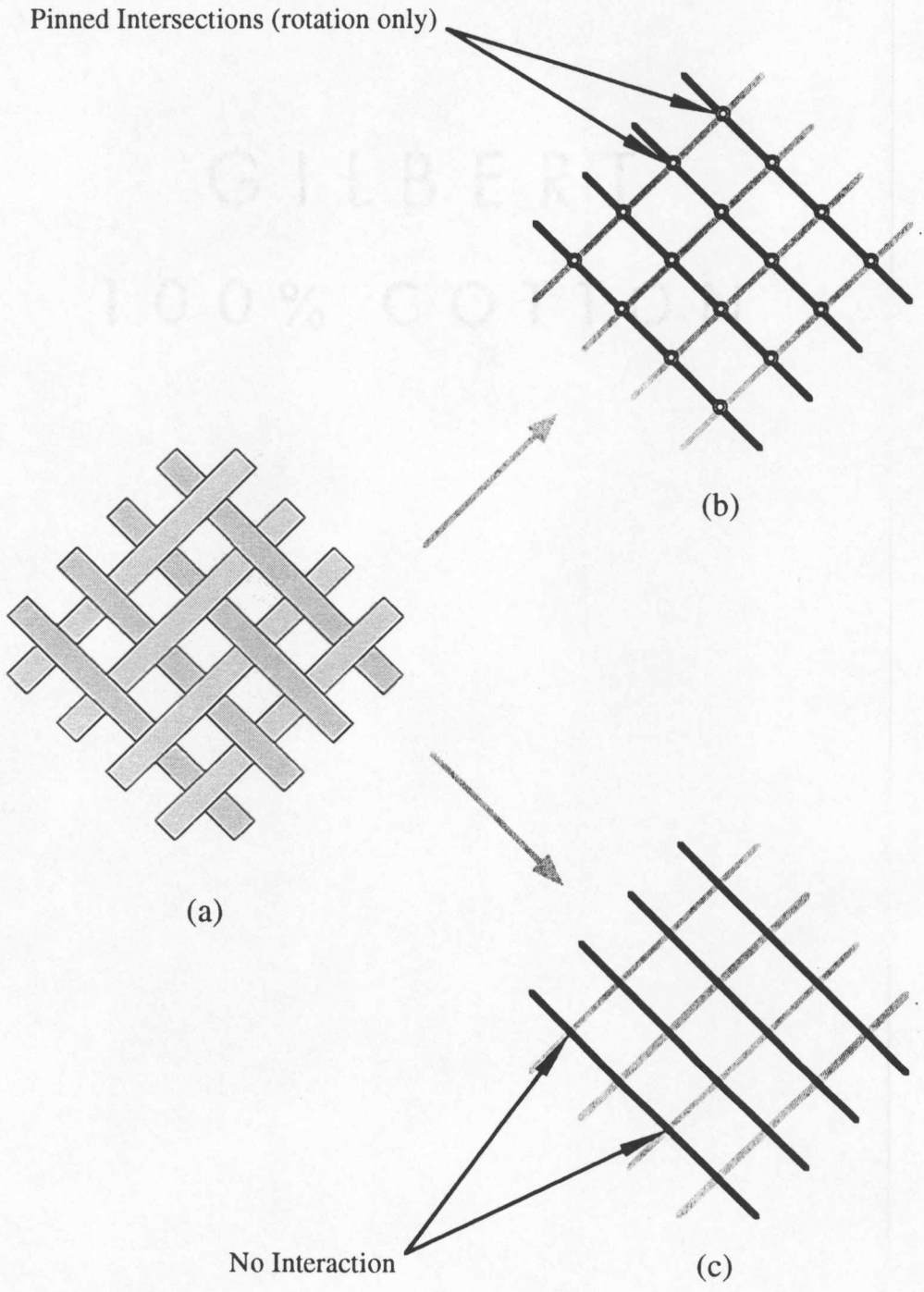

Figure 4.1: Unit cells for three cases: (a) actual pattern of the braided sleeves, (b) Chebyshev model of the sleeve allowing only rotation at tow intersections, and (c) geodesic model of the sleeve with no interaction between tows.

internal and external loading, the sleeve may be modeled as an axisymmetric net.

With the assumption of axial and reflection symmetries, and upon the selection of a model for the intersections, the geometry of a braided sleeve in the reference configuration is completely determined by its nominal diameter and its braid angle. Commercial sleeves are specified by material, nominal diameter and braid angle. Braids are available commercially in a variety of different materials and the braid angle is usually thirty or forty-five degrees. Axial and reflection symmetry are intrinsic to the commercial braiding process. However, a key issue for defining the statical-geometric behavior of the sleeve and thus predicting the shape of the sleeve under loads is the nature of the sleeve intersections. This parameter is not specified by sleeve manufacturers or in literature and is therefore the focus of this chapter.

This key issue is resolved by means of an experimental study. Single braided sleeves were placed in uniform axisymmetric tension. The resulting shapes were then observed and the configuration data was obtained. These data were compared with analytical results from each of the candidate models developed analytically in Chapter 3. From this comparison, a model for the braided sleeve was selected, indicating a dominant mechanism at array intersections.

4.2 Procedure for Single-Sleeve Membrane Fabrication

As already noted, the experiments consisted of pulling braided sleeves uniformly and axisymmetrically. A tensioning device was used to apply force the sleeves. The features of this device relevant to the single sleeve experiments are presented herein and shown in Figure 4.2. For a detailed discussion of the tensioning apparatus and all of its

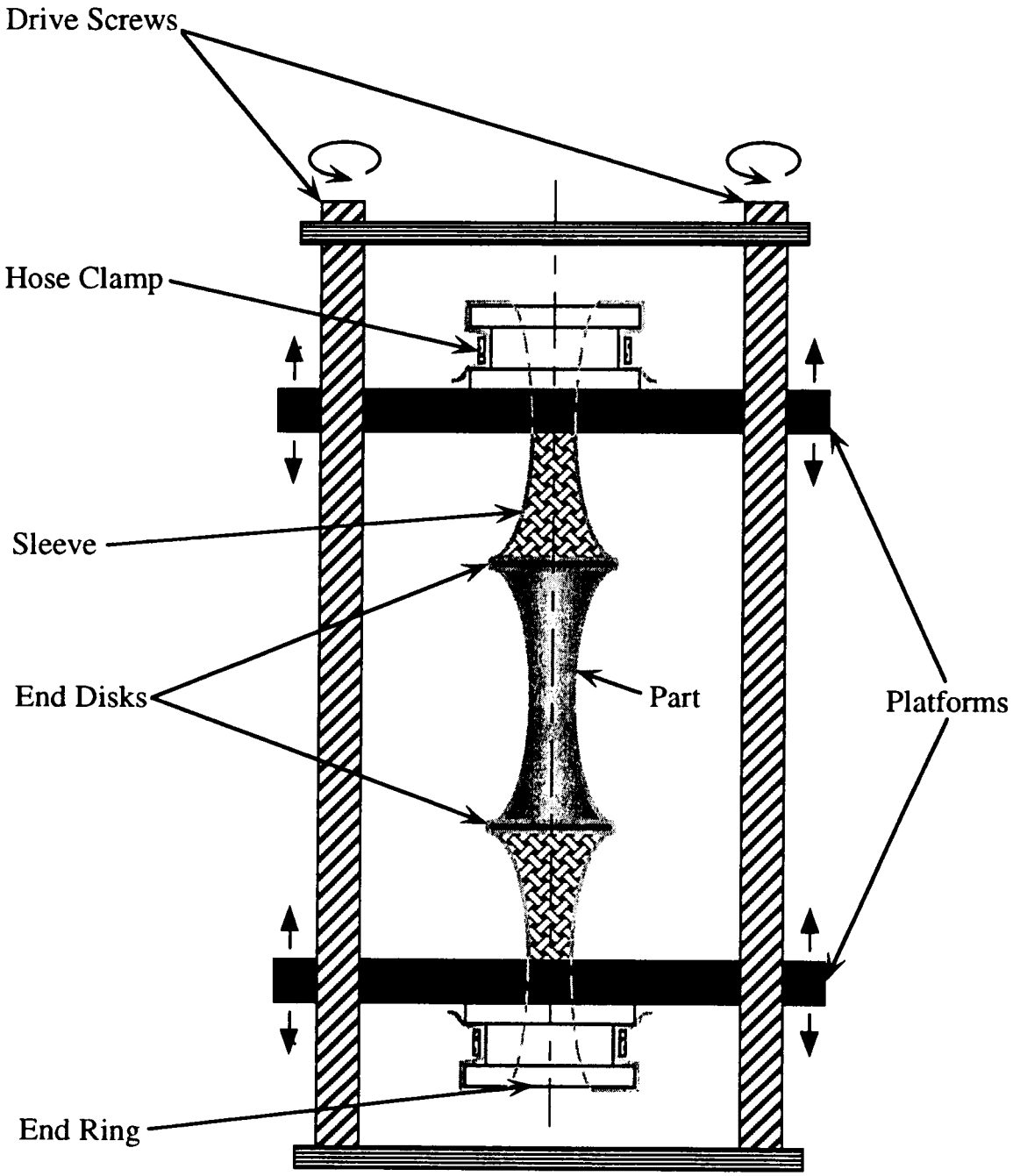

Figure 4.2: Schematic diagram of the device used to place the braided sleeves in uniform, axisymmetric tension.

features, refer to Chapter 5, Section 2 and Appendix B. The device required for these experiments consists of a set of two circular platforms which are moved by drive screws. A sleeve is attached to circular end rings which are then attached to the platforms of the device. Two end disks are placed inside the sleeve to form the desired shape. When tension is applied by turning the drive screws in tandem, the sleeve assumes a shape based on the size and placement of the end disks.

The experiments involved fiberglass sleeves with braid angle of 45° and two nominal diameters, 9" and 11". To fabricate test membranes, pieces of sleeve were weighed and cut. Based on the diameter of a given test sleeve, an end ring was selected. The sleeve was fed through the center of the end ring and then folded back over the outer surface of the ring. A hose clamp was used to secure the end of the sleeve to the ring. A teflon band was taped over the adjustment screw along the inner surface of the hose clamp to prevent the clamp from damaging the sleeve. The clamp was tightened to the extent necessary for holding the sleeve to the end ring, but to an amount which would still permit the sleeve some slippage under a nominal load.

On the tensioning device, two end disks were placed a predetermined distance apart. The sleeve-grip assembly was fixed to the top platform and carefully pulled over the end disks. The second grip was then attached to the unclamped end of the sleeve in a manner similar to the first grip attachment. Again, the hose clamp was tightened only enough to prevent slippage. Alignment was obtained by applying tension and allowing the sleeve to slip through the grips until all tows were engaged uniformly. When appropriate alignment was obtained, the first clamp was tightened. The sleeve was then pulled through the second grip until the sleeve surface appeared uniform. At this point the hose clamp on the bottom grip was hand tightened.

When the sleeve was secured within the tensioning device, an epoxy resin (Epon 828/V40 with 1:1 mixture) was spread on the area of the sleeve between the end disks using a brush. The epoxy was allowed to cure at room temperature for twenty four hours while maintaining the tension, resulting in the formation of a hardened membrane. The composite membrane was then removed from the tensioning device by first loosening the hose clamps and removing the grip rings from both ends of the sleeve. The end disks were then removed from the ends of the thus formed sleeve/membrane, which was subsequently separated from the device. The dry sleeve at each end of the resin-impregnated area was removed. The membrane was then sanded to remove any surface irregularities caused by excessive amounts of epoxy, and the shape of its surface was recorded by a measuring device.

4.3 Evaluation of Membrane Geometry

The membrane geometry was evaluated by a measuring device which consisted of three parts: a turntable, a caliper with a depth gauge, and a machinist's height measurer. A schematic of this device is shown in Figure 4.3. The tip of the depth gauge on the caliper acts as a locator, which can be positioned touching the surface of the rotating shell at different elevations to map the surface in three dimensions.

The turntable was marked at the desired angles of measurement, e.g., 0°, 45°, 90°, etc., and turned to the zero degree setting. A membrane was placed on the turntable such that its axis corresponded to the axis of table rotation. By moving the caliper along the height measurer and then extending the depth gauge until it touched the membrane, data describing the profile curve of the membrane were obtained. The caliper was moved at one inch intervals parallel to the axis of the membrane and profile curves were measured

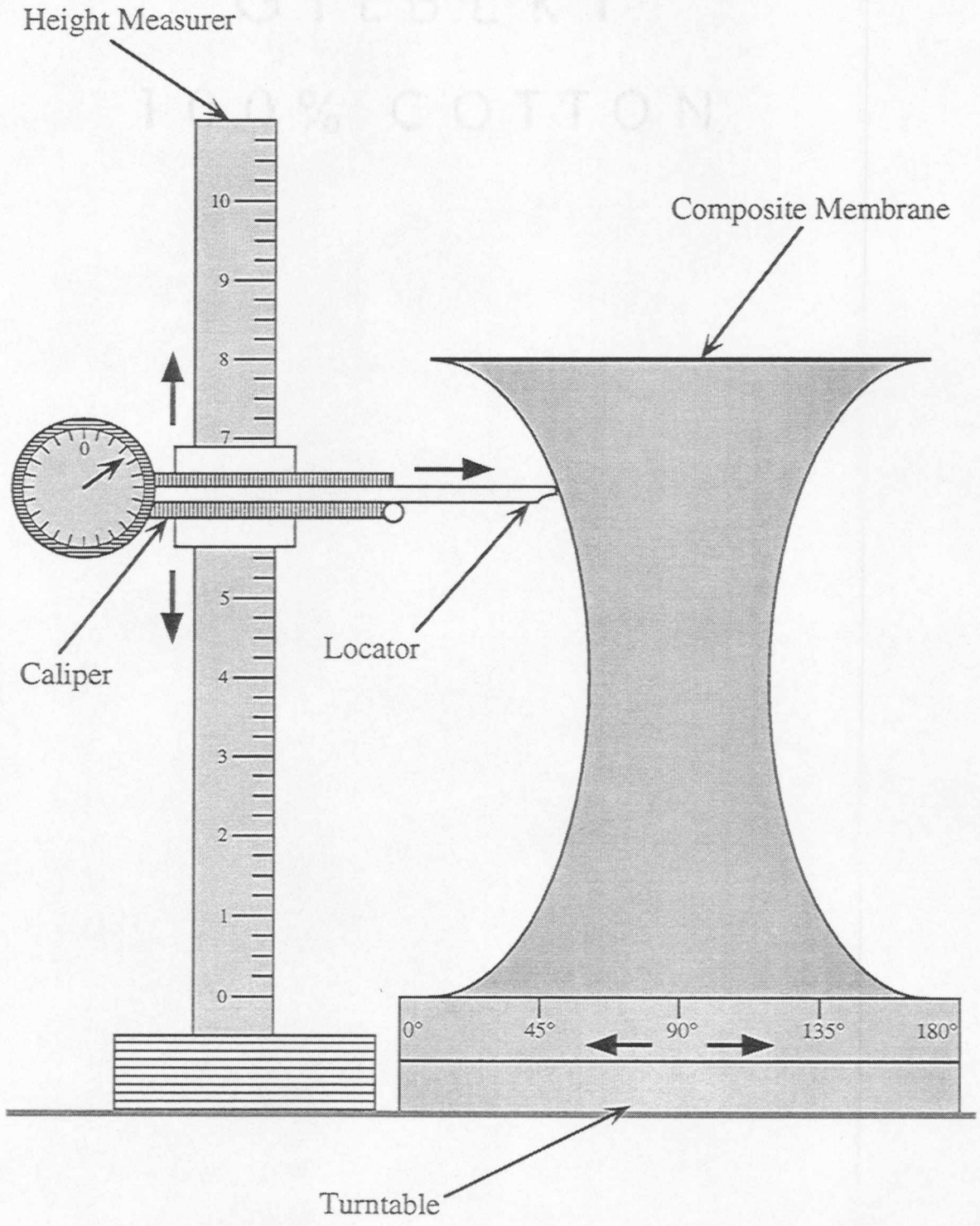

Figure 4.3: Schematic diagram of the measuring device used to obtain the membrane geometric data.

every 45°.

A description of the membrane in cylindrical coordinates was desired so that the data could be directly compared to the results of the analytical solutions in Chapter 3. However, it was not practical to measure the radius r directly. Instead, the evaluation device measures the distance from the height measurer to the surface of the shell. This distance, denoted by δ, must be converted into a radial coordinate by the following procedure. First, a reference circle on the turntable is marked. Then the distance between this reference and the turntable's axis of rotation, denoted r_d, is measured. The caliper is calibrated so that $\delta = 0$ corresponds to the reference circle. The radial coordinate is thus obtained from the measurement of δ by the formula:

$$r = r_d - \delta$$

The resulting data form a discrete mesh which describes the surface of the shell. Eight profile curves were taken from each of three membranes to be compared to the analytically predicted profile curves. In addition, since the foregoing numerical description generated a three dimensional image of the shell surface, it enabled the evaluation of the degree of axial symmetry. This data was used to quantify consistency in specimens thereby improving the quality of the fabrication technique.

4.4 Results

Computer programs were written in ANSI C to generate profile curves for each net model from equations (115) and (139). Listings of these programs are contained in Appendix A. The Legendre elliptic integral in (139b) was expressed by Carlson's elliptic

integrals for computational convenience[2]. Equation (115) was used to calculate the profile for a geodesic net. Equations (139) were used to calculate the profile for a Chebyshev net. These results are shown with experimental data in Figures 4.4 and 4.5 for membranes with axial lengths of ten inches and seventeen inches, respectively. It is clear from these figures that the profiles generated from the Chebyshev model provide a much better approximation to the actual shape of the composite membrane than the geodesic meridians. Physically, this indicates that translation of the tows with respect to one another is severely restricted by the tightness of the braid and the friction at tow intersections.

[2] Use of Carlson's elliptic integrals in numerical computations is discussed in [16].

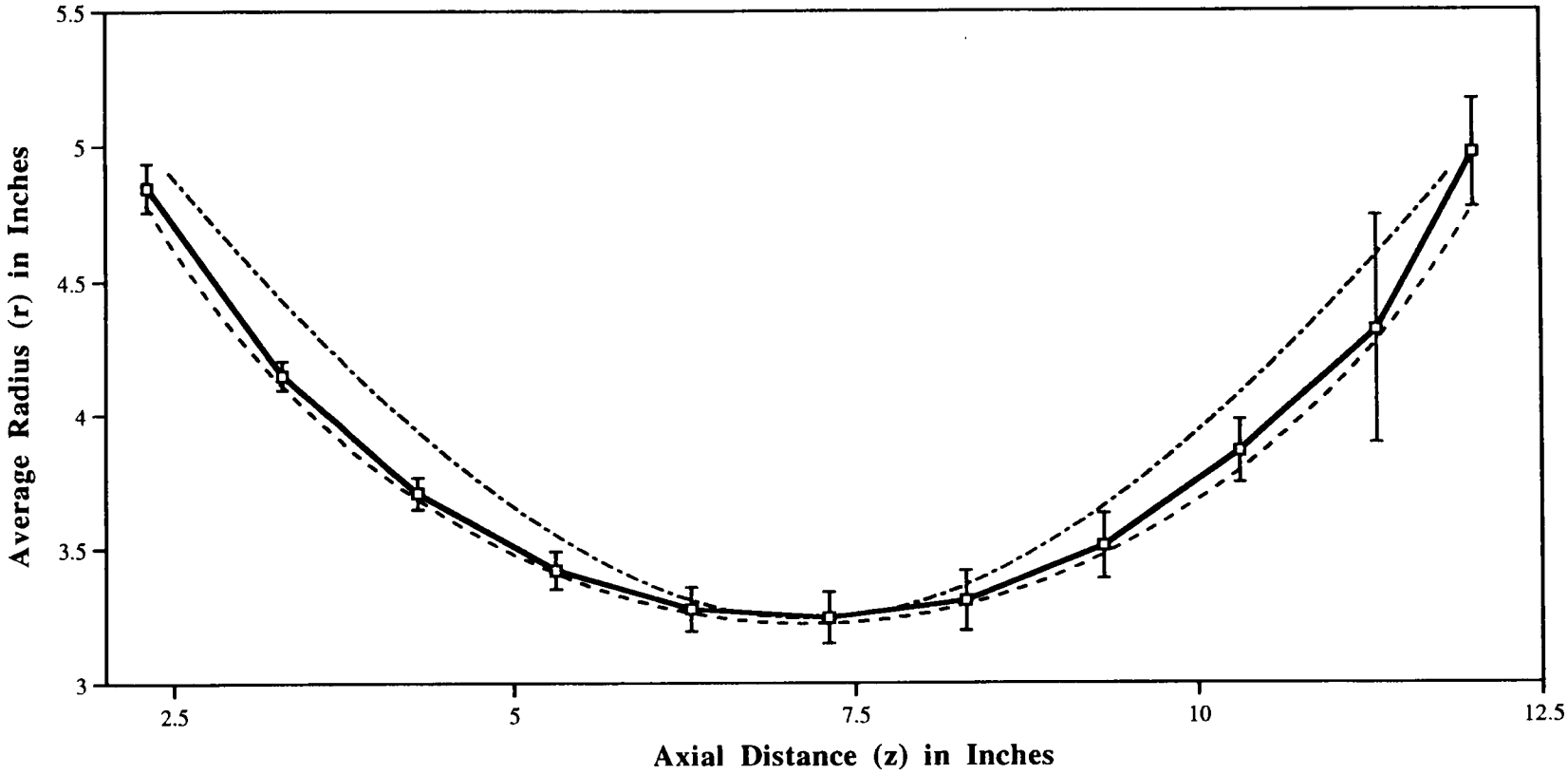

Nominal Diameter: 9 in

End Diameter: 10 in

Axial Length: 10 in

Average Experimental Meridian

Theoretical Chebyshev Meridian

Theoretical Geodesic Meridian

Figure 4.4: Experimental results and theoretical predictions for membrane with 10 inch axial length.

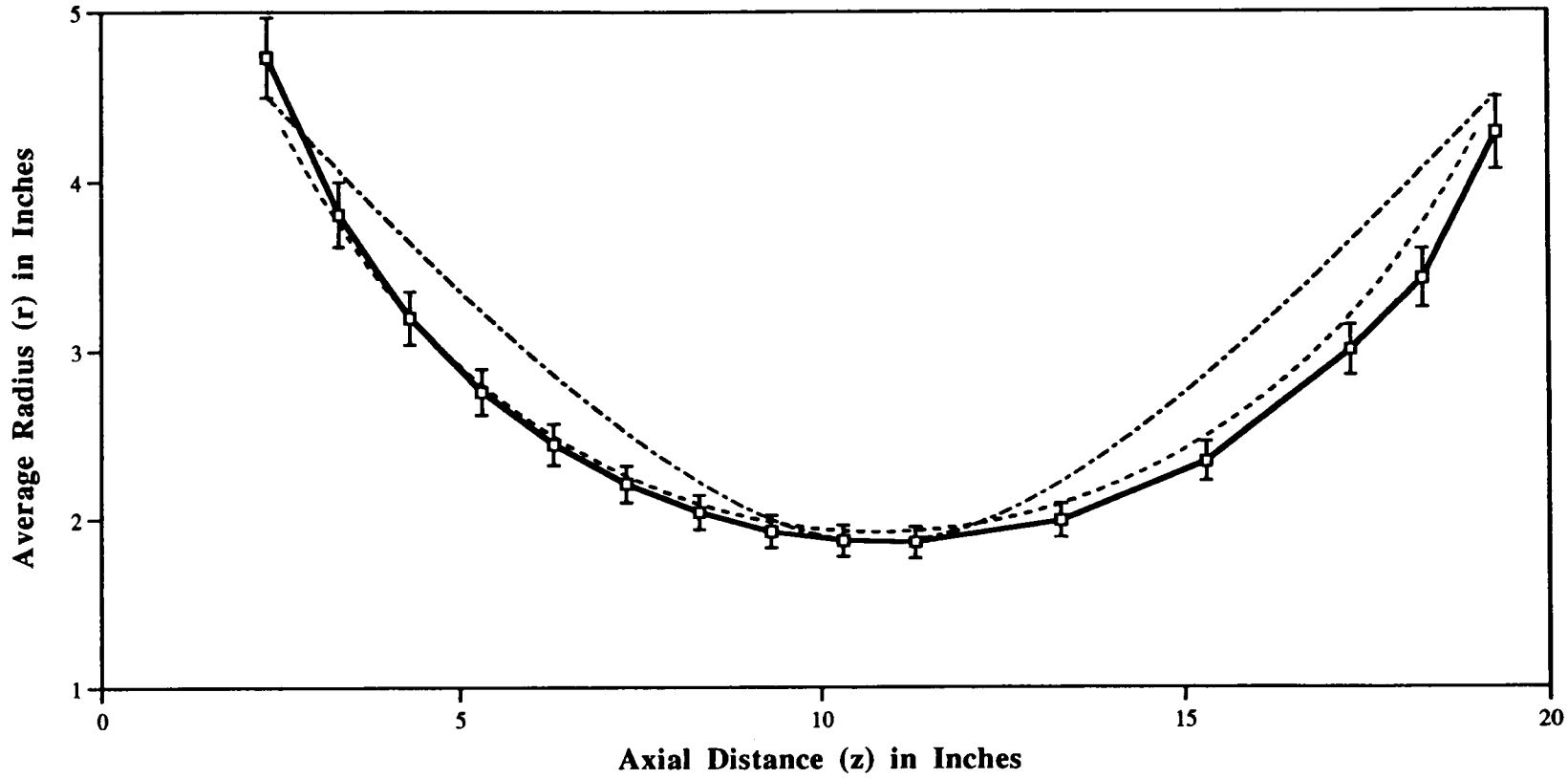

Figure 4.5: Experimental results and theoretical predictions for membrane with 17 inch axial length.

CHAPTER 5

Feasibility of Fabricating Composite Shells by Statically Controlled Geometry

5.1 Basic Considerations

We now turn to demonstrating the feasibility of producing shells by statically controlled geometry. In Chapter 4, the Chebyshev net was determined experimentally to be the best model of a braided sleeve for the present considerations. Composite membranes were produced by tensioning single braided sleeves, adding a polymer matrix and curing. These membranes are examples of structures produced by statically controlled geometry. Paralleling composite laminate plate fabrication, the single sleeve may be augmented by additional sleeves to produce thicker, "stacked" structures. However, the concept of such "stacking" or, more appropriately, nesting of several sleeves has implications beyond simply producing a thicker part. Nesting sleeves also allows greater control over the shape of the resultant shell.

With the net model established, it is possible to use the geometric results derived for Chebyshev nets in Chapter 3 to motivate an approach to simultaneously produce a thicker structure and increase the versatility of statically controlled geometry. Using equations (139), the meridians of two engaged sleeves having nominal diameters of nine inches and eleven inches with identical end diameters and axial lengths are shown in Figure 5.1. Before engagement of the sleeve tows, there is no topological reason that the sleeve with larger nominal diameter cannot be placed inside the sleeve with smaller nominal diameter. When the sleeves are engaged in such a configuration, there will be

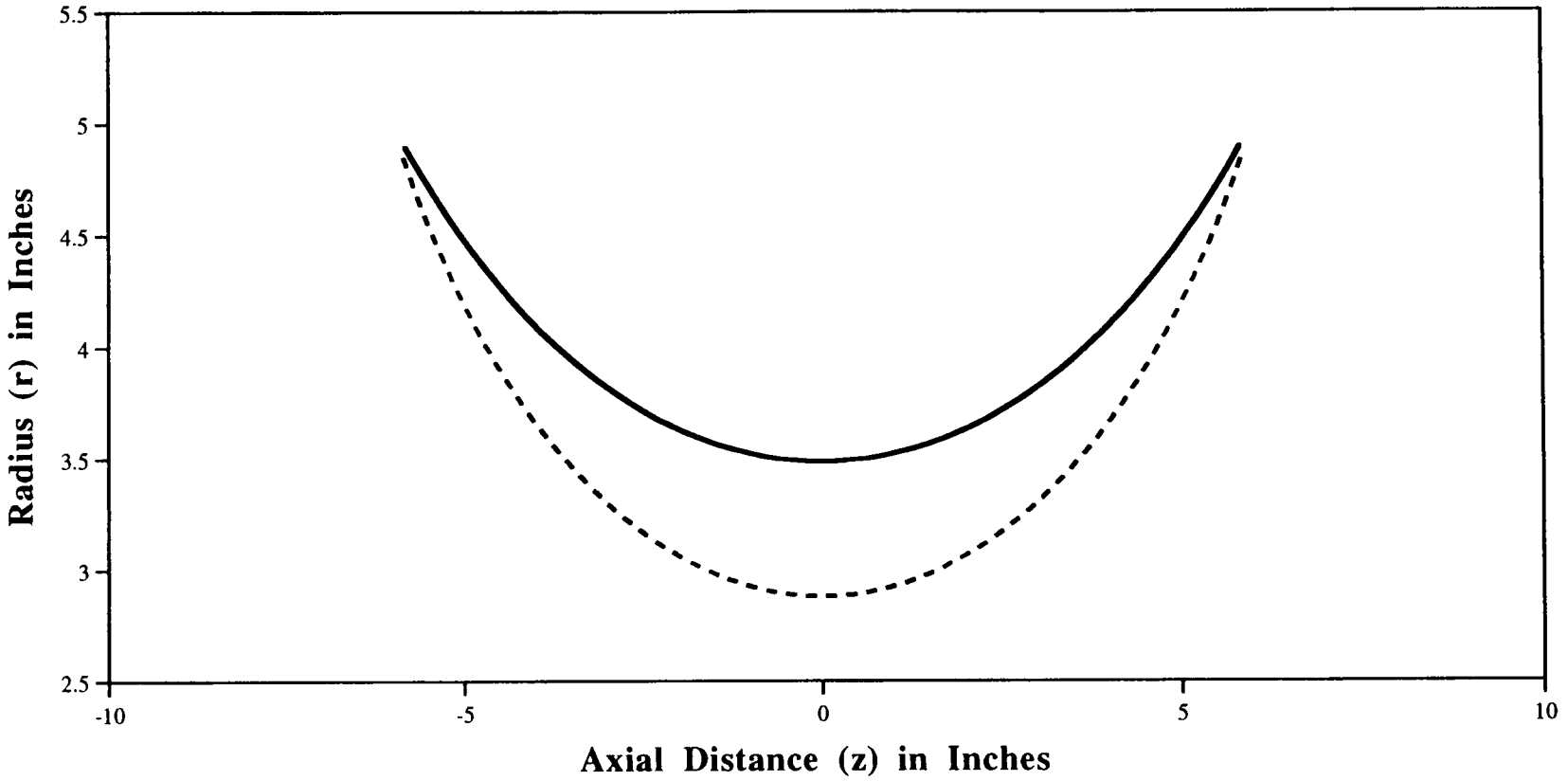

End Diameters: 10 inches

Axial Length: 10 inches

——— 11 inch nominal diameter

- - - - - 9 inch nominal diameter

Figure 5.1: Theoretical profile predictions for Chebyshev nets with nominal diameters of 9 inches and 11 inches.

interaction between the sleeves similar, in principle, to a shrink fit.

It is now conceivable that profile curves occupying the space between the two asymptotic meridians shown in Figure 5.1 may be obtainable from different patterns of tension on the two sleeves. Kuznetsov and Weitsman have derived analytical results for this case in [4]. A nested assembly may be formed by placing a braided sleeve of larger nominal diameter into a braid of smaller nominal diameter. Different shapes may be produced by varying the pattern of tension on a nested assembly, thus achieving a statically controlled geometry. We now turn to the possibility of fabricating composite shells from these nested assemblies of sleeves.

The difference between a membrane and a shell is that a shell is capable of supporting bending loads, while a membrane is not. The simplest example of a braided composite shell fabricated by statically controlled geometry is constructed from a single sleeve under tension with rigid rings added to each end of the sleeve. These single sleeves are similar to the membranes discussed in the foregoing chapter, but the rigid end rings curtail kinematic deformation of the membrane ends. The cured sleeve reinforced in this manner is capable of supporting bending loads, and is therefore a shell. A cured nested assembly is also capable of supporting bending loads

Since single sleeves under tension always have negative Gaussian curvature, their nesting will yield an anticlastic shell. To obtain a greater variety of shapes, an inflatable bladder may be inserted within the inner sleeve and used to apply hydrostatic pressure by injecting fluid into the bladder. This technique may be used for producing clastic shells with positive Gaussian curvature. Similarly, other external loads such as clamps and indentors could be used to shape the nested assembly. The selective use of different braided sleeves in a nested assembly along with the incorporation of inflatable bladders

and clamps enables the manufacturing of a variety of rotationally symmetric shapes. Conceptual diagrams of fabrication for the cases of an anticlastic shell involving a two-sleeve nested assembly and a clastic shell utilizing an inflatable bladder are shown in Figure 5.2 and Figure 5.3, respectively.

Finally, utilizing plates with non-circular geometries as end disks for forming the membrane geometry, it should be possible to produce non-axisymmetric membranes and shells. However, the details of such shapes go beyond the scope of this work.

5.2 Tensioning Device

The tensioning device mentioned in Section 4.2 in conjunction with the sleeve model experiments was designed to produce nested assemblies and internal bladders, as well as single sleeve membranes. There were three basic requirements for the tensioning device. The first is that it must uniformly and axisymmetrically pull at least two nested sleeves with independent levels of tension. The second is that it must allow surface loading mechanisms, such as inflatable bladders, to be applied. Finally, it must accommodate different sizes of sleeve and allow different configurations for sleeves of common size. Available equipment was found insufficient for the purpose of tensioning and loading sleeves to a wide variety of shapes, therefore a device was designed and constructed. It was constructed according to the specifications detailed in Appendix B. A schematic of the tensioning device is shown in Figure 5.4. The device consists of four platforms (P1, P2, P3, P4). The two bottom platforms (P3, P4), hereafter called holding platforms, are fixed to four threaded shafts (S1, S2, S3, S4) by tightening eight nuts around each platform. The holding platforms are intended to be stationary during the tensioning process, but they can be adjusted by manipulating the holding nuts. The four

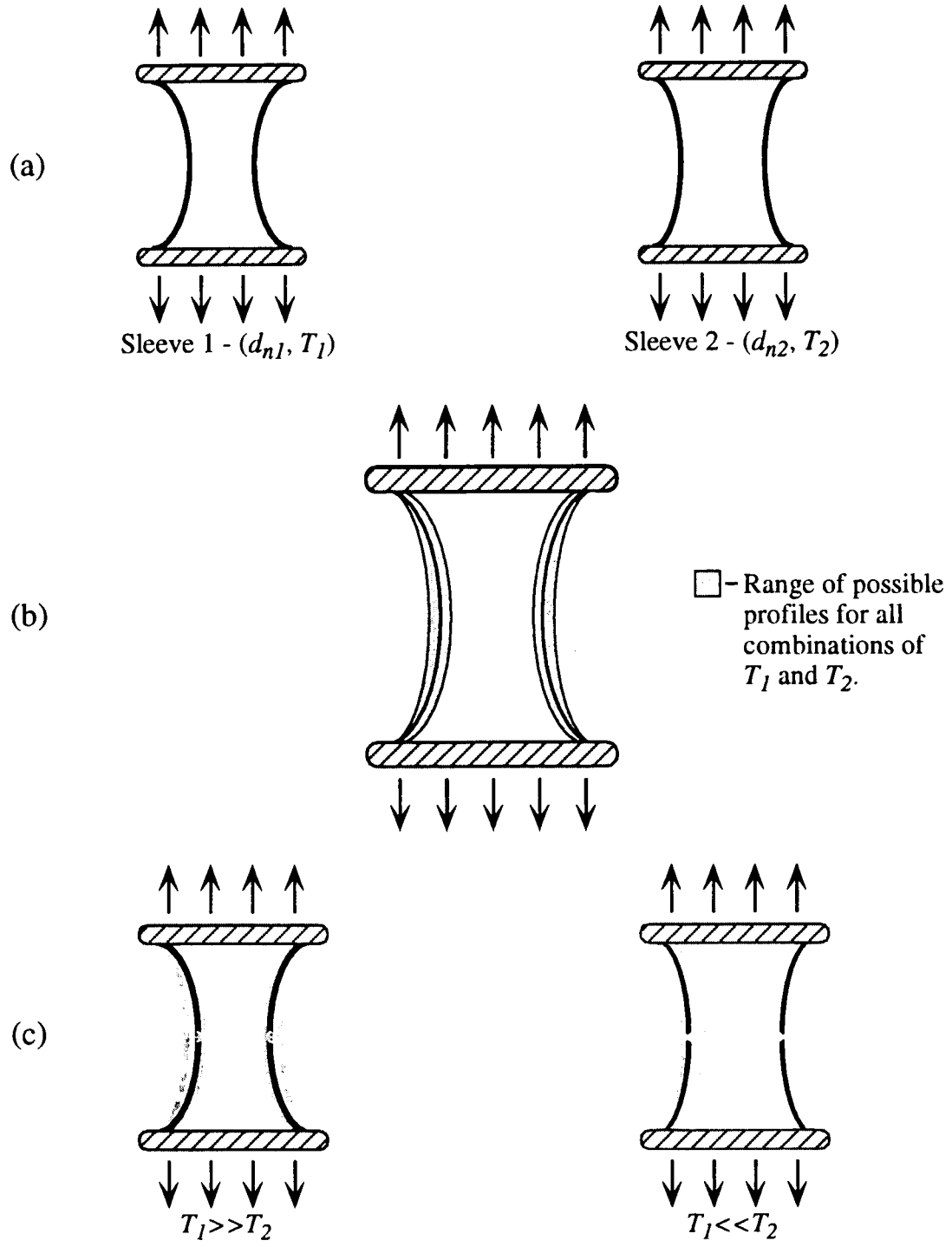

Figure 5.2: (a) Asymptotic configurations for sleeves 1 and 2 when $d_{n1}<d_{n2}$, (b) sleeves are nested with some combination of T_1 and T_2 to form an assembly, (c) extreme cases for which the assembly approaches its asymptotic limits. (d_n-nominal diameter, T-tension).

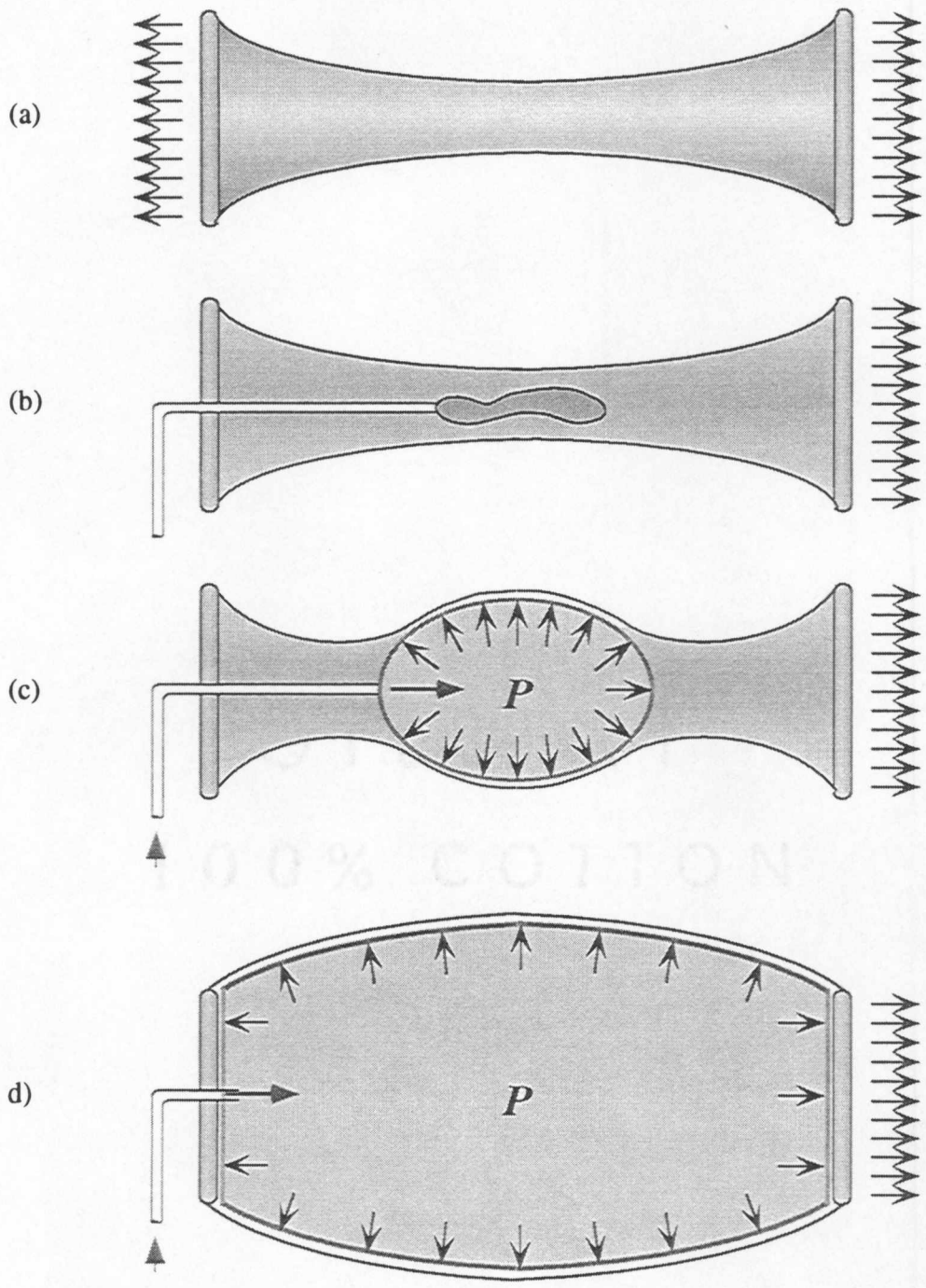

Figure 5.3: Conceptual diagram for producing a clastic shell: (a) a sleeve or nested assembly under nominal tension, (b) an inflatable is inserted into the structure, (c) fluid is pumped into the inflatable to produce internal pressure, (d) a prescribed shape is obtained corresponding to a required level of pressure.

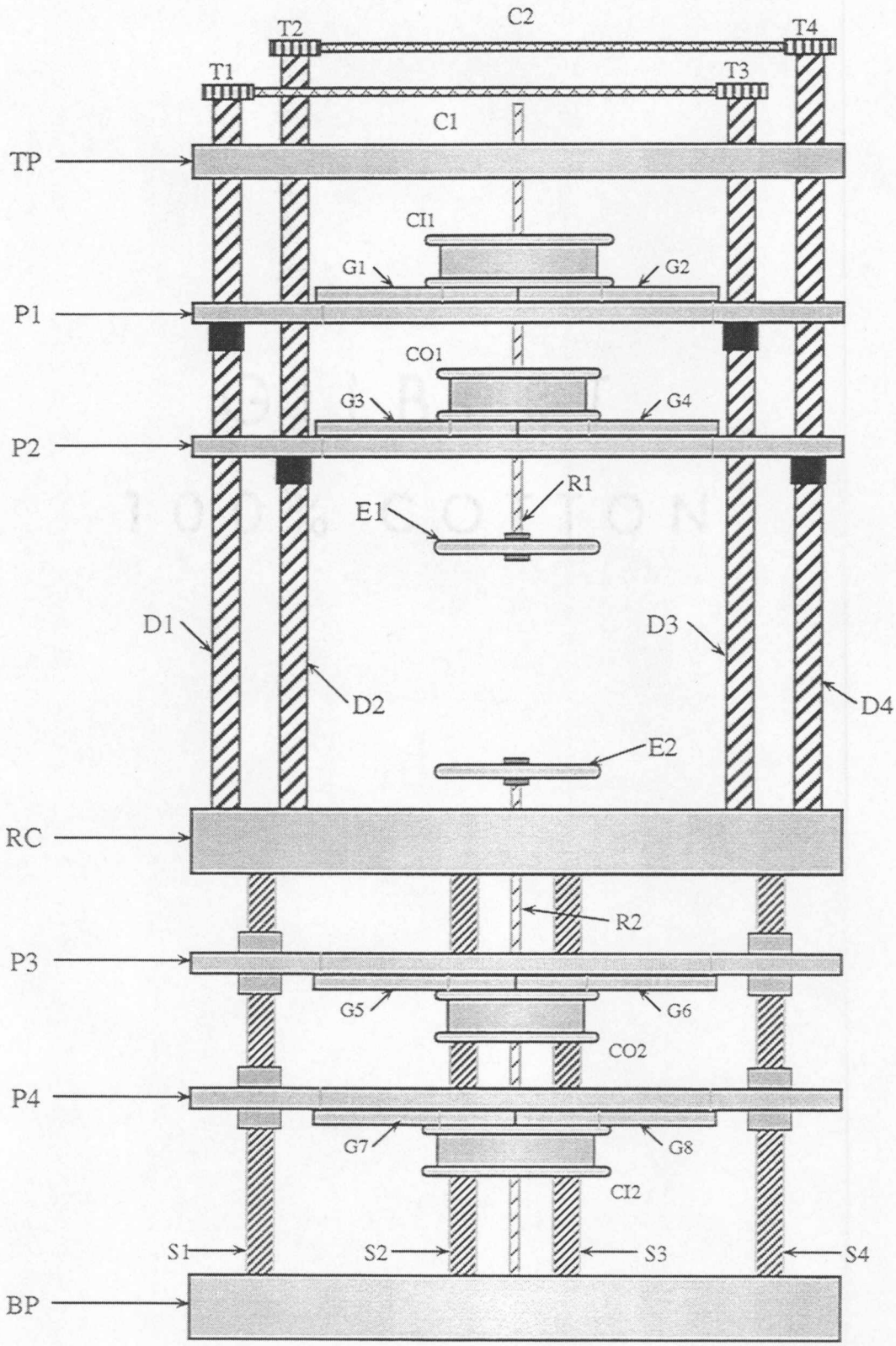

Figure 5.4: Schematic diagram of the tensioning device.

threaded shafts are fixed between a bottom plate (BP) and a reinforcing center ring (RC). The bottom plate is bolted to the floor and the assembly is oriented vertically. Four thrust bearings are embedded in the top of the reinforcing ring. The thrust bearings support four drive screws (D1, D2, D3, D4). The two upper platforms (P1, P2), which will be referred to as the top and bottom tensioning platforms, are each equipped with two ball bearing nuts centered between the inner and outer diameters of the platforms and offset 180° from one another. The platforms are configured so that each pair of ball bearing nuts rides on a separate pair of drive screws. A top plate (TP) maintains the alignment of the four drive screws.

Sprockets (T1, T2, T3, T4) are attached to the tops of the four drive screws above the top plate (TP). Two closed chains (C1, C2) are used to couple the sets of drive screws corresponding to the two platforms (P1, P2). Finally two crank nuts are fixed to the tops of two of the sprockets. Turning one of the crank nuts rotates two of the shafts and turning the other nut rotates the other two shafts. When the crank nut is turned with a wrench, the coupled shafts associated with that nut rotate. This rotation causes the platform supported on that pair of screws to move or apply tension to the sleeve. This tension may be maintained after removing the torque from the drive by placing a pin between the chain and one of the sprockets.

Two end disks (E1, E2) define the axial length of the part. The top part end disk (E1) is suspended from the top plate (TP) along the central longitudinal axis of the device by a rod (R1). Similarly, the bottom part end disk (E2) is supported by a rod (R2) attached to the bottom plate (BP). The ends of the support rods are threaded and each part end disk is fixed to its rod by two opposing nuts. The distance between the part end disks defines the part region, or the area of the sleeve that will eventually be impregnated with resin. The part end disks define the end geometry of the shell and may have any shape,

but they must fit inside both sleeves of the assembly without damaging either of the sleeves. Photographs of the tensioning device are shown in Figure 5.5.

5.3 Procedure for Shell Fabrication

Single sleeves were placed in the tensioning device and grasped in the manner described in Section 4.2. However, to implement the internal loading necessary to fabricate a shell from a nested assembly or internal inflatable, some additional steps must be incorporated. The procedure for fabricating a shell from a nested assembly is discussed and the additional steps for applying internal pressure with an inflatable bladder are included.

First, two part end disks were placed in the tensioning device a prescribed distance apart. The part end disks were wrapped in release film and their outer edges were lined with release tape. The disks were then treated with a release agent. If an inflatable bladder were to be utilized, it was placed between the part end disks. Balloons and rubber balls were used as inflatable bladders. The fluid supply hose was fed through a hole in one of the disks and attached to the inflatable. The bladder was deflated enough to allow it to be inserted into the sleeves without resistance.

Away from the device, a circular end ring (CO1) was attached to one edge of the outer sleeve. This attachment is achieved with a hose clamp around the sleeve and end ring. Then a second end ring (CI1) was attached to one edge of the inner sleeve. Since the nominal diameter of an inner sleeve was larger than the nominal diameter of the associated outer sleeve, the end rings that grasp the inner sleeve were larger also. Consequently, the free end of the inner sleeve was threaded through the outer sleeve end

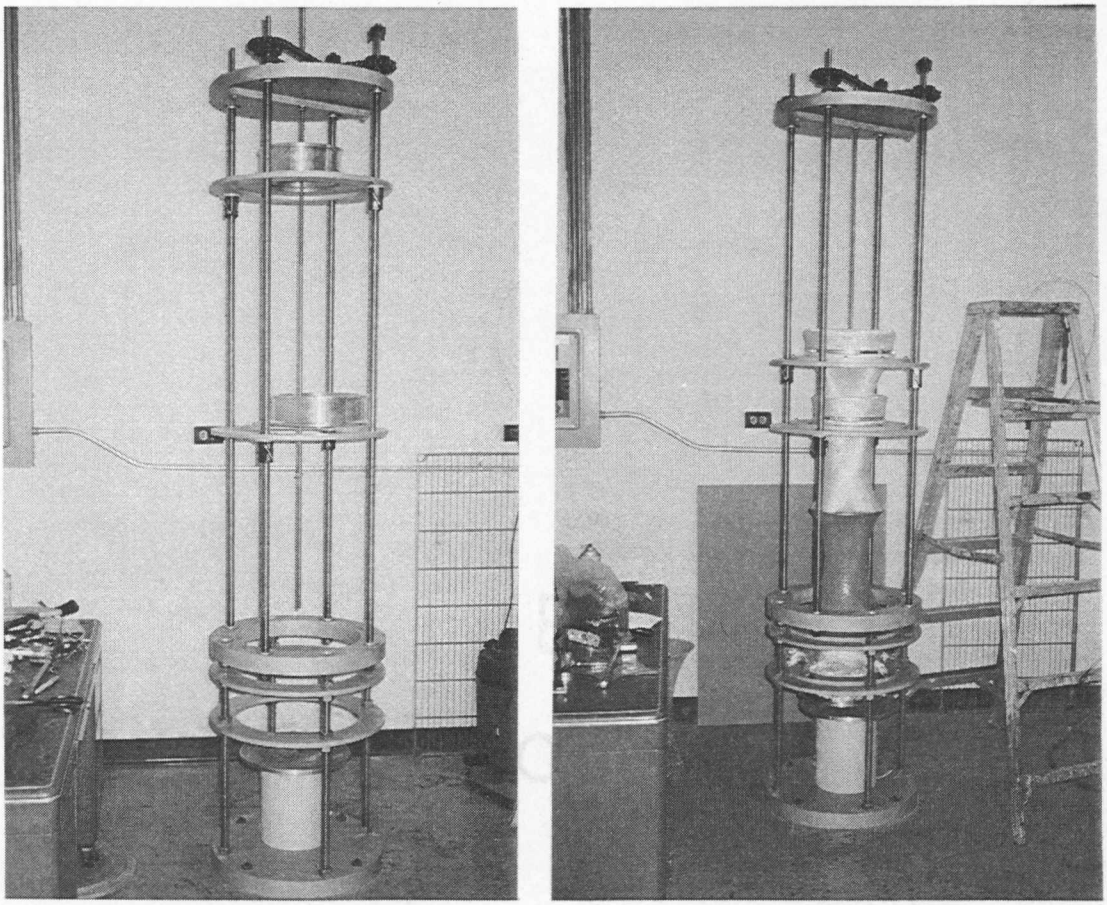

Figure 5.5: Photographs of the tensioning device.

ring (CO1).

The nested sleeves were placed inside the tensioning device. The end ring of the inner sleeve (CI1) was attached to the top tensioning platform (P1) by fixing two semi-circular grips to the top platform (G1, G2). Each end ring must have two associated grips. When these grips are fixed to a platform, they form a circular plate with a hole in the center. The diameter of this hole is less than the outer diameter of the end ring so that the end ring is supported and the sleeve passes through the center hole. Similarly, the end ring of the outer sleeve was attached to the bottom tensioning platform with a corresponding pair of grips (G3, G4).

The inner sleeve was rolled over both of the part end disks. At this point, the distances between the center ring (RC) and each of the tensioning platforms (P1, P2) were adjusted so that the end of the inner sleeve was situated below the bottom holding platform (P4). A second end ring (CI2) was attached to the edge of the inner sleeve with a hose clamp and the grips (G7, G8) were installed on the bottom holding platform (P4). The outer sleeve was fed over the part end disk and gently straightened. The bottom tensioning platform (P2) was adjusted so that the end of the sleeve extended below the top holding platform (P3) enough to allow attachment of the final end ring (CO2). However, the end ring was not yet attached. Instead, the outer sleeve was rolled back up so that only the inner sleeve covered the region between the end disks.

The hose clamps holding the inner sleeve were set to a nominal tension which allowed the sleeve to slip when pulled, but did not permit the end rings to become detached from the sleeve. The inner sleeve was then pulled until all tows were uniformly engaged, in a manner outlined in Section 4.2. Upon obtaining the uniform engagement and eliminating slack spots in the sleeve, the hose clamps were manually tightened with a

screwdriver.

Epon 828 epoxy resin was mixed with V40 hardening agent with a one-to-one stoichiometric ratio. The resulting matrix material was then brushed onto the inner sleeve within the part region. Epoxy was applied from the bottom part end disk to a circle approximately one inch below the top part end disk. This dry band is incorporated because when the sleeve was pulled, it was observed that stretching occurred. It is desirable not to wet the sleeve outside the part region, because the cured epoxy outside the part end disks will complicate their removal from the resulting shell.

Next, the outer sleeve was rolled back down over the part end disks to cover the wet part of the inner sleeve. The final end ring (CO2) was attached to the remaining edge of the outer sleeve and attached to the top holding platform by grips. The procedure to uniformly engage the tows was repeated for the outer sleeve and all hose clamps were tightened. Epoxy resin was then applied to the outer sleeve within the part region, again allowing a dry band within the region to account for sleeve stretching.

If an inflatable were placed inside the assembly, then fluid was pumped into the bladder to manipulate the shape of the nested assembly and generate internal pressure. The drive screws were turned to apply tension to each sleeve. A torque wrench was used to obtain a prescribed torque on each set of drive screws and a pin was utilized to maintain the tension in the sleeve. The epoxy was allowed to cure at room temperature for at least twenty four hours before the shell was removed from the tensioning device. After removal from the device, parts were postcured for three hours at 125° C.

5.4 Feasibility of Statically Controlled Geometry

To demonstrate the feasibility of statically controlled geometry, several shapes were produced using the foregoing equipment and procedure. Membranes of revolution were successfully manufactured by statically controlled geometry during the experiments of Chapter 4. In addition to these, several demonstration shells were fabricated to show the versatility of the technique. An anticlastic shell made up of two nested sleeves is shown in Figure 5.6. Two clastic shells fabricated by inserting inflatables into braided sleeves and applying internal hydrostatic pressure are shown in Figure 5.7 and Figure 5.8. Non axisymmetric shells were also produced to demonstrate that the method is not limited to fabrication of shells of revolution. A membrane produced by offsetting the semi-major axes of two elliptical end plates by 90° is shown in Figure 5.9. As these figures show, widely different shapes may be obtained by statically controlled geometry.

Finally, two identical single-sleeve membranes were fabricated with identical parameters to demonstrate the repeatability of the process. These two membranes are shown together in Figure 5.10.

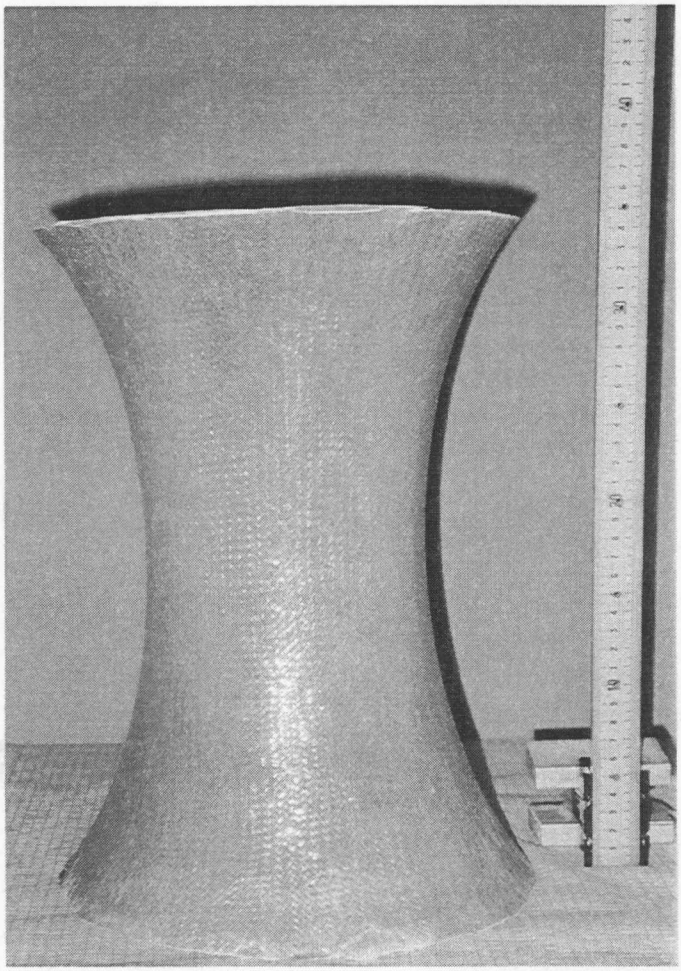

Figure 5.6: Example of a shell fabricated from a nested assembly of two sleeves.

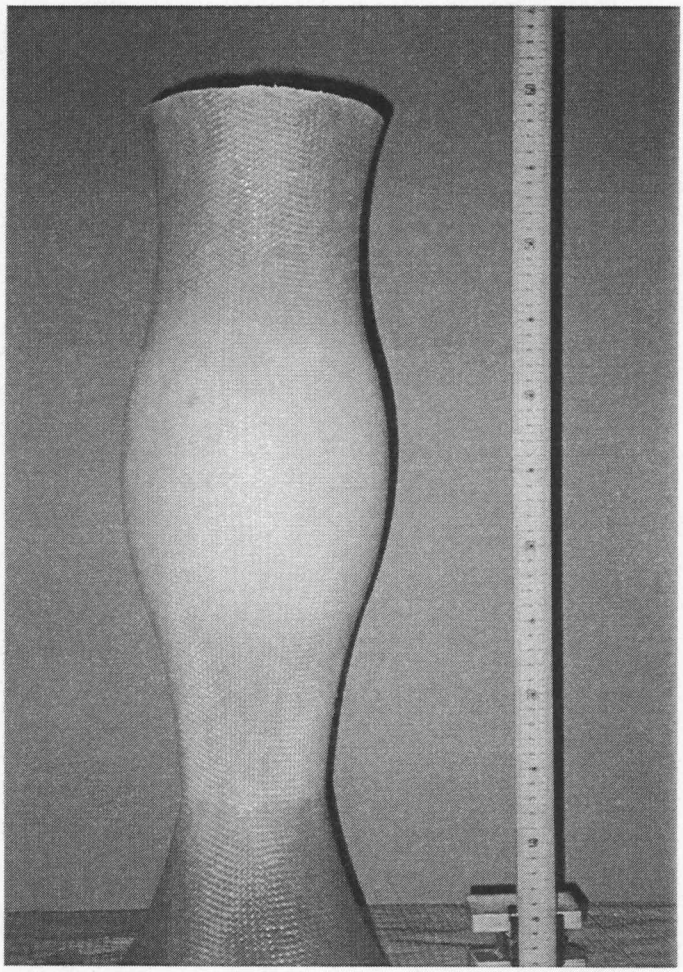

Figure 5.7: A clastic shell with positive Gaussian curvature produced by internal pressure.



Figure 5.8: Example of a clastic shell fabricated with internal pressure and external loads (indicated by white bands around the shell).

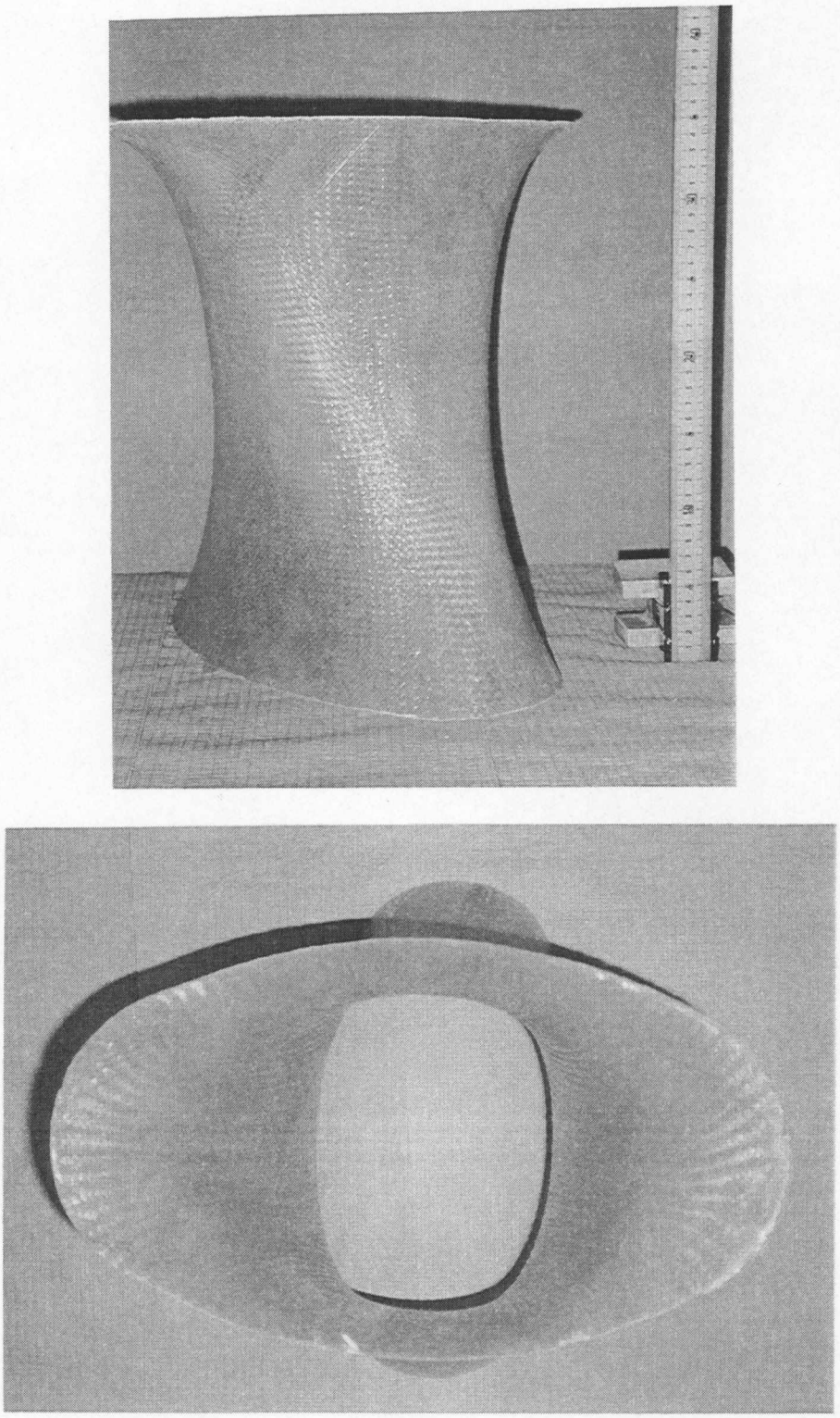

Figure 5.9: Shell without rotational symmetry fabricated with elliptical end disks.

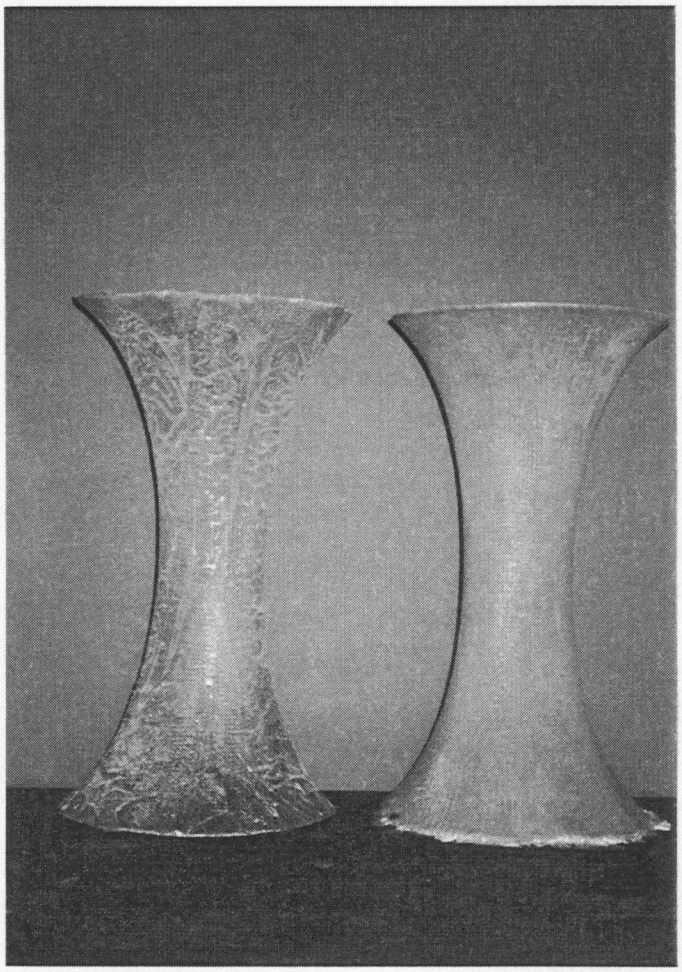

Figure 5.10: Two identical rotationally symmetric membranes with 10 inch end diameters and 17 inch axial length.

CHAPTER 6

Conclusion

6.1 Summary and Conclusions

The goal of this work has been to establish the feasibility of statically controlled geometry as a method for fabricating composite shells. The first step toward this goal was to establish the nature of the interaction between tows at intersections and thereby choose a sleeve model. The only way to unequivocally determine the braided sleeve model was by performing experiments with actual braided sleeves and comparing observed behavior to theoretical predictions. Two theoretical models were available: the geodesic net and the Chebyshev net. Experiments were performed on braided sleeves under uniform, axisymmetric tension to take advantage of the available analytical solutions for asymptotic geodesic and Chebyshev nets. The Chebyshev net was found to be the best approximation to the actual behavior of the sleeve.

With the capability to predict the geometry of a nested assembly, it was desired to demonstrate that producing composite shells was possible. A special tensioning device was built to tension two sleeves with independent levels of tension. The device was also constructed to allow an inflatable to be placed inside the nested assembly to produce shells with positive Gaussian curvature. Using the tensioning device, several composite shells were fabricated. By producing a variety of shells with different shapes, the versatility of the technique was demonstrated.

There are several potential advantages of statically controlled geometry as a

fabrication technique for composite shells. The first is that shells may be produced without using a mandrel or mold. A mandrel is necessary for filament winding, lamination, and direct braiding, but not in the present circumstance of statically controlled geometry. Eliminating the need for a mandrel is a significant step toward reducing manufacturing costs. Another advantage is that, unlike filament winding, no complex computer-controlled system is required. The equipment required to fabricate shells with statically controlled geometry is relatively simple.

Statically controlled geometry is remarkably versatile. Sleeves may be braided, transported, and stored before the shell is actually produced. Then the sleeves may be shaped into the desired geometry by statics. This shaping aspect of the process utilizes simple technology, and could be set up in non-standard manufacturing environments such as at sea or in space. Impregnation of sleeves with resin may take place during the braiding of component sleeves, or during the fabrication of the shell itself.

Statically controlled geometry could be utilized in conjunction with other techniques (e.g., filament winding or lamination). The statically generated structures could be used as a mandrels that are actually incorporated into the final part. In addition to the simple mechanisms presented herein, the shape of the composite shell may be controlled by adding indentors and similar constructions to apply loads to the sleeve. Notably, although most of the shells in this work exhibit rotational symmetry, the new fabrication technique is not limited to that case. A shell with elliptical ends was fabricated to demonstrate that point.

One of the most notable features of this technique is that it is not limited to any particular material system. All shells fabricated for this work were made from fiberglass sleeves and epoxy resin. However, in principle the method could be implemented for

ceramic matrix composites in addition to various polymeric matrices. This possibility extends the potential of statically controlled geometry to a much greater range. One of the primary difficulties with the manufacturing of ceramic composites involves the machining of parts. Statically controlled geometry could provide significant savings in the machining cost of ceramic composite parts by producing desired shapes directly.

This work has demonstrated that braided sleeves may be modeled as Chebyshev nets. The feasibility of the fabrication technique was explored by constructing a special tensioning device and imparting tension on actual braided sleeves. Composite membranes were fabricated from single sleeves. Composite shells were then fabricated by nesting two sleeves. By inserting an inflatable into an assembly, clastic shells were produced. Finally, a sleeve was pulled in a non-axisymmetric configuration to produce a membrane without rotational symmetry. These model shells demonstrate that statically controlled geometry can be used to fabricate shells with a variety of geometries. Ultimately, the advantages of statically controlled geometry can provide a cost effective fabrication technology for composite shells.

6.2 Suggestions for Future Work

The technology for extending the principles of statically controlled geometry to industrial use should be explored. Currently used parts, with geometries that could be feasibly manufactured with the statically controlled geometry technique, should be identified in industry. These parts could then be constructed using the new method. By comparing statically controlled geometry to other methods of fabrication involving both advanced and traditional materials, actual quantitative cost/benefit analyses could be executed. The method must be refined to bring reproducibility within the confidence

intervals required by industry.

Curing methods and appropriate resins should be considered, along with the utilization of prepreg sleeves, which would simplify manufacturing and enhance the shell properties. A suitable scheme for "bagging" the part for resin consolidation and reduction of voids should be pursued. In principle, tensioning devices that may be placed in autoclaves or furnaces are feasible.

The nature of braided sleeves has been established as a Chebyshev net by examining the behavior of the net in a uniform tension field, however experiments should be performed on sleeves in other configurations to determine circumstances under which this model may break down. The tensioning device designed for this work needs improvement, most significantly in instrumentation. To advance the technique to the next level of complexity, a device capable of independently tensioning more than two sleeve at one time must be developed.

The mechanics methodology for the analysis of stress and material deformation of the resultant shell remains to be formulated. In addition to the shell theory applied to different geometries, the questions of anisotropy and inhomogeneity in the shell need to be addressed. Anisotropic shell theory exists but must be tailored to address some of the unique features that result from the use of braided components on curved surfaces. These features include varying thickness, varying fiber volume fraction, and variability of reinforcement orientation embodied in the change in net angle within the surface generated by a braided sleeve. A model addressing these issues needs to be developed, followed by the implementation of stress and deformation analysis. Due to the generally non-linear nature of shells, it will be necessary to develop computational schemes to obtain quantitative results.

REFERENCES

REFERENCES

1. Groves, S. E. "Characterizing the Failure of Composite Structures." *Mechanical Engineering* **113** (1991): 57-60.

2. Peters, S. T. and Humphrey, W. D. "Filament Winding." in *Engineered Materials Handbook, Vol. 1: Composites*, Ed. T. J. Reinhart, ASM International, Metals Park, Ohio (1987): 503-518.

3. Kuznetsov, E. N. and Weitsman, Y. J. United States Patent #5,340,625 (1993).

4. Kuznetsov, E. N. and Weitsman, Y. J. "A New Method of Fabricating Composite Shells." *International Journal of Solids and Structures*, **31:1** (1993): 65-74.

5. Struik, D. J. *Differential Geometry*. Addison-Wesley, Reading, Massachusetts (1961).

6. McConnell, A. J. *Applications of Tensor Analysis*. Dover, New York, New York (1957).

7. Nakahara, M. *Geometry, Topology and Physics*. Institute of Physics Publishing, Philadelphia, Pennsylvania (1990).

8. Shulikovsky, V. I. *Classical Differential Geometry*. (In Russian) Nauka, Moscow (1963).

9. Kuznetsov, E. N. *Underconstrained Structural Systems*. Springer-Verlag, New York, New York (1991): 161-218.

10. Kuznetsov, E. N. "Kinetoelastostatics of Axisymmetric Nets." *ASME Journal of Applied Mechanics*, **53** (1986): 891-896.

11. Kuznetsov, E. N. "Axisymmetric Static Nets." *International Journal of Solids and Structures*, **18:12** (1982): 1103-1112.

12. Pipkin, A. C. "Equilibrium of Tchebychev Nets." *Arch. Rat. Mech. Anal.* **85** (1984): 81-97.

13. Pipkin, A. C. and Rivlin, R. S. "Minimum-weight Design for Pressure Vessels Reinforced with Inextensible Fibers." *ASME Journal of Applied Mechanics* **30** (1963): 103-108.

14. Rivlin, R. S. "The Deformation of a Membrane Formed by Inextensible Cords." *Archive of Rational Mechanics and Analysis* **2** (1959): 447-476.

15. Voss, A. "Ueber ein neues Princip der Abbildung krummer Oberflächen." *Math. Ann.* **19** (1882): 1-26.

16. Press, W. H., et al. *Numerical Recipes in C*, 2nd ed. Cambridge University Press, New York, New York (1992): 261-269.

APPENDICES

APPENDIX A

Computer Programs for Membrane Prediction

This appendix contains the source code, written in ANSI C, for the computer programs used to generate theoretical profile data for geodesic and Chebyshev asymptotic rotationally and reflectionally symmetric nets. These routines are based on the equations presented in Chapter 3.

Asymptotic Geodesic Prediction

```
#include <stdlib.h>
#include <stdio.h>
#include <math.h>

/ *     GEODESIC Net profile prediction:
        Given the input of sleeve equatorial radius, shell axial length, and constrained
        end diameter, this program calculates profile data for the resulting one-sheet
        hyperboloid of revolution
* /

/ *     Function Prototypes     * /
/ *             In this module: * /

void                    LFeed(void);
void                    Flush(void);

void    LFeed( void)
{
        printf("\n");
}

void    Flush( void )
{
        while ( getchar() != '\n' )
        ;
}

void    main( void )
{
        int i, flag, numOfPoints;
        double  rNom, L, eD, graphOffset, zmin, zmax, Pi=3.141592654;
        double re, u, r, r2, RefAngle1, RefAngle2, f, fmid;
```

```
        double dr, rMin, rMin2, rEnd, b, du, z, rt;
        char    fileName[10], dummy;
        FILE *fp;

/* Set up output file for console output -------- */
        printf("Enter file name (10 chars max): \n");
        scanf("%s", fileName)
        strcat(fileName,".dat");
        fp=fopen( fileName, "w");

        LFeed();
/*  Get  Data  ----------------------------------- */
        printf("Enter sleeve equatorial radius:  ");
        scanf("%Lf", &rNom); LFeed();
        printf("Enter axial dimension       : ");
        scanf("%Lf", &L);     LFeed();
        printf("Enter end diameter          : ");
        scanf("%Lf", &eD);    Flush();
        LFeed();        LFeed();

/* Calibrate to Experimental Graph ? ------------ */
        printf("Would you like to calibrate to an experimental graph? ");
        dummy=getchar(); LFeed();
        if ((dummy == 'n') || (dummy =='N'))
        {
                zmin = 0.0;
                zmax = 0.0;
        }
        else
        {
                printf("\tEnter Zmin   => ");   scanf("%Lf", &zmin);
                printf("\tEnter Zmax   => ");   scanf("%Lf", &zmax);
        }

        rEnd=eD/2.0;
        L= L/2.0;
        re=rNom;

/ *             Find the reference angle which satisfies the end conditions      * /
        RefAngle1       = Pi/18.0;                      / *     10°     * /
        RefAngle2       = Pi/2.0;                       / *     90°     * /
        rMin            = sin(RefAngle1)*re;
        rMin2           = sin(RefAngle2)*re;
        r       = sqrt( DSQR(re)+(DSQR(L*rMin)/( (re+rMin)*(re-rMin) )) );
        r2      = sqrt( DSQR(re)+(DSQR(L*rMin2)/( (re+rMin2)*(re-rMin2) )) );
        f=r-rEnd;
        fmid=r2-rEnd;

        rt=f<0.0  ?  (dr=rMin2-rMin,  rMin):(dr=rMin-rMin2,rMin2);
        while (fabs(rEnd-r) > 0.0001)
        {
```

```
            rMin=rt+(dr*=0.5);
            r       = sqrt( DSQR(re)+(DSQR(L*rMin)/( (re+rMin)*(re-rMin) )) );
            fmid    = r-rEnd;
            if (fmid<=0.0) rt=rMin;
        }
        printf("rMin=%Lf\n",rMin);
        b=asin(rMin/re)*180.0/Pi;
        printf("Reference angle = %Lf\n",b);

        numOfPoints = 30;
        u       = 0.0;
        graphOffset     = zmin + (zmax-zmin)/2.0;
        du      = L / (double)numOfPoints;
        i=1;  r=0.0;

        while( (u<=L) && (r<rEnd) )
        {
            r       = sqrt( DSQR(re)+(DSQR(u*rMin)/( (re+rMin)*(re-rMin) )) );
            z       = u;
            fprintf(fp,"%Lg\t%Lg\n",  z+graphOffset,  r  );
            fprintf(fp,"%Lg\t%Lg\n",  graphOffset-z,  r  );
            u       += du;
            i++;
        }
        fclose(fp);

}
```

Asymptotic Chebyshev Prediction

The routines "rf()" and "rd()" are Carlson's elliptic integrals. These functions are found in [16].

```
#include <stdlib.h>
#include <stdio.h>
#include <math.h>

/ *     Given the input of sleeve nominal diameter, shell axial length, and constrained
        end diameter, this program calculates the equatorial radius that will
        result.  This radius may then be used to evalute the constant cos(beta)/sin(theta)
        for a Chebyshev net.
* /

/ *     Function Prototypes     * /
/ *             In this module: * /

void                    LFeed(void);
void                    Flush(void);
double                  rf(double x, double y, double z);
double                  rd(double x, double y, double z);
```

```
void    LFeed( void)
{
        printf("\n");
}

void    Flush( void )
{
        while ( getchar() != '\n' )
        ;
}

void    main( void )
{
        int i, flag, numOfPoints;
        double  dNom, L, eD, graphOffset, zmin;
        double re, u, v, a, R1, R2, k, sh, ch, ch2, m, umax, r;
        double tol, zguess, oldre, dx, rMax, a2, rEnd,b, du, z, zmax;
        char    fileName[10], dummy;
        FILE *fp;

/* Set up output file for console output -------- */
        printf("Enter file name (10 chars max): \n");
        scanf("%s", fileName);
        strcat(fileName,".dat");
        fp=fopen( fileName, "w");

        LFeed();
/*   Get   Data   ----------------------------------   */
        printf("Enter sleeve nominal diameter:  ");
        scanf("%Lf", &dNom); LFeed();
        printf("Enter axial dimension       : ");
        scanf("%Lf", &L);     LFeed();
        printf("Enter end diameter          : ");
        scanf("%Lf", &eD);    Flush();
        LFeed();        LFeed();

/* Calibrate to Experimental Graph ? ------------ */
        printf("Would you like to calibrate to an experimental graph? ");
        dummy=getchar(); LFeed();
        if ((dummy == 'n') || (dummy =='N'))
        {
                zmin = 0.0;
                zmax = 0.0;
        }
        else
        {
                printf("\tEnter Zmin   => ");    scanf("%Lf", &zmin);
                printf("\tEnter Zmax   => ");    scanf("%Lf", &zmax);
        }

        rMax=sqrt(2.0)*dNom/2.0;
```

```
rEnd=eD/2.0;
L= L/2.0;

tol     = 0.005;
zguess = 0.0;
oldre   = rEnd;
dx      = -rEnd;

while (fabs(zguess-L) > tol)
{
        re      =  oldre+(dx*=0.5);
        R1      =  rEnd/re;
        R2      =  re/rMax;
        a       =  sqrt(1.0-DSQR(R2))  *rMax;
        v       =  (log(R1 + sqrt((R1*R1) - 1.0)));
        sh      =  sinh( v );
        k       =  re/a;
        m       =  (1.0 + k*sh)*(1.0 - k*sh);
        ch2     =  DSQR(sh) +1.0;
        printf("a=%Lf\tv=%Lf\tsh=%Lf\tk=%Lf\n",  a,  v,  sh,  k);
        printf("ch2=%Lf\tm=%Lf\n",  ch2,  m);
        zguess = a*sh*( rf( ch2, m, 1.0 ) -(DSQR( sh*k )*rd(ch2,m,1.0)/3.0));
        r       =  cosh(v);
        printf("len=%Lf\tr=%Lf\tre=%Lf\n",  zguess,  r,  re);
        if (zguess<L)   oldre = re;
        LFeed();
}


printf("%Lf",  re);
LFeed();

numOfPoints = 30;
a       =  sqrt(1.0-DSQR(re/rMax))  *rMax;
b       =  re;
k       =  b/a;
u       =  0.0;
umax    =  log( (rEnd/re) + sqrt( DSQR(rEnd/re) - 1.0 ) );
graphOffset     =  zmin + (zmax-zmin)/2.0;

du      =  umax / (double)numOfPoints;
for (i=1; i<=numOfPoints; i++)
{
        sh      =  sinh( u );
        ch      =  cosh( u );
        ch2     =  DSQR( ch );
        r       =  b*ch;
        m       =  (1.0 + k*sh)*(1.0 - k*sh);
        z       =  a*sh*( rf( ch2, m, 1.0 ) -(DSQR( sh*k )*rd(ch2,m,1.0)/3.0));
        fprintf(fp,"%Lg\t%Lg\n",  z+graphOffset,  r  );
        fprintf(fp,"%Lg\t%Lg\n",  graphOffset-z,  r  );
```

```
        u       += du;
        if (u>umax) u=umax;
}
fclose(fp);}
```

APPENDIX B

Design Specifications for the Tensioning Device

This appendix contains the specifications for the tensioning device discussed in Chapter 5. It contains design drawings for each component of the tensioning device.

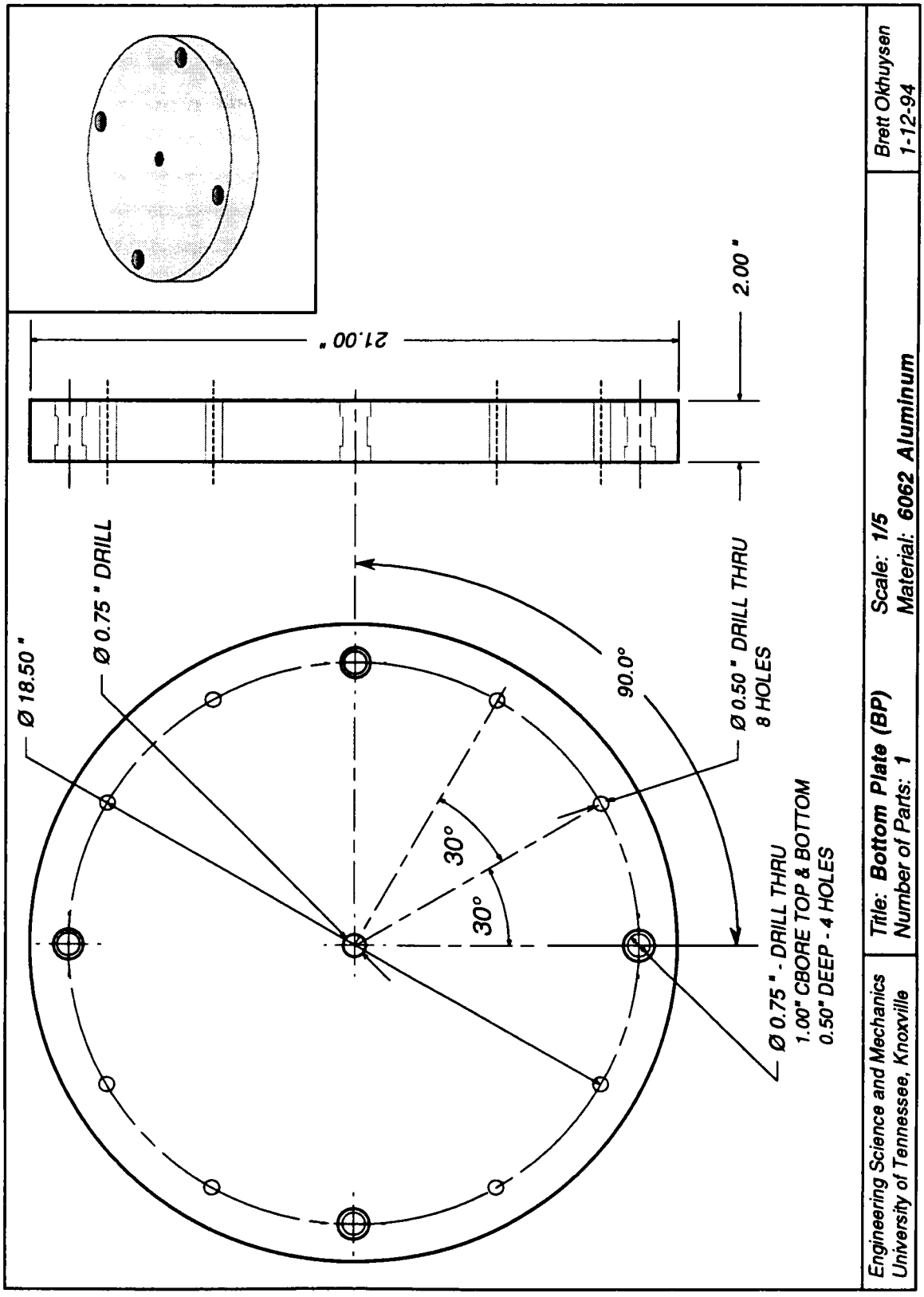
Ø 18.50 "
Ø 0.75 " DRILL
21.00 "
2.00 "
90.0°
30°
30°
Ø 0.50 " DRILL THRU
8 HOLES
Ø 0.75 " - DRILL THRU
1.00" CBORE TOP & BOTTOM
0.50" DEEP - 4 HOLES
Engineering Science and Mechanics
University of Tennessee, Knoxville
Title: Bottom Plate (BP)
Number of Parts: 1
Scale: 1/5
Material: 6062 Aluminum
Brett Okhuysen
1-12-94

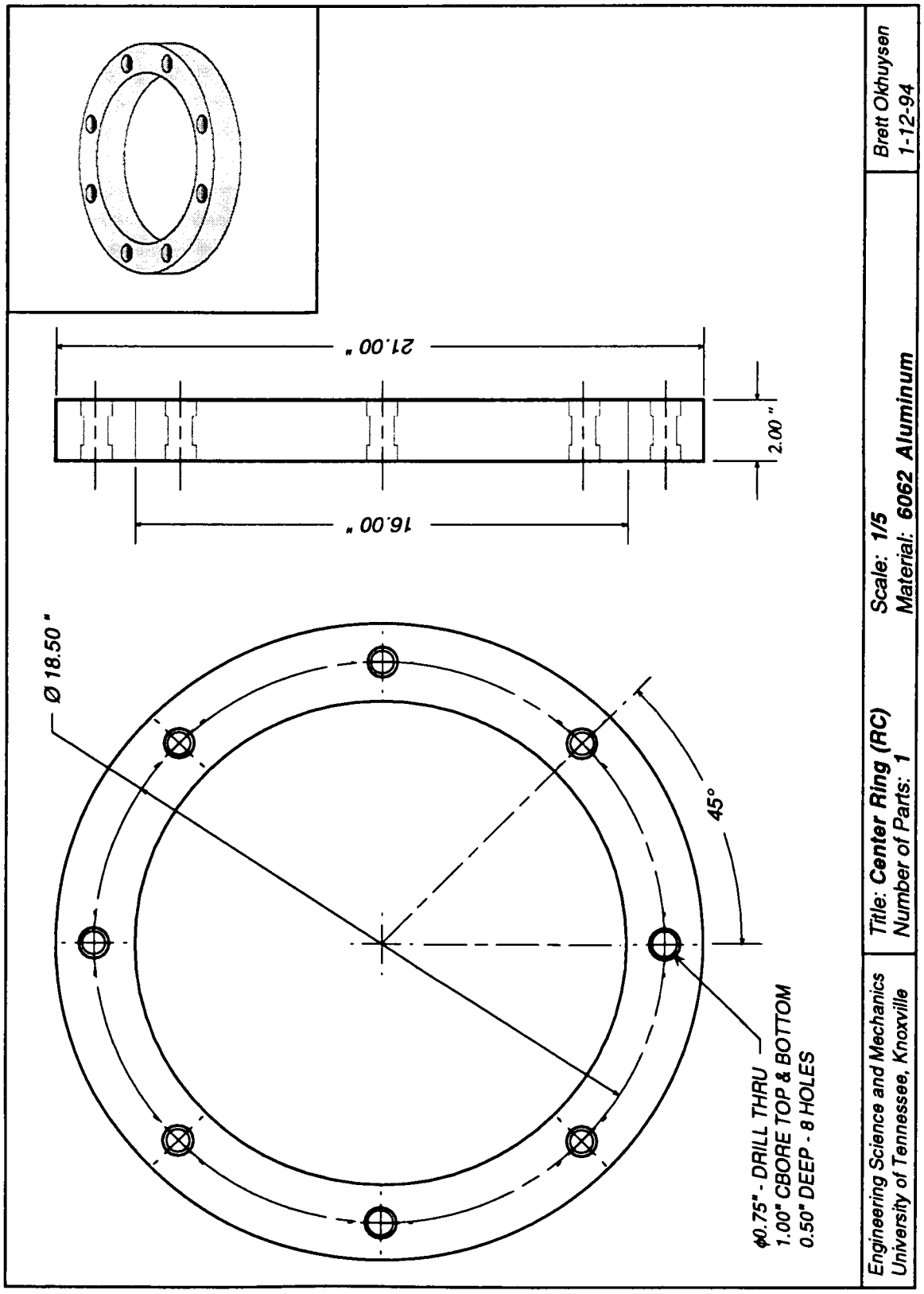
21.00 "
16.00 "
2.00 "
Ø 18.50 "
45°
ϕ0.75" - DRILL THRU
1.00" CBORE TOP & BOTTOM
0.50" DEEP - 8 HOLES
Engineering Science and Mechanics
University of Tennessee, Knoxville
Title: Center Ring (RC)
Number of Parts: 1
Scale: 1/5
Material: 6062 Aluminum
Brett Okhuysen
1-12-94

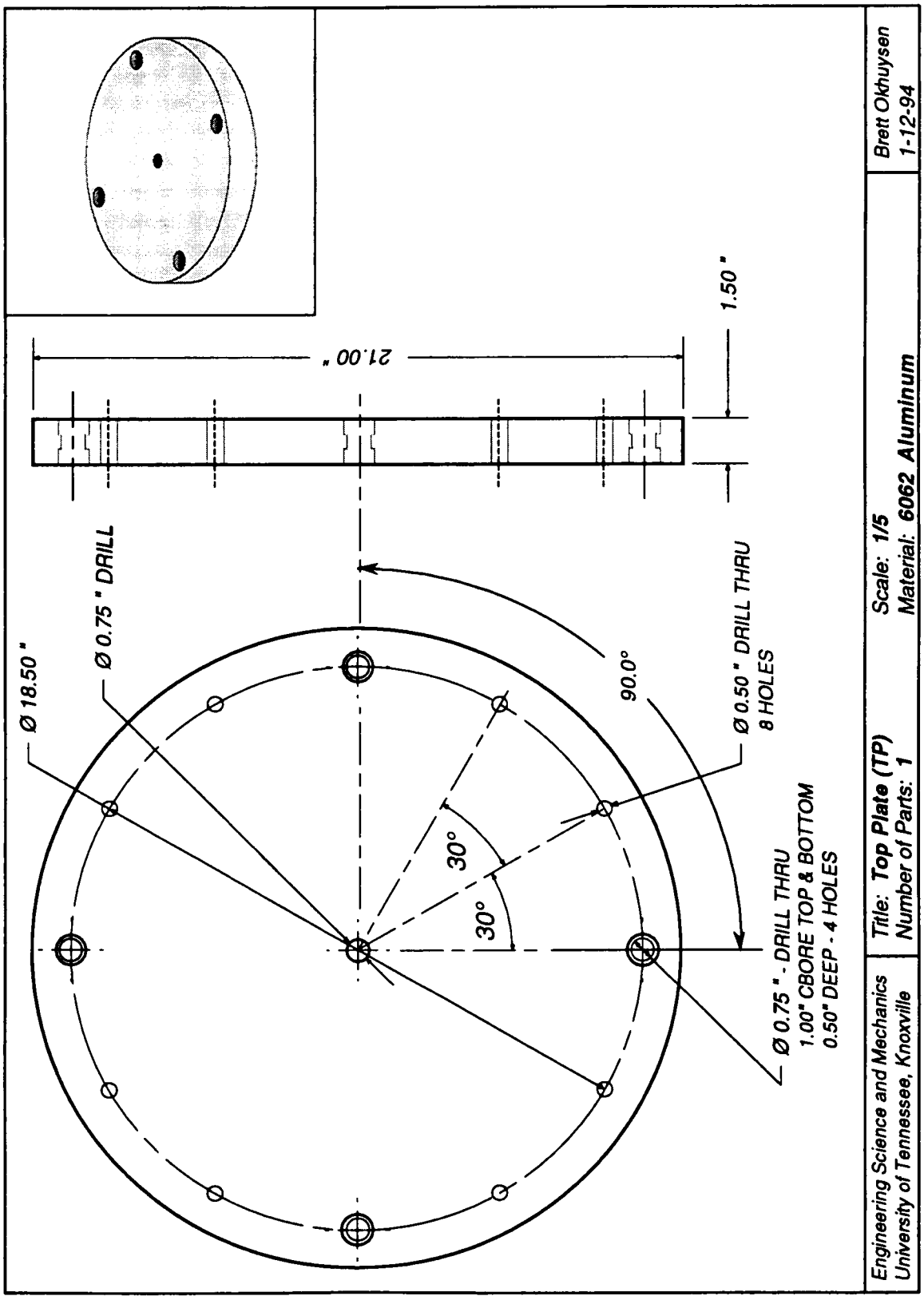
Ø 18.50 "
Ø 0.75 " DRILL
Ø 0.75 " - DRILL THRU
1.00" CBORE TOP & BOTTOM
0.50" DEEP - 4 HOLES
30°
30°
90.0°
Ø 0.50 " DRILL THRU
8 HOLES
21.00 "
1.50 "
Engineering Science and Mechanics
University of Tennessee, Knoxville
Title: Top Plate (TP)
Number of Parts: 1
Scale: 1/5
Material: 6062 Aluminum
Brett Okhuysen
1-12-94

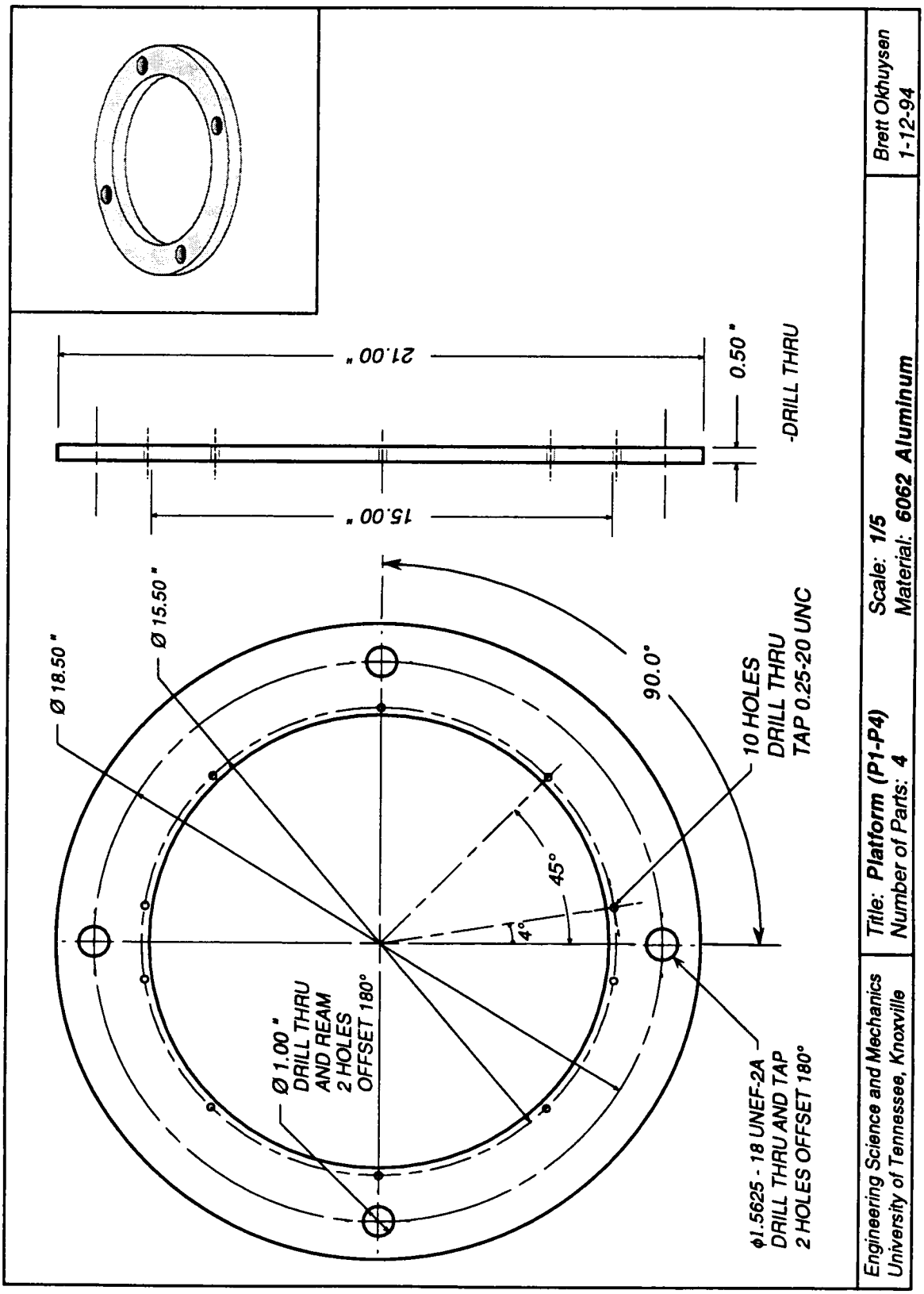
21.00 "
15.00 "
0.50 "
-DRILL THRU
Ø 18.50 "
Ø 15.50 "
90.0°
10 HOLES
DRILL THRU
TAP 0.25-20 UNC
45°
4°
Ø 1.00 "
DRILL THRU
AND REAM
2 HOLES
OFFSET 180°
ϕ1.5625 - 18 UNEF-2A
DRILL THRU AND TAP
2 HOLES OFFSET 180°
Engineering Science and Mechanics
University of Tennessee, Knoxville
Title: Platform (P1-P4)
Number of Parts: 4
Scale: 1/5
Material: 6062 Aluminum
Brett Okhuysen
1-12-94

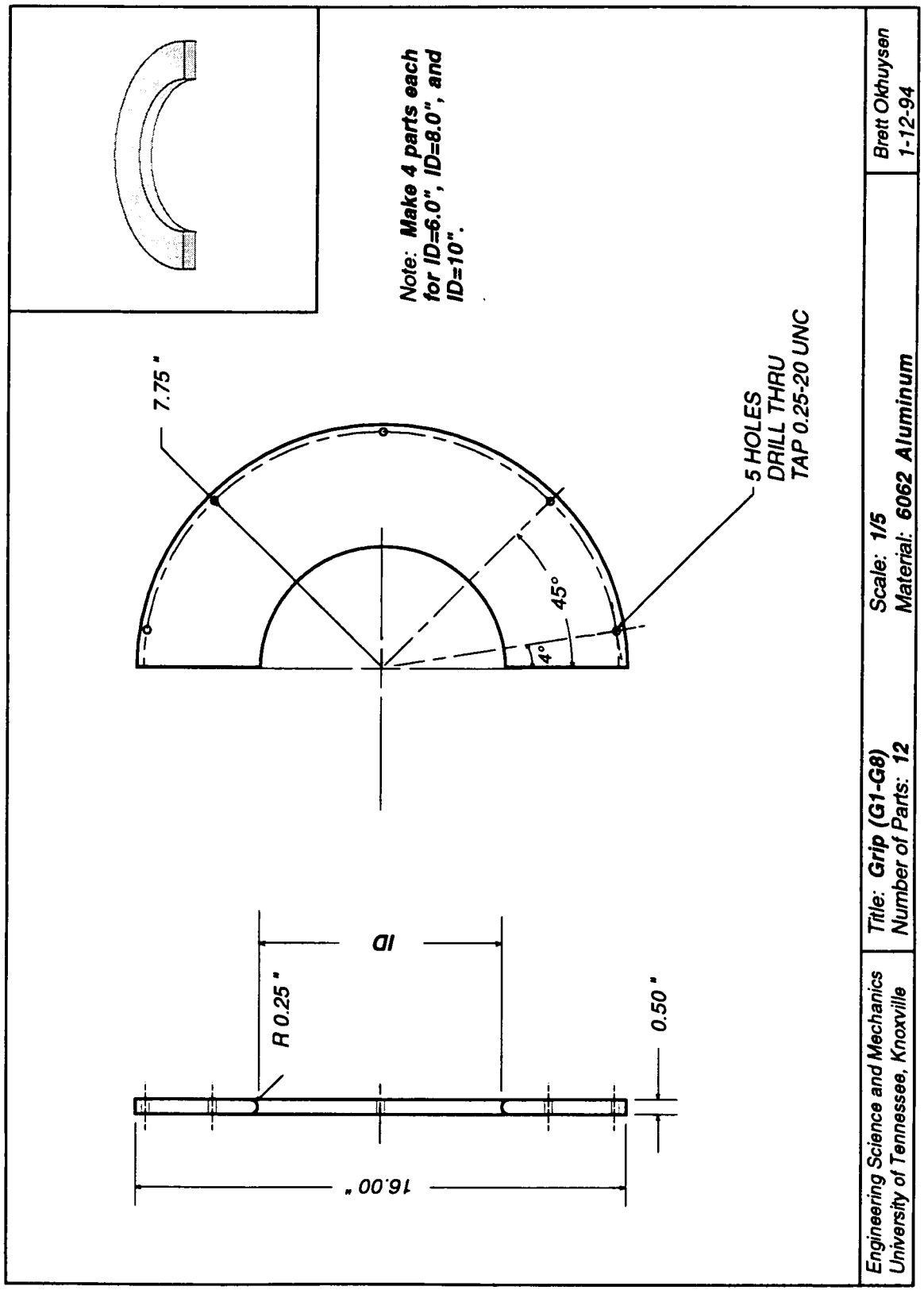
Note: Make 4 parts each for ID=6.0", ID=8.0", and ID=10".
7.75"
5 HOLES
DRILL THRU
TAP 0.25-20 UNC
45°
4°
ID
R 0.25"
0.50"
16.00"
Engineering Science and Mechanics
University of Tennessee, Knoxville
Title: Grip (G1-G8)
Number of Parts: 12
Scale: 1/5
Material: 6062 Aluminum
Brett Okhuysen
1-12-94

NTS

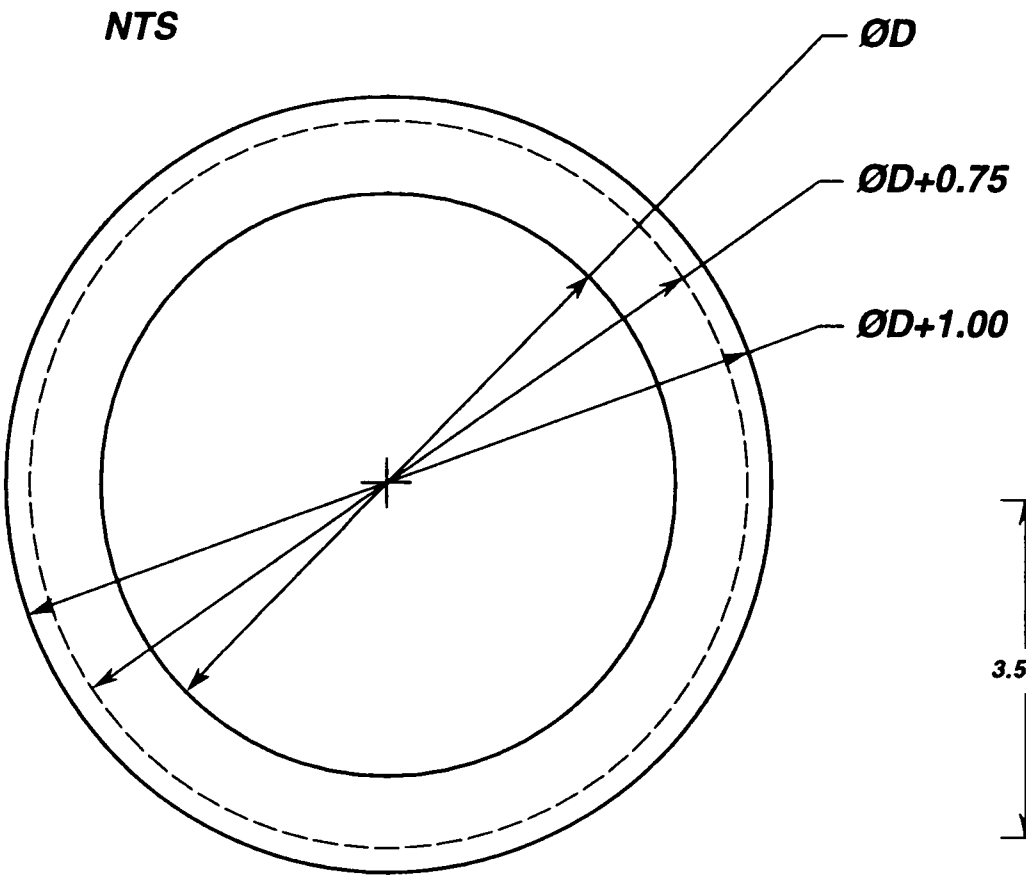

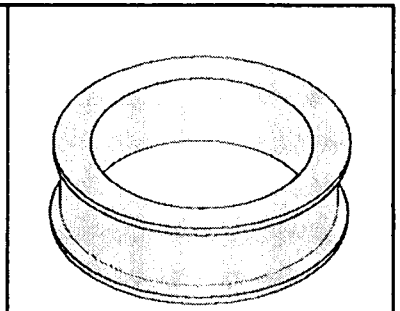

RING CROSS SECTION

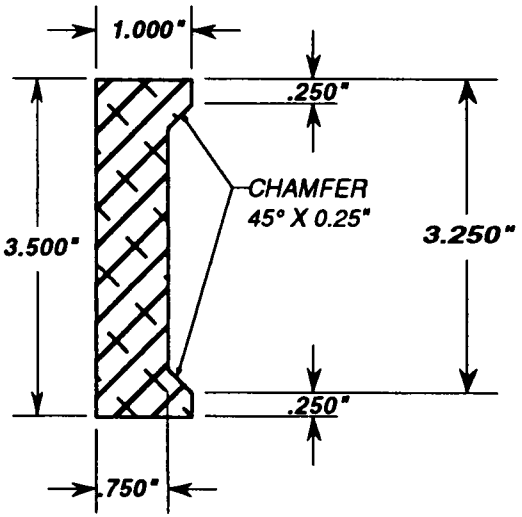

Notes: **Break all edges**
Make two rings each for
D=6.0", D=8.0", and D=10.0"

Engineering Science and Mechanics University of Tennessee, Knoxville	Title: **Sleeve End Ring** Number of Parts: **6 (CIn,COn)**	Scale: **1/2** Material: **6062 Aluminum**	Brett Okhuysen 1-12-94

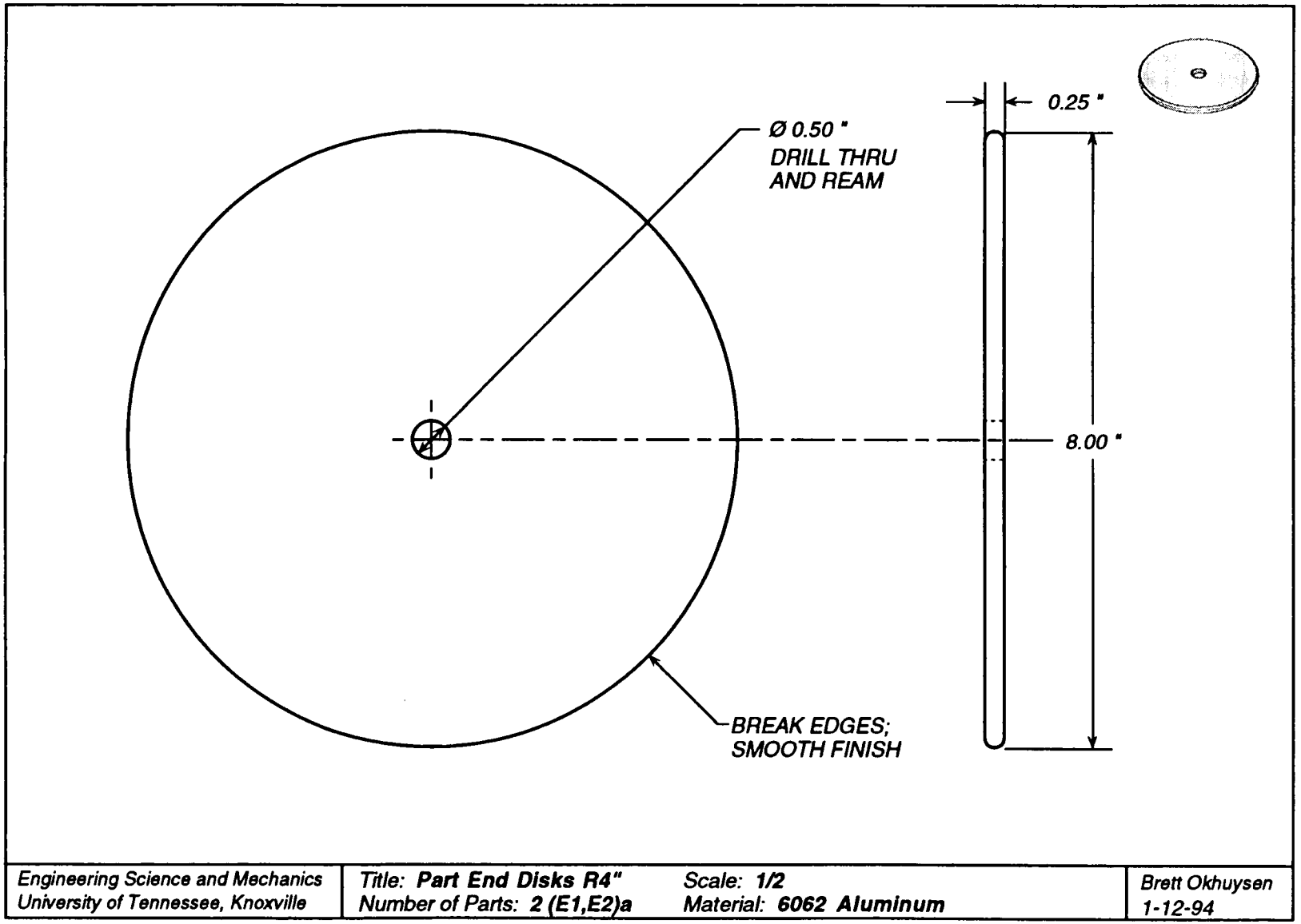

Engineering Science and Mechanics University of Tennessee, Knoxville	Title: **Part End Disks R4"** Number of Parts: **2 (E1,E2)a**	Scale: **1/2** Material: **6062 Aluminum**	Brett Okhuysen 1-12-94

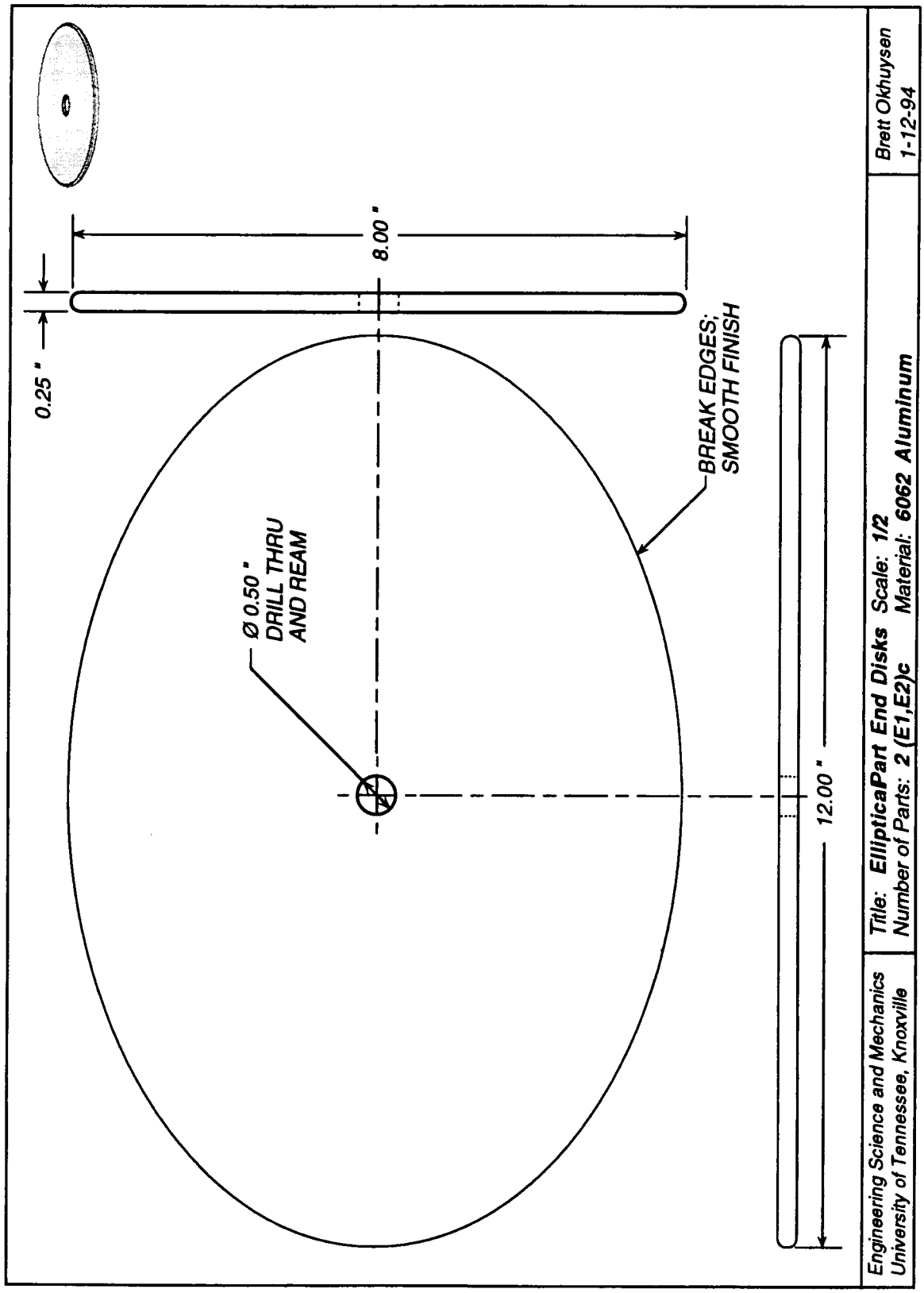
0.25 "
8.00 "
Ø 0.50 "
DRILL THRU
AND REAM
BREAK EDGES;
SMOOTH FINISH
12.00 "
Engineering Science and Mechanics
University of Tennessee, Knoxville
Title: EllipticaPart End Disks Scale: 1/2
Number of Parts: 2 (E1,E2)c Material: 6062 Aluminum
Brett Okhuysen
1-12-94

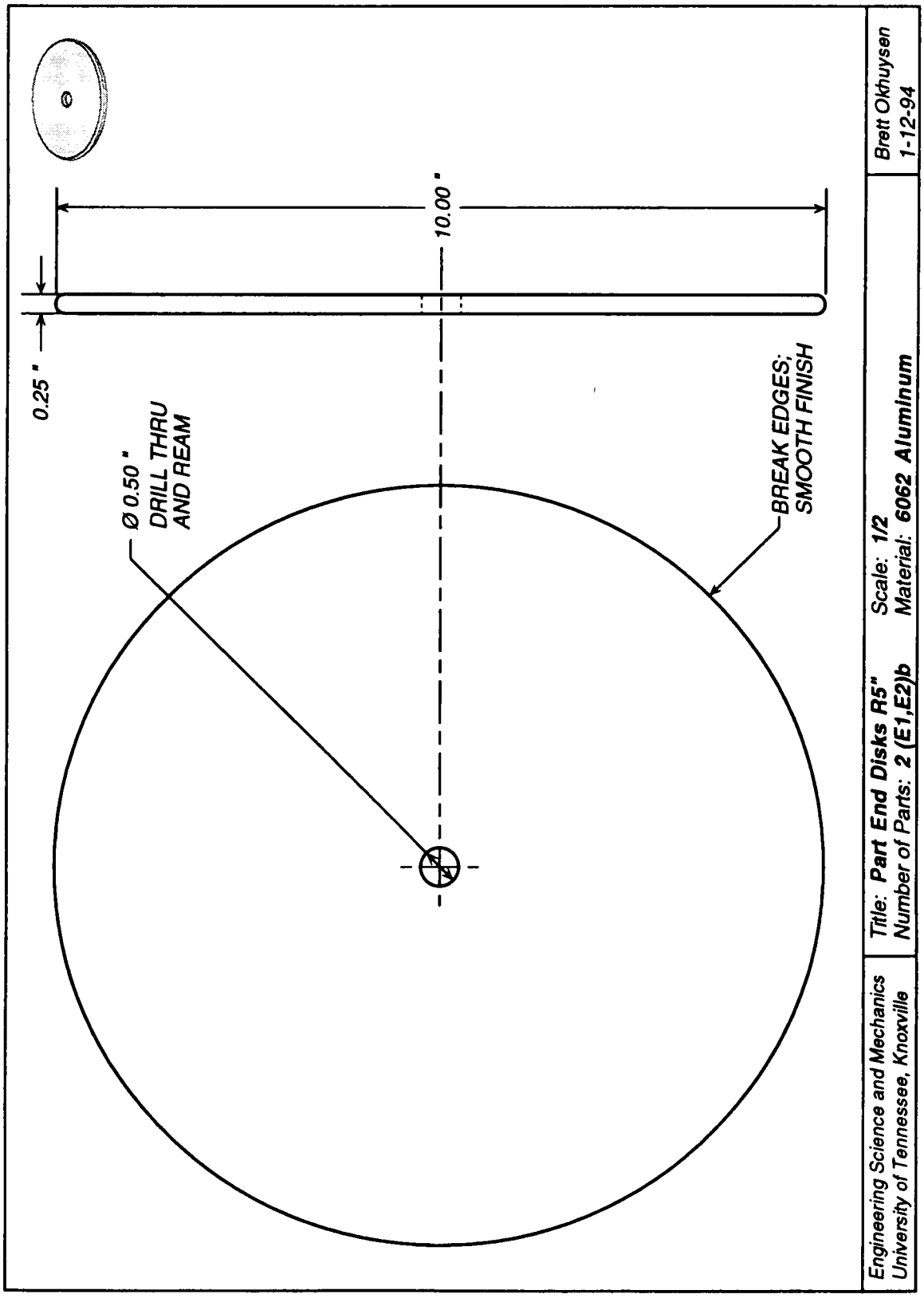
0.25 "
10.00 "
Ø 0.50 "
DRILL THRU
AND REAM
BREAK EDGES;
SMOOTH FINISH
Engineering Science and Mechanics
University of Tennessee, Knoxville
Title: Part End Disks R5"
Number of Parts: 2 (E1,E2)b
Scale: 1/2
Material: 6062 Aluminum
Brett Okhuysen
1-12-94

PARTS LIST

ALL UNITS IN INCHES

CODE	DESCRIPTION	QUANTITY
KS	3/16 x 2 SQUARE STOCK KEY	4
HN1	1 - 8 UNC-2B HEX NUT	24
HN2	3/4 - 10 UNC-2B HEX NUT	16
LW	3/4 REGULAR LOCK WASHER	16
HN3	1/2 - 13 UNC-2B HEX NUT	8
S1-S4	1 - 8 UNC-2A x 28" THREADED SHAFT	4
TB	THRUST BEARING 3/4" ID - 1" OD x 1"	16
BB	BALL BEARING NUT	4
D1-D4	1" x 72" SCREW STOCK	4
T1-T4	SPROCKET: 5/8" ID WITH 1/8x3/16 KEYHOLE	4
C1,C2	CHAIN	2
HC1	1/2 - 13 UNC-2A x 4" HEXAGON CAP SCREW	8
HC2	1/2 - 13 UNC-2A x $1\frac{1}{2}$" HEXAGON CAP SCREW	4
HC3	1/4 - 20 UNC-2A x 7/8" HEXAGON CAP SCREW	40
R1	1/2 - 13 x 92" THREADED SHAFT	1
R2	1/2 - 13 x 32" THREADED SHAFT	1
PW1	1.062 x 2.000 x 0.134 TYPE A PLAIN FLAT WASHER	16
PW2	0.531 x 1.062 x 0.095 TYPE A PLAIN FLAT WASHER	8

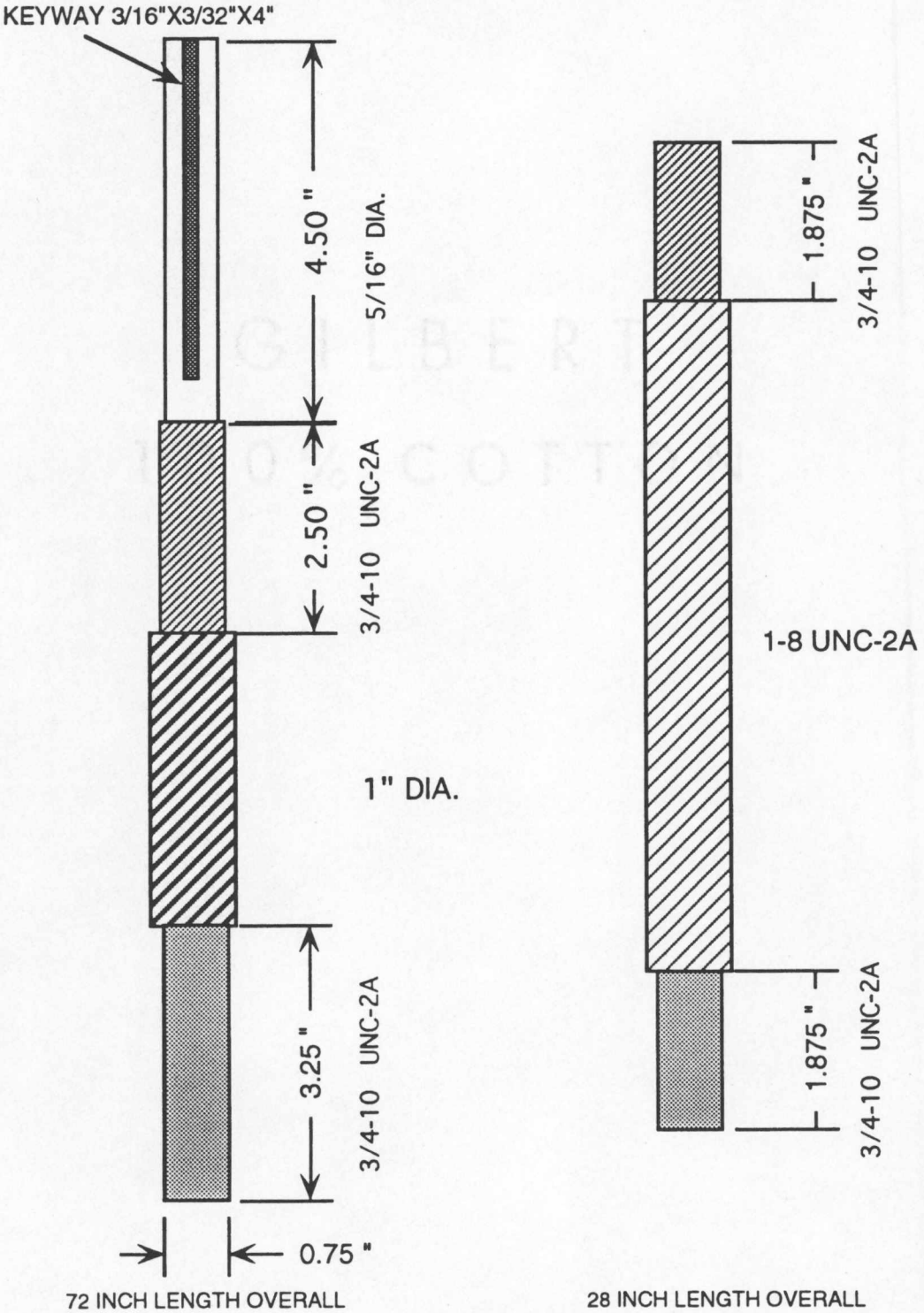

D1-D4 **S1-S4**

THREADED SHAFTS

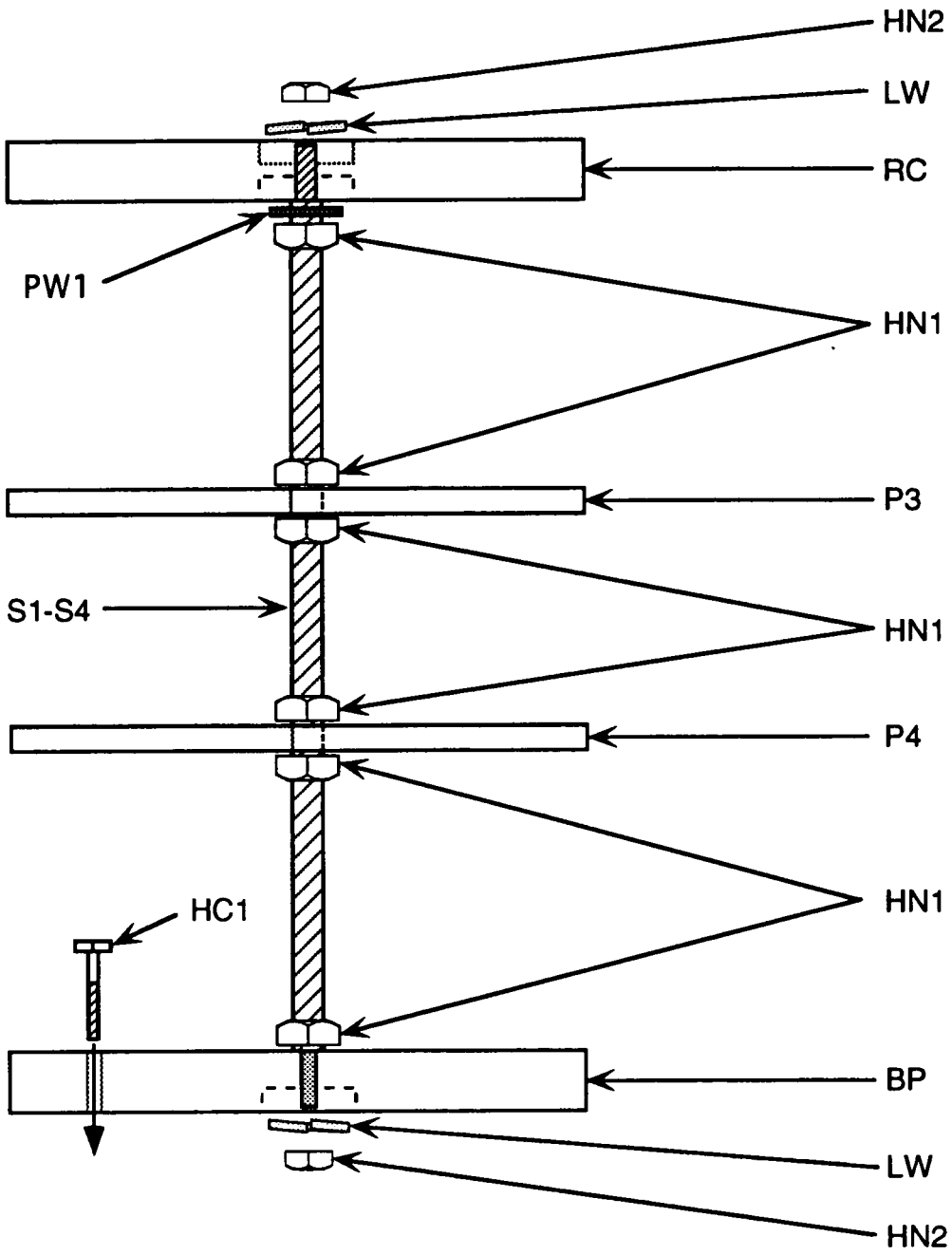

BOTTOM ASSEMBLY

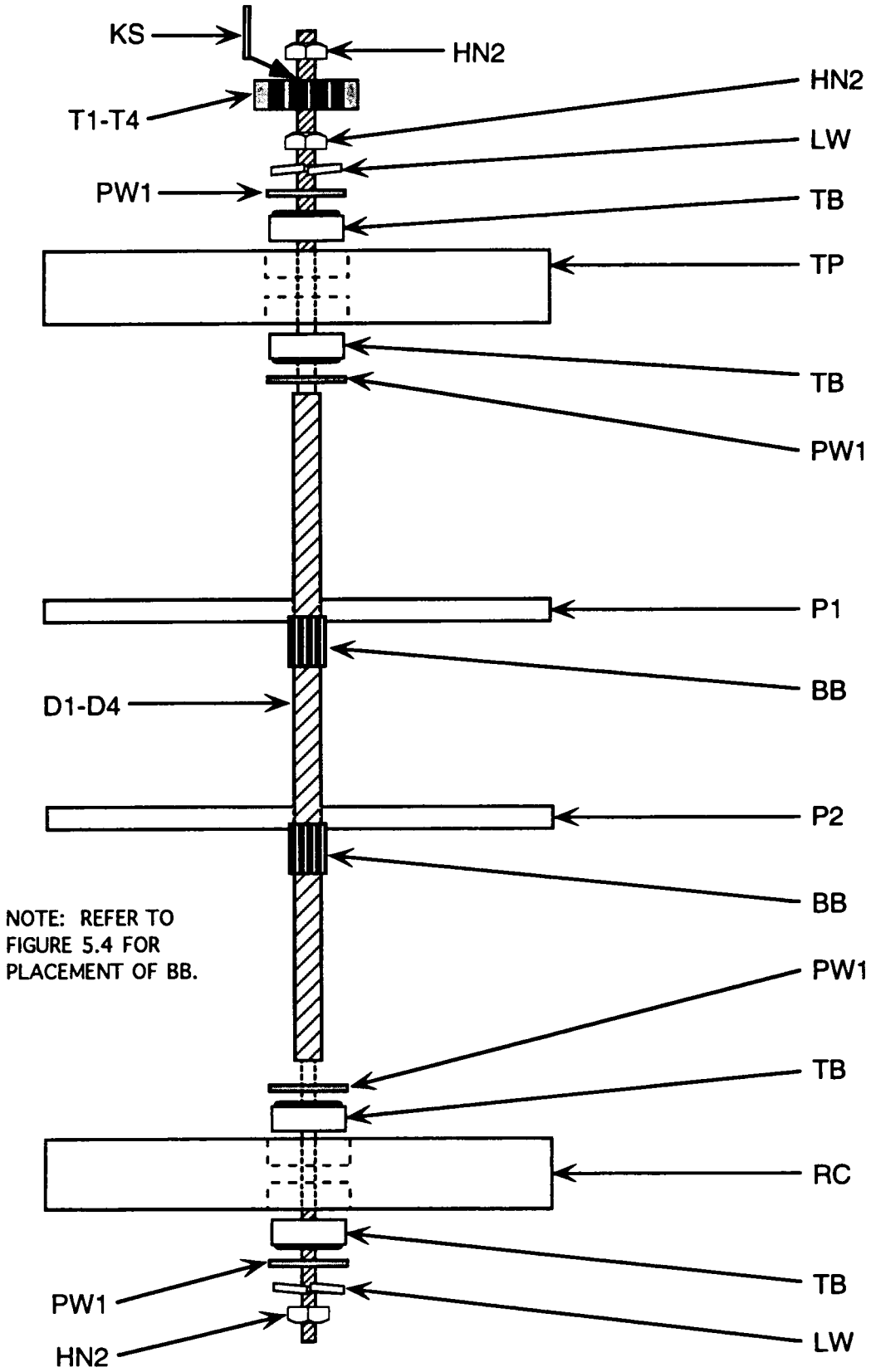

TOP ASSEMBLY

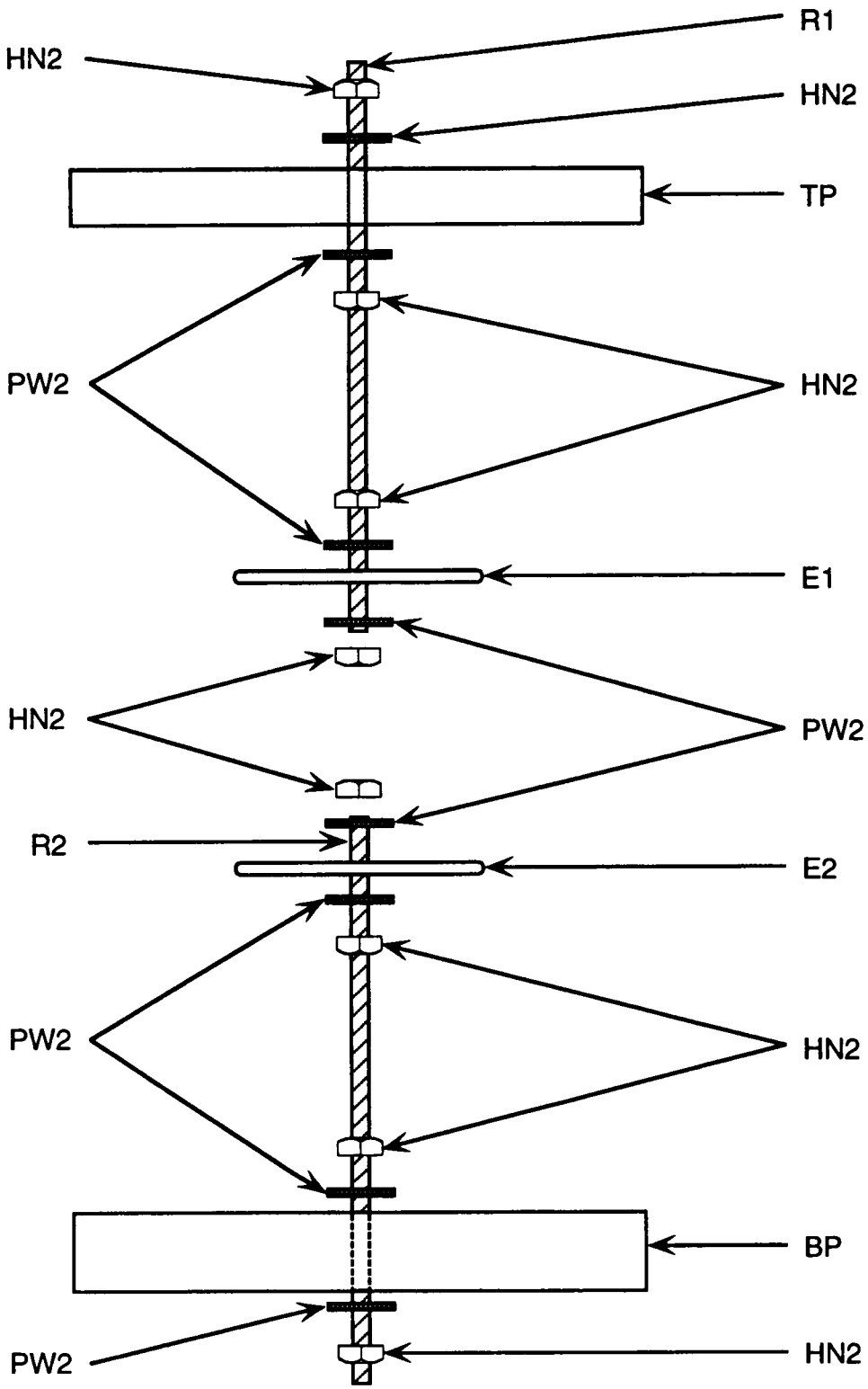

PART END DISK ASSEMBLY

VITA

Brett Samuel Okhuijsen was born in Columbus, Georgia. After spending many years in Savannah, Georgia, he moved to New York and later to Idaho. He attended high school at Bishop Kelly High School in Boise, Idaho. He then moved to Knoxville, Tennessee, and attended the University of Tennessee, Knoxville where he received a Bachelor's Degree in Engineering Science and Mechanics specializing in computational mechanics.

In his second year of undergraduate study, Brett was exposed to research for the first time through the a research assistantship in the Department of Physics. This assistantship led to a summer internship at the Joint Institute for Heavy Ion Research at Oak Ridge National Laboratory. Further into his undergraduate studies, Brett participated in the cooperative engineering program, which led him to work for the Naval Air Warfare Center in Warminster, Pennsylvania. The co-op experience led him to the field of composite materials. He continued his education at the University of Tennessee and became captivated by theoretical mechanics. Brett received a Master's Degree in Engineering Science in August 1995.

In August of 1995, he will begin work on a Ph. D. degree in theoretical mechanics under the supervision of Professor Dusan Krajcinovic at Arizona State University.